COMBINED EXPERIMENTAL AND MODELING STUDIES REVEAL NEW MECHANISMS IN T CELL ANTIGEN RECOGNITION

A Dissertation
Presented to
The Academic Faculty

by

William Rittase

In Partial Fulfillment
of the Requirements for the Degree
Doctor of Philosophy in the Department of Mechanical Engineering
Woodruff School of Mechanical Engineering

Georgia Institute of Technology
August 2018

COMBINED EXPERIMENTAL AND MODELING STUDIES REVEAL NEW MECHANISMS IN T CELL ANTIGEN RECOGNITION

Approved by:

Dr. Cheng Zhu, Advisor
School of Mechanical Engineering
Georgia Institute of Technology

Dr. Susan Thomas
School of Mechanical Engineering
Georgia Institute of Technology

Dr. Melissa Kemp
School of Biomedical Engineering
Georgia Institute of Technology

Dr. Manu Platt
School of Biomedical Engineering
Georgia Institute of Technology

Dr. Todd Sulchek
School of Mechanical Engineering
Georgia Institute of Technology

Date Approved: June 29, 2018

[To Melissa and Willow]

ACKNOWLEDGEMENTS

I would like to thank many people for their contribution to getting me to this point in my life. First, I would not be here if not for my professors at Bucknell who gave me my first research position and advised me towards this path in the first place – Dr. Keith Buffinton and Dr. Steven Shooter. I would like to thank my current advisor, Dr. Cheng Zhu, for his understanding and advice in all aspects of academia, and the financial support to keep this work going. Additionally, all Zhu lab members, past and present, have been influential in some part of this work; I would especially like to thank Dr. Kaitao Li, Dr. Prithiviraj Jothikumar, Dr. Jin-sung Hong, and Dr. Chenghao Ge for their discussions on many of the topics, and Dr. Fang Kong for his assistance on HAFM development. I would like to acknowledge my friends and family, especially my parents, for their emotional cheerleading and support throughout these many years. And most importantly, I could not have done this without my wife Melissa who has trusted and supported me through the ebbs and flows during this process.

TABLE OF CONTENTS

ACKNOWLEDGEMENTS **iv**

LIST OF TABLES **viii**

LIST OF FIGURES **ix**

LIST OF SYMBOLS AND ABBREVIATIONS **xi**

SUMMARY **xiii**

CHAPTER 1. Introduction **1**

CHAPTER 2. Background **5**
2.1 T cells in immunity **5**
2.1.1 Thymic development 5
2.1.2 T cell activation 6
2.1.3 T cell subsets 7
2.2 T cell antigen recognition through the TCR **8**
2.2.1 TCR-pMHC structure 9
2.2.2 TCR signalling and regulation 10
2.2.3 Antigenic and self pMHC origins 12
2.3 Models of TCR antigen recognition and self-peptide discrimination **13**
2.3.1 Receptor occupancy model 13
2.3.2 Kinetic segregation 14
2.3.3 Kinetic proofreading and extensions 15
2.3.4 Role of force in antigen recognition 16
2.3.5 Models for the role for coreceptors in antigen discrimination 17
2.4 Motivation and significance of research **18**

CHAPTER 3. Experimental materials and methods **19**
3.1 Cells and proteins **19**
3.2 Bead preparation **19**
3.3 Site density measurement **20**
3.4 Microcantilever preparation and calibration **20**
3.5 Statistical analyses **21**
3.6 Dynamic micropipette assay using HAFM **21**
3.7 Lck inhibition treatment **22**
3.8 Cholesterol oxidase treatment **22**
3.9 Cholesterol sulfate treatment **22**

CHAPTER 4. Development and validation of a horizontal atomic force microscope **24**
4.1 Background **24**
4.2 Development of instrumentation **27**
4.2.1 Hardware design 27

4.2.2 Software libraries 30
4.3 Validation of instrumentation 30
4.3.1 Hallmarks of AFM 30
4.3.2 Micropipette assay 31
4.3.3 Force clamp and rupture force assays 35
4.4 Discussion and future directions 39

CHAPTER 5. Transient ligand memory in TCR antigen recognition 41
5.1 Background 41
5.2 Memory index 42
5.3 Verification of TCR memory in cellular environment 44
5.4 Analysis of purified TCR:pMHC systems 45
5.5 Mechanism exploration by dynamic input micropipette assay 47
5.5.1 Dynamic input micropipette assay 47
5.5.2 Effects of ligand potency on TCR ligand memory 48
5.5.3 Generalized linear regression model of TCR memory 51
5.5.4 Lck assists in triggering long periods of adhesion 52
5.5.5 Cholesterol binding to TCR inhibits ligand memory 56
5.6 Modeling and simulation of TCR ligand memory 59
5.7 Discussion and future studies 67

CHAPTER 6. Role of mechanical force in CD8 coreceptor binding and its impact on T cell tolerance 73
6.1 Introduction 73
6.2 Experimental data 75
6.3 Long-lived bond formation is a diffusion limited process 78
6.3.1 Survival distributions indicate multiple bond states 78
6.3.2 Force-induced recruitment models cannot explain data 80
6.3.3 Force-induced PDD formation promotes catch-bond response 86
6.4 Model and simulations on proposed mechanism explain experimental data 89
6.4.1 Proposed mechanism for catch-bond behaviour in thymocyte selection 90
6.4.2 Simulations on proposed mechanism 92
6.5 Discussion and future studies 97

CHAPTER 7. Conclusions and future directions 103

APPENDIX A. Matlab code for simulation of TCR memory mechanism 105
A.1 Code for cholesterol binding model 105
A.2 Code for get kinetic parameters function 108
A.3 Code for one touch function 109
A.4 Code for SSA function 110
A.5 Code for model evaluation script 110
A.6 Code for memory index evaluation and plotting script 112

APPENDIX B. Matlab code for Markov chain survival distribution fitting 116
B.1 Code for fitting algorithm 116
B.2 Code for gathering data function 119

B.3 Code for scanning parameter space 120
B.4 Code for running the different cases and finding lowest residual function 122
B.5 Code for simulating a single Markov chain function 124
B.6 Code for finding error residuals function 126
B.7 ODE equations for Markov transition 127

APPENDIX C. Matlab code for simulation of CD8 catch-bond mechanism 130
C.1 Code to run BFP assay for one ligand, several CD8:Lck fractions 130
C.2 Code to determine bond lifetimes for one cell and pair function 131
C.3 Code for get kinetics function 136
C.4 Code to determine the probability of rupture before clamp function 138
C.5 Code to select a lifetime function 138
C.6 Code to compile data function 139
C.7 Code to plot lifetimes and extract data from workspace script 140

REFERENCES 142

LIST OF TABLES

Table 1. Comparison of single molecule measurement techniques and their assays 26
Table 2. HAFM primary components 27
Table 3. Simulation parameters for mechanism investigation 62
Table 4. TCR ligand memory mechanism simulation parameters 63
Table 5. Twenty best parameter fits by statistical model 65
Table 6. Best parameter fits by statistical model with outliers removed 67
Table 7. Simulation parameters for CD8 thymocyte binding mechanism 95

LIST OF FIGURES

Figure 1. Cartoon depiction of MHC Class structure 10
Figure 2. Principle components of atomic force microscopy 24
Figure 3. Diagram of different HAFM molecular origins 27
Figure 4. Photodiode board circuitry 29
Figure 5. HAFM hardware development requires maximal use of space 30
Figure 6. AFM signal hallmarks 31
Figure 7. HAFM micropipette assay outline 34
Figure 8. HAFM micropipette data stability 35
Figure 9. Demonstration of HAFM force clamp assay 37
Figure 10. HAFM cell-cell force separation characteristics 38
Figure 11. Memory index for several TCR:pMHC systems 45
Figure 12. Purified TCR:pMHC memory index 46
Figure 13. Confirmation of adhesion in different 1E6 TCR ligands 49
Figure 14. TCR ligand memory dependence on peptide potency 50
Figure 15. Normalized memory index dependence on ligand potency 51
Figure 16. TCR ligand memory dependence on contact and waiting times 52
Figure 17. Impact of Lck inhibition on adhesion frequency and ligand memory 54
Figure 18. Lck inhibition decreases probability of triggering upregulated adhesion periods 56
Figure 19. Cholesterol oxidase treatment effects on TCR ligand memory 57
Figure 20. Addition of cholesterol sulfate reduces TCR memory in a dose-dependent fashion. 58
Figure 21. Simulation mechanism outline 61
Figure 22. Micropipette simulation algorithm outline 64
Figure 23. Experimental data vs. simulated parameter fitting using statistical methods 66
Figure 24. Comparison between Hill coefficient and ligand memory in moderating binding sensitivity 70

Figure 25. Positively selecting ligands form catch-bonds while negatively selecting ligands form slip bonds in the presence of CD8 76
Figure 26. Addition of Lck inhibitor removes catch bond promotion by CD8 77
Figure 27. Catch bonds arise from two possible survival distributions 79
Figure 28. Force-induced recruitment mechanism 81
Figure 29. Double exponential fit adequately predicts fraction of PDD bonds 82
Figure 30. Formation of PDD unlikely after pulling of TCR:pMHC bond 84
Figure 31. Formation of PDD unlikely after pulling of CD8:MHC bond 85
Figure 32. Transient species deviations under force 87
Figure 33. Markov chain connection diagram for determination of survival distribution 88
Figure 34. Fraction of PDD bonds correlates with catch-bond behavior. 89
Figure 35. Proposed mechanism for catch-bond behavior in thymocyte negative selection 91
Figure 36. BFP simulation algorithm flow diagram 93
Figure 37. Outline of system interactions 94
Figure 38. TCR:pMHC force induced Lck activation function 96
Figure 39. Simulated vs. Experimental thymocyte lifetime vs. force 97
Figure 40. Simulated BFP data indicates high Q4R7 sensitivity to mechanism 97

LIST OF SYMBOLS AND ABBREVIATIONS

2D	Two-Dimension(al)
AFM	Atomic Force Microscopy
APC	Antigen Presenting Cell(s)
BFP	Biomembrane Force Probe
BSA	Bovine Serum Albumin
CD	Cluster of Differentiation
CI	Confidence Interval
Co-IP	Co-ImmunoPrecipitation
DI	Deionized
DMSO	Dimethyl Sulfoxide
HAFM	Horizontal Atomic Force Microscopy
i.i.d	Independent and Identically Distributed
Ig	Immunoglobulin
ITAM	Immunoreceptor Tyrosine-based Activation Motif
LAT	Linker for the Activation T cells
MFP	Molecular Force Probe

P_a	Probability of Adhesion
PBS	Phosphate buffered saline
PDD	Pseudo-Dimer of Dimers
pMHC	(peptide) Major Histocompatibility Complex
RBC	Red Blood Cell
SA	Streptavidin
SLP-76	SH2-domain-containing Leukocyte Protein of 76 kDa
SSA	Stochastic Simulation Algorithm
TCR	T Cell Receptor
ZAP-70	Zeta-chain-Associated 70 kDa tyrosine Phosphoprotein

SUMMARY

T cells of the immune system recognize small antigen peptide fragments loaded onto Major Histocompatibility Complex (MHC) molecules through their T Cell Receptor (TCR). The recognition of antigenic pMHC by the TCR is an extremely sensitive and specific process, discriminating as few as a single antigenic pMHC from the self majority while remaining tolerant to uninfected cells. This unique sensitivity and specificity have been intensely studied, but much is still unknown regarding mechanisms surrounding the antigen recognition process.

In the following studies, a Horizontal Atomic Force Microscope (HAFM) was developed to assist in parsing this unique behavior. Utilizing this system, periods of upregulated adhesion, called TCR ligand memory, were investigated between 1E6 TCR and a panel of pMHC of varying potency. The strength of these periods of upregulated adhesion, indicative of an upregulated sensitivity to antigen, inversely correlated with antigen potency. Inhibition of proximal signaling molecule Lck decreased the triggering of these periods, but did not significantly affect their duration. Interestingly, membrane cholesterol oxidation by cholesterol oxidase eliminated TCR ligand memory all together. Treatment with cholesterol sulfate, a naturally occurring analog of cholesterol, depleted TCR ligand memory in a dose-dependent fashion. This behavior was simulated to extract estimates of kinetic parameters and showed that TCRs upregulated their kinetics several magnitudes very quickly upon initial antigen recognition. This mechanism is a way to increase antigenic sensitivity and increase antigen rebinding to further cell activation.

Additionally, OT-1 double positive thymocytes were probed by pMHC using a Biomembrane Force Probe (BFP) with different ligands under the presence of CD8, a coreceptor which also binds MHC independently of TCR. Negatively selecting ligands resulted in catch-bonds, and positively selecting ligands resulted in slip bonds. This process relied on the kinase activity of Lck. Simulation-based analysis on these data sets indicated that this mechanism was not the result of passive processes. Force induced formation of long-lived bonds, indicating that mechanical forces are priming formation of a larger complex which enhances lifetime. These bonds dominate the average lifetime and result in catch-bond behavior. Simulations of the BFP assay suggest that mechanotransduction by the TCR resulted in active heterodimerization of CD8 and TCR via interactions between intracellular tails of CD3(TCR) and Lck(CD8). This mechanism results in additional upregulation of binding kinetics for increasing antigen capture and rebinding to promote signaling, thereby also increasing antigen sensitivity and discrimination.

CHAPTER 1. INTRODUCTION

The human body is remarkably complex machine. With the discovery of the first cells by Robert Hook in the 17th century [1] and the further formulation of cell theory over a century later [2], we know that this complex machine is composed of trillions of cells seamlessly working together to perform tasks necessary for us to survive. If we add to it the complexity of the cellular machinery and all its levels of regulation, the problem of understanding the human body in all its intricacies is simply mind-boggling, possibly outside the capacity for human knowledge. From this scope, the entire premise of survival and disease becomes overwhelming.

Ultimately, the goal of understanding the human body is to give context to the diseases which disrupt it, leading to better and more informed treatments. Despite the pathology of disease being seen largely at a systems level, diseases in the human body, spanning from autoimmune disorders to the common cold, originate or interact at the cellular level [3]. This cellular activity eventually manifests itself in affecting system level functions. Therefore, if we center our search for understanding diseases by examining the fundamental effector units – the cells themselves – then we can begin to understand specific aspects of these diseases. This approach narrows the range of potential treatments and streamlines the identification of clinical intervention points.

As alluded to earlier, the cell itself is a remarkably complex machine. If the cell is a machine, the proteins are the principle components which perform its function. Therefore to understand the cell, we must begin by understanding the proteins themselves. Several layers of difficulty convolute the investigation of proteins, but it primarily originates from

the inability to adequately visualize their processes. Proteins are smaller than the diffraction limit (approximately 10 nm). Therefore, the field uses a variety of techniques to circumvent this limitation. Entire subfields are dedicated to one of a few of these assays. Some visualize protein movement and organization by tagging proteins with fluorescent dyes or other markers through specialized microscopy techniques [4]. Others visualize their modifications in bulk assays such as Western blot techniques [5] and flow cytometry [6] after probing interactions by modifying proteins or providing different stimuli. Entire fields are dedicated to simply visualizing a single protein's structure or binding properties [7]. All this data is later disseminated by review papers and text books to draw conclusions about the inner workings of the cell.

Despite the vast amount of available data by molecular biology approaches, predictions were, and still frequently are, generalized as unquantified influences, such as upregulation of activity, on other molecular interactions. These influences are outlined as static connection diagrams which describe the influences of multiple molecular pathways. From a homeostatic perspective, this helps to better understand what gives rise to many cellular behaviors. However, if a molecule can be activated, inhibited, expressed or degraded by a series of other controlled reactions, all under the influences of external factors such as molecular expression or micro-environmental cues, homeostatic influences cannot suffice to understand the complexity of even a single molecule's influence on the system as a whole.

Computational systems biology approaches attempt to unify the vast amount of information available from molecular biology to converge on the true interaction network. This, in turn, will lead to a better understanding of the cell itself and further progress the

goal of better and more informed disease treatments. There are considered two arms of the computational systems biology [8], data-mining and simulation-based analysis. Moving forward, the focus will be on simulation-based analysis.

Much of the focus of simulation-based analyses is placed on kinetics rates and affinities of receptor-ligand binding. The Zhu lab has developed several techniques to assist in measuring the kinetics of receptor-ligand interactions spanning across two membranes – called two-dimensional, or 2D, kinetics – which are critical in governing communication between to cells in contact. Because membranes of cells act to isolate the intracellular machinery which governs cell responses, intercellular communication across membranes is a cornerstone of cell-cell communication. This communication stems from several factors, but a significant influence is the result of receptor-ligand interactions linking two opposing membranes, allowing signals to be directly transmitted from cell to cell. How quickly receptors bind and dissociate, governed by the on- and off-rates of the interaction respectively, are critical parameters in shaping the response.

However, in many experimental 2D kinetics assays, the receptor-ligand interaction is in the cellular context, allowing modifications and signaling to occur; the cell is often thought of as being "tickled" with its ligand by the experimenter. It is natural to assume that this "tickling" may induce changes to the cell over time as the result of prior binding events, yet the result is often summarized as a single kinetic rate or affinity and correlated with complex behaviors which are often significantly downstream of binding. In essence, although the presented information is more easily digested by the reader, some information in the series of binding events is lost by the use of summary parameters, similar to the loss of information in molecular biology approaches discussed previously. In this manuscript,

simulation-based analyses will be used in tandem with experimental assays to draw more information from these complex 2D binding assays.

The focus of this manuscript will be on a primary molecular interaction of the adaptive immune response – that of the T Cell Receptor (TCR) binding to its ligand, a peptide fragment loaded onto Major Histocompatibility Complex (pMHC). From its discovery in 1982-83 [9-11], a significant amount of study has been aimed toward understanding its function and regulation. However, despite the large body of research into its role in adaptive immunity, the biophysical aspects of discrimination of foreign peptides are still incompletely understood. The majority of the difficulty arises from the fact that antigenic pMHC, those coming from foreign pathogens, are typically low in number compared to self pMHC, those which are naturally displayed on the surface of all cells in the body [12]. Therefore, the TCR must have enough power to detect low amounts of antigen on infected or diseased cells, while also not eliciting a response to healthy cells expressing only self pMHC.

Much of the focus of antigen recognition and discrimination has been placed on the kinetics of the interaction, making it an excellent study for the 2D kinetic assay tools in the Zhu lab and simulation-based analyses. In this study, a new tool was developed in the Zhu lab, Horizontal Atomic Force Microscopy (HAFM), to assist in performing some of the assays required to investigate TCR kinetic regulation. This tool was used to investigate transiently upregulated TCR-pMHC binding periods which are thought to enhance the discriminatory capabilities of the TCR. Lastly, a mechanism controlling the mechanical activation of TCR and binding of coreceptor CD8 in thymocytes to enhance antigen discrimination was investigated through simulation-based analyses.

CHAPTER 2. BACKGROUND

2.1 T cells in immunity

In brief, there are two main components to our immune systems - innate and adaptive immunity – composed of many different cell types originating from the bone marrow [13]. Innate immunity provides the first line of defense to invading pathogens, and relies heavily on recognition of generic patterns. T lymphocytes, or T cells, are a major component of the body's adaptive immune system, the second line of defense, which depends on innate immune functions to develop a response. After pathogen clearance, adaptive immunity has the ability to recognize the same pathogen upon future infection and expedite its clearance.

2.1.1 Thymic development

T cells begin as pluripotent hematopoietic stems cells in the bone marrow, and transition to the thymus for training. Here, they are referred to as thymocytes, and are not yet involved in immune functions. In the thymus, thymocytes undergo development of a functional TCR, positive selection by appropriate self pMHC binding, and determination of lineage fate [14-16]. In short, the thymus positively selects T cells to respond to self pMHC, a response called tonic signalling which is required for T cell survival [17], while eliminating cells which respond too strongly in a process called negative selection [18]. This results in a pool of cells which do not respond adversely to healthy cells, but which has the possibility of recognizing non-self, or antigenic peptides; the reasoning for such a mechanism will become more clear in Section 2.2.3. After thymocytes undergo the selection process, naïve T cells leave the thymus and enter circulation.

2.1.2 T cell activation

The series of events required for T cell activation after infection is well-defined. First, antigen from the infected site is delivery through innate recognition or other passive processes through the lymphatic system to a draining lymph node and presented on Antigen Presenting Cells (APCs). After antigen delivery to the lymph nodes, naïve T cells have the ability to recognize pathogenic pMHC in the lymph nodes through their specific TCR and become activated by forming a well-characterized, complex structure between T cell and APC known as the immunological synapse [19-22]. Subsequently, the cells undergo clonal expansion. This expansion leads to a large pool of effector cells with the same TCR recognizing the same pathogenic pMHC. These cells either return to circulation and the site of infection to identify and kill other infected cells presenting the same pathogenic MHC or release cytokines which help prime other immune cells to boost other proximal or humoral immune responses [13, 23]. Once the pathogen has been removed from the body by this response, a small number of the remaining effector cells transition into a memory state to act upon future infection by the same or similar pathogens [24].

It is important to note that these are only the classical responses induced by antigen recognition. There are several other subtypes of T cells that behave differently or have other roles (discussed further in section 2.1.3.2). Additionally, the picture is very complex, involving many other molecular and biochemical players which act to modulate the response. However, the basic progression of the activation cycle is similar – antigen uptake, presentation in the lymph nodes, TCR recognition, expansion, recirculation, further TCR recognition in tissues, and lastly, effector response.

2.1.3 T cell subsets

As the field of immunology develops, many different subsets of T cells are defined, all with differential behaviours and responses. We will briefly go over some of them here. However, as the literature grows, these subsets are more guidelines than fixed points. Cells have remarkable plasticity; switching between subsets has been known to occur and concrete classifications of cell behaviours is being constantly revised [25].

2.1.3.1 Classical T cell subsets: CD4+ vs. CD8+ T cells

The coreceptors CD8 and CD4 bind to MHC class I and II, respectively, independent of the TCR binding site to enhance the activation upon antigen recognition [26]. In addition to their role in antigen recognition (discussed in Section 2.3.5), the presence of either coreceptor is exclusive and indicates a specific lineage fate [13]. CD8+ positive cells are the effective targeted killers of the immune system. Upon pathogenic pMHC recognition in the lymph nodes, differentiated cytotoxic effector CD8+ T cells are the foot soldiers of the immune system that seek out and kill other infected cells throughout the body to prevent the spread of disease. Naturally, there are subsets of these (discussed in [27]). If CD8+ cells are the foot soldiers, CD4+ cells are their diverse set of commanders, playing multiple roles to orchestrate the defense through the release of different cytokines. These include T_H1, T_H2, T_H9, T_H17, T_H22, T_{reg}, and T_{FH} [28] although there are subsets of even these cell subtypes [29-32]. These cells display wide variety of roles range from upregulating innate responses and antibody production to shutting down even these same roles.

Both CD4+ and CD8+ positive cells however require initial antigen recognition through their TCR, albeit by different means. CD8+ positive cells recognize only class I pMHC, which is expressed on all cell types throughout the body. They must be able to eliminate any cell that is infected while not allowing the pathogen to spread by tightly controlling their disposal by apoptosis. However, CD4+ cells, which have TCRs only recognizing only class II pMHC, only respond to professional APCs. The different MHC classes allows a delineation of effector functions, stemming from how the peptides are processed. More will be discussed about this in Section 2.2.3.

2.1.3.2 Non-classical subsets

Although not necessarily important to this study, it is important to note that there are several other subsets of T cells that do not necessarily recognize pMHC; their responses to antigen through different receptors may be similar and the mechanisms by which they are triggered could be related. Natural Killer T cells recognize glycolipids presented on another molecule, CD1d [33, 34]. Mucosal Associated Invariant T cells respond to MR1 bound vitamin B metabolites, although their function is more innate and less adaptive [33, 34]. Up to this point, all mention of TCR has been of the majority αβ heterodimer, although there is another subset of T cells expressing a different form - γδ - aptly named γδ T cells, reviewed in [35]. From this point forward, all mention of TCR will be αβ.

2.2 T cell antigen recognition through the TCR

The TCR is the central node of T cell activation and the primary molecule of interest for this study. Since its discovery nearly in the early 80s [9-11], a significant amount of research has uncovered several aspects key to how it recognizes antigen and signals

activation of the cell. Some of that will be reviewed in this section. There are several key aspects to understanding any receptor-ligand interaction – the structure and signaling capacities. In the case of TCR-pMHC interactions, it is also critical to understand the origins of the peptides themselves. These concepts will be discussed in this section.

2.2.1 TCR-pMHC structure

The αβTCR is a membrane-bound heterodimer of immunoglobulin (Ig)-like chains encoded by several different gene regions – variable, diversity, joining, and constant – which are organized during thymic development [36]. Due to somatic rearrangement of these regions, there are a theoretically estimated 10^{15} to 10^{20} unique combinations of TCRs [37], although practical limitations constrain the true diversity to around 10^{7}-10^{8} [38]. Each T cell will express only one of these unique combinations. Considering that each TCR and can cross-react with possibly several different pMHCs, the potential peptide sequences which can be recognized by T cells is enormous.

On the pMHC side, the structure is slightly simpler, but no less diverse due to MHC class restriction and the presence of two components – both the peptide and the MHC itself. Class I and II MHC have slightly different structures. MHC Class I is composed of three globular domains, α1-α3, stabilized by Beta-2 Microglobulin (Figure 1A). The short peptide sequence, approximately 8-12 amino acids in length, sits in a groove between the α1 and α2 domains. MHC Class II is composed of two chains consisting of two domains each - αβ. The longer peptide sequence (>11 amino acids) sits in the groove between the α_1 and β_1 domains (Figure 1B).

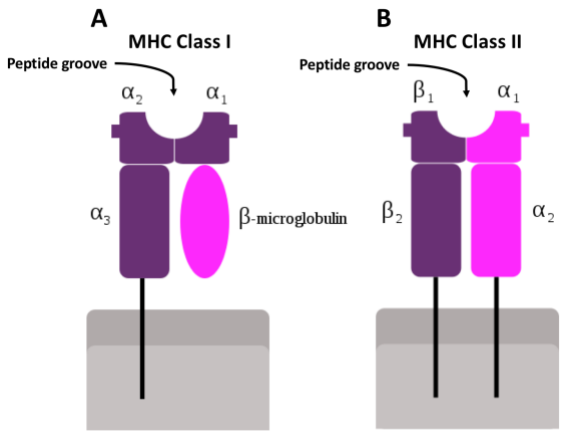

Figure 1. Cartoon depiction of MHC Class structure

(A) MHC Class I structure. Peptide sits in groove between α_1 and α_2 domains. (B) MHC Class II structure. Peptide resides between α_1 and β_1 domains. Figure adapted from [39]

The majority of the TCR diversity is encoded by the variable region most distal to the cell membrane. Due to the massive diversity of the TCR pool, many different structures must be resolved to make generalizations about the origins of ligand recognition. Since the first TCR-pMHC structure was first resolved by x-ray crystallography in 1996 [40], over 100 different structures have been solved. Six TCR loops, CDR1-3 for each chain, govern the interaction with both the MHC and peptide [41, 42]. TCRs tend to overlap the peptide at a well-conserved binding angle (see [43] for binding angles), with the CDR loops making contacts on the peptide. However, some CDR loops also contact the MHC itself [41, 43], indicating that the TCR recognizes aspects of both the MHC and peptide.

2.2.2 TCR signalling and regulation

Due to the cell membrane barrier isolating cellular machinery, information from outside the cell must be transferred across the membrane in the form of receptor-ligand binding. Typically, information from binding produces signalling in the form of a biochemical signal inside the cell. The TCR only carries a short intracellular domain and

does not contain any intracellular signalling domains of its own. Therefore, this information transfer relies wholly on another molecular interaction, the interaction between TCR and CD3 subunits that organize themselves around the TCR. Stoichiometric assays have determined there are three CD3 dimers - δε, γε, and ζζ – that non-covalently associate with the TCR, each containing one or more Immunoreceptor Tyrosine-based Activation Motifs (ITAMs) required for biochemical signalling [41, 44]. These ITAMs become phosphorylated upon activation of the T cell [45]. The initial phosphorylation of ITAMs and accumulation of signal, referred to as TCR triggering or TCR activation, is a central event in the activation of T cells. As few as a single antigenic pMHC interaction can result in cell activation [46-48]. Therefore, understanding the regulation of this information transfer is critical in understanding the immune response.

The sequence of events in TCR triggering is well described in the literature. Briefly, CD3 ITAMs in a resting T cell are thought to be buried in the membrane where they are not accessible for phosphorylation due to the strong negative charge of the inner leaflet and positively charged sequences on the CD3 tails [49, 50]. Upon pMHC engagement, the ITAMs are exposed for phosphorylation by Src family tyrosine kinase Lck [51]. After an ITAM has been doubly phosphorylated, Syk family kinase Zeta-chain-Associated 70 kDa tyrosine Phosphoprotein (ZAP-70) can bind through its tandem SH2 domains, releasing an inhibitory state and enabling it to become phosphorylated (by Lck or trans-phosphorylated by other ZAP-70), stabilizing an active conformation. ZAP-70 then begins a chain of events by phosphorylating many different molecules, primarily scaffolding or signalling proteins such as Linker for the Activation T cells (LAT) and SH2-domain-containing Leukocyte

Protein of 76 kDa (SLP-76) [52, 53]. These molecules continue a cascade of activation, resulting in full T cell activation.

TCR activation is a very dynamic process involving multiple levels of regulation; this begins at the TCR itself. In a resting T cell, the TCR resides in nanodomains and clustered by lipid rafts on resting T cells [54, 55], which concatenate upon antigen recognition into large microclusters symptomatic of immunological synapse formation. Receptor pre-clustering controls receptor sensitivity [56] and has been shown to be relevant with TCR [54, 57]. In addition to the clustering effects of lipid rafts, cholesterol binds the TCR, resulting in downregulation of signalling [55, 58-60]. This indicates several levels of control at the TCR level.

Intracellular regulation of signalling occurs at many points. Lck has several different phosphorylated forms, each with different kinetics [61], to regulate initial ITAM phosphorylation rates. ZAP-70 and the ITAMs also have their own levels of regulation discussed previously. In addition, phosphatases and other kinases, such as SHP isoforms and Csk, control the phosphorylation patterns of these molecules, typically themselves under the control of co-stimulatory and co-inhibitory receptors [62]. In summary, the TCR signalling complex is chaotic, but tightly controlled, through a combination of factors [63].

2.2.3 Antigenic and self pMHC origins

Antigens are any substance that induces your body to produce a specific antibody for it; however, it is more broadly used to define any toxin or foreign substance that induces an immune response. Traditionally, MHC class I and II molecules present peptides to be recognized by CD8+ and CD4+ T cells, respectively. The origins of the peptide fragment

depend on the source of the protein – intracellular peptides for MHCI and exogenous peptides for MHCII. However, the presented peptides derive from proteolysis by the proteasome [64] and is occurring in healthy or infected cells. Importantly, this process is does not discriminate between proteins of different origins; it simply degrades those which have been targeted for degradation.

Therefore, if a virus begins hijacking the cell, pieces of the proteins it expresses which are not expressed by a healthy cell will become expressed alongside those of the natural protein fragments. The result is pMHC are both antigenic and self. However, due to the dominance of self-proteins in the cell, self-peptides dominate the expression [12, 65]. This is a critical point. TCRs must be able to differentiate small differences in the peptide sequence to determine if a cell is infected while maintaining tolerance (not triggering) to a cell expressing only self-peptides. The result of faulty recognition can have dire consequences on the body in the form of autoimmune diseases. This discrimination is a crucial factor under significant investigation. However, to date, the discriminatory capabilities of TCR antigen recognition have not been reconciled with the high sensitivity of antigen detection [51]. Previous efforts to do so will be summarized in Section 2.3.

2.3 Models of TCR antigen recognition and self-peptide discrimination

Mathematical models and simulation-based analysis have been used to elucidate many different mechanisms in receptor activation [8]. Beginning soon after the discovery of the TCR, its mechanism has been under investigation through computational simulations and mathematical modelling. This will be discussed in this section.

2.3.1 Receptor occupancy model

One of the earliest models of TCR signalling, named receptor occupancy or affinity-based model, assumes that the response of the T cell is governed by the fraction of TCRs bound to pMHC. This model gained popularity in many circles because of the TCR's similarity to many other receptors and basic tenants of pharmacology with its origins the early 20th century [66]. Because antigenic MHCs have higher affinity, it is believed that they alter the balance, inducing more TCRs to bind and shift the signalling across the threshold towards activation. Despite the concept being very popular in explaining the T cell response [67-69], it only seems to hold true to thymocytes [70, 71]. The existence of significant contradictory evidence suggests affinity may play a role, but it is not the only factor [45, 51, 72]. Therefore, in the human body, it is likely that some amount of tonic signalling is induced by receptor occupancy due to its tuning at the thymic selection level, but the knowledge that a single antigenic MHC binding event induces responses [47, 48] brings to question this mechanism playing a significant role in pathogen clearance.

2.3.2 Kinetic segregation

The concept of kinetic segregation originated as an alternative model based on the observation that receptor-ligand interaction of similar sizes segregated into small microdomains upon T cell activation during immunological synapse formation [73]. It is known that the membrane-bound phosphatase CD45, which lacks any known ligand, regulates the kinase activity of Lck [61, 74]. Due to its large ectodomain (~45nm) and the relatively small intermembrane distance of the TCR:MHC complex (~15nm), passive minimization of membrane bending energy leads to segregation of CD45 from TCR:MHC complexes over time [75, 76]. This isolation promotes kinase restricted zones where high kinase activity phosphorylates CD3 intracellular tails, resulting in T cell signalling. As

evidence for this mechanism, deletion or shrinking of extracellular CD45 domains has been shown to reduce TCR-CD45 isolation and eliminate T cell activation [76]. Due to the low number of antigenic pMHC on the surface of cells, it is unlikely to be the primary factor in initial TCR triggering. Kinetic segregation likely plays a role in immunological synapse formation and propagation of TCR signalling, adding a signalling amplification layer leading to full T cell activation, but does not provide the means for the initial triggering events.

2.3.3 Kinetic proofreading and extensions

TCR recognition of antigenic peptides exhibits qualities of high specificity and sensitivity. As TCRs scan the surface of an APC, they will experience lots of noise in the form of self-pMHC, but will only respond after encountering antigen; this is termed sensitivity, as the TCR must be extremely sensitive to the presence of antigen to respond above the noise [21, 47, 77]. Additionally, a single amino acid point mutation in the peptide fragment can also completely change the response – that is, the TCR responds specifically for a certain pMHC and will not trigger when it does not engage antigen peptide [78].

Although kinetic segregation and receptor occupancy models may be instrumental in propagating TCR signalling, the initial triggering mechanism, i.e. the first triggering event leading to activation, is still under debate. The first attempt at modelling this mechanism was the kinetic proofreading mechanism adapted by McKeithan [79] from DNA replication models. He suggested that upon binding, modifications began occurring to the TCR at a specific rate. Once a significant number of modifications had been made, the TCR was considered fully active. If the TCR:pMHC complex dissociates before full

activation, the TCR reverts to an unmodified resting state. In this simple model, specificity is increased with higher modification number, but at the cost of sensitivity due to the stochastic nature of receptor-ligand dissociation.

As a consequence of this model, the primary kinetic factor in TCR signaling would be the rate of dissociation. The model suggests that a low off rate interaction should be able to produce a signal, whereas a high off rate ligand should not. However, this has been found incomplete, as 2D kinetic measurements of the off rates of ligands of differential potency have shown little variation [80, 81]. The model has been modified to include rebinding to include the influence of on rate [82], feedback loops including downstream signaling molecules [83-85], effector responses [86], and conformational modifications [87]. Each adds to the complexity of the model, but provides a new framework for antigen sensitivity and specificity. Likely, the truth lies in some form of kinetic proofreading, but not at the simplistic level presented by McKeithan. Because of the strength of this model, an extension of the kinetic proofreading model will be utilized in future chapters.

2.3.4 Role of force in antigen recognition

Mechanical forces have been known to be act on receptors to induce responses, a concept broadly termed as mechanotransduction. The concept of mechanical force in TCR triggering was first proposed as a mechanism to resolve the complex sensitivity/specificity interplay by Ma and colleagues in 2008 [88]. Experimental and structural evidence has shown that mechanical pulling and/or torques on the TCR can induce signalling [89-93]. Additionally, agonist TCR:pMHC bonds have been shown to have increased lifetime with force, a counterintuitive phenomenon called a catch bond [94], which could increase the

bond duration for kinetic proofreading [92]. In fact, signalling could not be provoked in the absence of force applied to the bonds and was specific to the pMHC interaction [92, 93]. It is believed that force on the TCR:pMHC translates through the CD3 ectodomains for intracellular ITAM dissociation from the membrane, resulting in phosphorylation and TCR activation [95]. The origins of mechanical stimulation *in vivo* may be the result of cytoskeletal rearrangement [96] or membrane fluctuations [97]. Although mechanotransduction may be a significant player in TCR triggering and cell activation, the field is still in its infancy; not much is understood about the specifics of this process.

2.3.5 Models for the role for coreceptors in antigen discrimination

The coreceptors CD4 and CD8 are both able to bind MHC independent of TCR binding, albeit very weakly [98, 99]. Each coreceptor can be bound intracellularly to Lck [100, 101]. It is believed that the coreceptors act to either stabilize TCR:MHC complexes [99, 102, 103], trap MHC close to membranes [104], or provide a mechanism for Lck delivery and propagate signalling [105, 106]. There are several caveats to these models. Coreceptor binding is not necessarily required for T cell activation [107] and can be dominated by strong agonist pMHCs [108]. Additionally, TCRs are activated in cytosolic Lck, not the Lck bound to coreceptor [109]. However, it is clear that both coreceptors bind to the TCR:pMHC complex and are required for *in vivo* activation.

Although there are a significant number of TCR binding/signalling simulation analyses, few involve coreceptors. Due to the presence of intracellular Lck which can bind CD3 ITAMs, coreceptors have the ability to form a pseudo-dimer of dimers (PDD) where there are three reversible bonds (TCR:MHC, CD8:MHC, Lck:CD3) playing a role to

stabilize the complex through close proximity. Chakraborty and colleagues suggested through modelling that this effect was minimal, but its lacks supporting experimental evidence [110]. Other recent models have suggested that the role of coreceptors relies solely on its ability to deliver Lck [111, 112]; similar to kinetic proofreading, the TCR:pMHC interaction discriminates by lasting long enough to "scan" coreceptors for the presence of Lck. Once one is found, the T cell activates. However, this model suffers from the same sensitivity/specificity exchange as kinetic proofreading models due to its heavy reliance on TCR:pMHC bond lifetime. At this time, the true role of CD8 in TCR antigen recognition is incompletely understood.

2.4 Motivation and significance of research

As summarized previously, the importance of the TCR in the human body cannot be understated. T cells play a substantial role in the adaptive immune system, and their TCR is the primary molecule in unleashing the T cell response. The motivation for this study is simple. There are many models of TCR triggering the initial cellular response, but none can adequately explain the high sensitivity and specificity of antigen recognition at the single pMHC level. Comprehensive understanding of this process is critical to initiating new waves of safer and better-informed immunotherapies. We believe that some critical information encoded in the TCR triggering process was previously not accessible by traditional assays. By using novel biophysical readouts of sensitive binding assays as a reflection of the underlying biological process, this study uncovers mechanisms surrounding the unique specificity and sensitivity in TCR antigen recognition through combined experimental and simulation-based analyses.

CHAPTER 3. EXPERIMENTAL MATERIALS AND METHODS

3.1 Cells and proteins

The TCR-deficient J.RT3-T3.5 Jurkat cell line transfected with 1E6 TCR (1E6-J) and the associated biotinylated pMHC were gifts from Dr. David Cole. 1E6-J cells were expanded a media of RPMI 1640 with L-glutamine supplemented with 10% fetal bovine serium and 1unit/mL penicillin/streptomycin (R10) in 37°C, 5% CO_2, then stored in R10 containing 10% dimethyl sulfoxide (DMSO) at -80°C or liquid nitrogen for future use. Cells were thawed and rested in R10 for a minimum of 24 hours before use. Cultures were maintained in 37°C, 5% CO_2, for up to two weeks. Media was changed every 48-72 hours to maintain 0.2-1 million cells/mL. Cells were taken as needed for experiments. Biotinylated pMHC was allocated into 20μg/mL vials, 10μL, in phosphate buffer saline (PBS) with 1% BSA and stored at -80°C and diluted with the same solution for coating purposes.

3.2 Bead preparation

Streptavidin-coated beads (SA beads) were prepared similarly to biomembrane force probe beads in [80]. 8.1 μm borosilicate glass beads were first covalently coupled with mercapto-propyltrimethoxy silane which was then covalently linked to tetravalent streptavidin-maleimide in PBS by overnight incubation at room temperature. Once prepared, SA beads were stored at 4°C in HEPES buffer with 1% BSA and taken as needed. SA beads were then incubated with biotinylated pMHCs for 1h at room temperature and then resuspended in HEPES buffer with 1% BSA.

3.3 Site density measurement

Site densities for TCR and pMHC were measured using flow cytometry and PE conjugated antibodies for the specific molecules [80]. pMHC: BB7.2, BD Pharmingen Cat#558570; TCR: IP26, Biolegend, Cat#306708. Cells and beads were incubated with antibodies at 10μg/ml in 50μl PBS without calcium and magnesium, 1% BSA, 25mM HEPES buffer at 4°C for 30min; The fluorescent intensity was measured by the BD LSR II flow cytometer and calibrated by the BD QuantiBRITE PE standard beads (BD Biosciences). To determine site densities, the total amount of surface protein was divided by the surface area of the cell or bead.

3.4 Microcantilever preparation and calibration

Microcantilever wafers were purchased from Bruker (OBL-10). Microcantilevers were cleaned in piranha solution (3:1 high concentration sulfuric acid to 30% hydrogen peroxide) for 30 minutes, rinsed in deionized (DI) water, placed in an ethanol bath for 5 minutes, and finally rinsed again in DI water. Cantilevers were functionalized in a 400μg/mL biotinylated BSA (Sigma Aldrich A8549) in PBS overnight in 37°C. After incubation, cantilevers were washed and placed in filtered PBS and stored for future use at 4°C for up to one week.

To calibrate the microcantilevers, an SA glass bead was picked up by the micropipette of the HAFM and aligned with the tip of the microcantilever. Piezo actuation of the micropipette moved the bead with constant velocity while the signal from the photodiode was recorded. The slope of the resulting distance (measured by the capacitive feedback sensor on the piezo) vs. signal curve was measured to calibrate photodiode

sensitivity to distance. Cantilever stiffness was then measured by the thermal fluctuation method [113].

3.5 Statistical analyses

Statistics were performed as noted in either MathWorks Matlab (R2015b), Python (Spyder 3.2.4) Microsoft Excel, or GraphPad Prism. Statistical analyses for calibration of simulation parameters was performed in R statistical packages. The process is currently under review [114].

Linear regression was performed in Matlab (R2015b) using first and second order covariates of the contact and waiting times and their effects with previous adhesion score. Those whose coefficients were not significantly non-zero were eliminated one at a time in order of least significant until all covariant coefficients were significantly non-zero.

3.6 Dynamic micropipette assay using HAFM

The procedure is outlined in Section 4.3.2. Briefly, a bead coated in the ligand is adhered to the microcantilever along the center axis through superfluous SA-biotin interactions. A cell is then aspirated by the micropipette and brought into contact with the bead. The indentation force was controlled between 20-30pN assuming a cantilever stiffness of 4pN/nm. The cell was then held in contact for a period of time between the uniform interval 0.25-5s. The cell was then retracted by piezo control. A bond was identified by a fast dissociation step by the photodiode signal. The cell was then permitted to rest for another period on the interval 0.25-5s, which was adjusted for retraction and

approach times accordingly. The experiments were limited to 300 contacts. Cells which tethered extensively or did not reach 150 contacts were removed from analysis.

3.7 Lck inhibition treatment

The lyophilized powder for small molecule inhibitor of Lck, CAS 213743-31-8, was purchased from Sigma-Aldrich (428205-M), dissolved in DMSO, and stored in aliquots for future use at 4°C. 500,000 cells/mL were treated in 4 or 20μM of the inhibitor or vehicle control in L15 media supplemented with 1% BSA and HEPES buffer for 30 minutes at room temperature, then placed in the HAFM chamber. Experiments were performed in the continuous presence of the inhibitor or vehicle control for no more than 2h.

3.8 Cholesterol oxidase treatment

Cholesterol oxidase lyophilized powder was purchased from Sigma-Aldrich, dissolved in PBS, and stored in aliquots for future use at -20°C. 500,000 cells/mL were treated in 1U/mL of the inhibitor or vehicle control in L15 media supplemented with 1% BSA and HEPES buffer for 1h at 37°C, then placed in the HAFM chamber. Experiments were performed in the continuous presence of cholesterol oxidase for no more than 2h.

3.9 Cholesterol sulfate treatment

Sodium cholesteryl sulfate was purchased from Sigma-Aldrich (C9523-25MG), dissolved in DMSO, and stored in aliquots for future use at -20°C. 500,000 cells/mL were treated in the noted concentrations of cholesterol sulfate or control in L15 media supplemented with 1% lipid-free BSA and HEPES for 1h at 37°C, then placed in the

HAFM chamber. Experiments were performed in the continuous presence of cholesterol oxidase for no more than 2h.

CHAPTER 4. DEVELOPMENT AND VALIDATION OF A HORIZONTAL ATOMIC FORCE MICROSCOPE

4.1 Background

Atomic Force Microscopy (AFM), a form of scanning probe microscopy, is a renowned instrumentation concept used to measure extremely small displacements (<1nm resolution) or forces (~1pN resolution). The most rudimentary AFM is composed of a microcantilever/laser/photodiode system. The laser is focused on the back of a microcantilever and reflected back to a photodiode. When the cantilever is deflected, the laser reflection will shift on the photodiode and an intensity change is measured (Figure 2). Within a small range of displacement, the intensity change on the photodiode is linearly proportional to the displacement. If desired, this displacement can be converted to force by calibration of the cantilever stiffness.

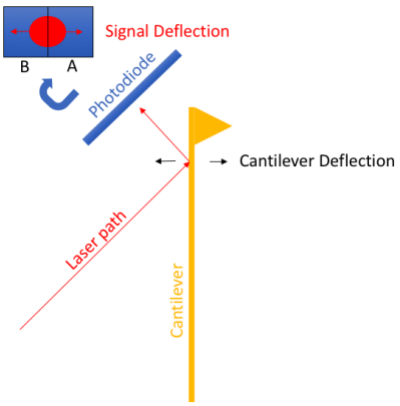

Figure 2. Principle components of atomic force microscopy
A laser is focused onto the back of a microcantilever. The reflection is measured on a photodiode of two sides (although four is also common for detection of torsion components). Movement of the cantilever in either direction will correspondingly move the laser reflection. This displacement can be calibrated to the signal. Signals can be measured at extremely high rates, limited only by computational resources.

AFMs have two general functions although others have been proposed. Primarily, commercial AFMs are used as imaging tools to measure a range of surface topographies, from biological to mechanical materials. The result is a 3D surface mapping of the material. However, they can be adapted to function as molecular force probes, which are important to the study of mechanical responses of receptor-ligand interactions. In these assays, a piezo-electric motor brings a functionalized AFM tip into and out of contact with the sample. With such a device, the dynamics of specific receptor-ligand interactions can be examined under mechanical force.

There are several methods of measuring similar kinetic properties of receptor-ligands interactions at the single molecule level. In essence, the method which can be used relies on the origins of the receptor-ligand pair, summarized in Table 1, although it must be noted that this list is not entirely comprehensive. In an ordinary AFM system, both molecules need to be purified and usually functionalized to the microcantilever through specific interactions; neither the receptor nor ligand can reside in the cellular context. Cell-purified molecule dynamics (where one molecule is in the cellular context, the other is purified) cannot easily be performed on the AFM. If a cell is adherent and can reach high confluence on the plate, it is possible to perform on AFM. Lastly, zero-force assays (thermal fluctuation) or measuring the interaction of two cells is nearly impossible.

Table 1. Comparison of single molecule measurement techniques and their assays

Instrument	Purified molecule force dynamics	Native cell-purified molecule force dynamics	Thermal fluctuation	Cell-cell force dynamics
Atomic Force Microscopy	X	some		
Biomembrane Force Probe	X	X	X	
Horizontal Atomic Force Microscopy	X	X		X
Optical Tweezers	X	X	X	
Magnetic Tweezers	X	X		

Adaptations of the AFM concept have made some of these assays more accessible. The addition of an objective and camera on the top of an AFM has provided the means of mounting cells or purified molecules onto cantilevers while being able to control their contact onto plated cells [115-118]. Other adaptations of added another camera/objective on the side to perform microscopy of the cells during and after contact [119, 120]. Recently, Ounkomol and colleagues have developed a new form of Horizontal Atomic Force Microscopy (HAFM) in which they mount the AFM under a microscope and replace the sample plane with micropipette aspiration control [121, 122]. Although Ounkomol's measurements primarily focused on mechanical force interactions, this setup had significant potential in many different assays outside the typical AFM scope (Table 1, Figure 3). We realized this system had the capacity to perform and automate the tedious micropipette assay [123]. Due to the nature of an automated system, the HAFM also has the potential to mediate long-term kinetic probing assays on cells to elucidate mechanisms involved in regulation of kinetics due to signaling. With these assays in mind, we decided to develop a HAFM and validate its utility.

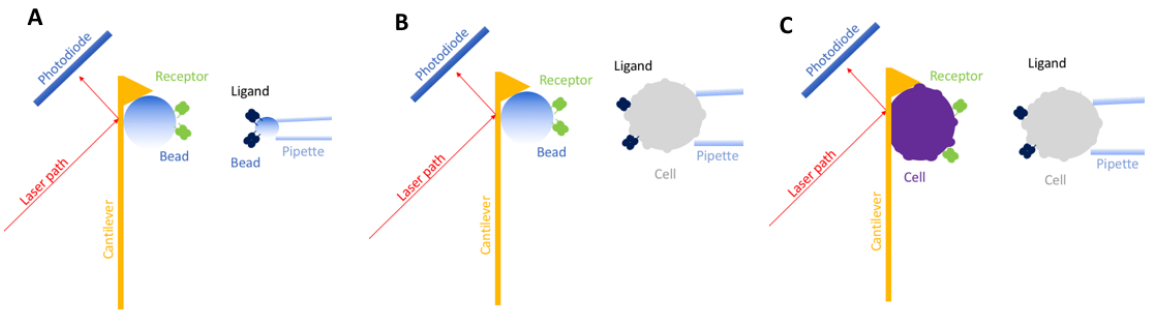

Figure 3. Diagram of different HAFM molecular origins
The HAFM can be used to perform force/displacement assays in the context of (A) purified molecule-purified molecule interactions, (B) purified molecule-cell interactions, (C) or cell-cell interactions.

4.2 Development of instrumentation

There are two different components to instrument design – hardware and software. Both were designed in tandem to operate the many different assays of the HAFM.

4.2.1 Hardware design

As mentioned earlier, a HAFM consists of several key components, but the physical system requires additional manipulation, control, and noise isolation components. Of the components, many were purchased from reliable suppliers (Table 2) with the exception the custom-designed hardware, consisting of the micropipette, photodiode board, and many machined components.

Table 2. HAFM primary components

Quantity	Manufacturer	Item Description	Item #
1	TMC	Tabletop Vibration Isolator	64-314
1	Dell	Computer/Monitor	Optiplex
1	NI	PCI card for A/D conversion	PCIe-6321
1	NI	Input/Output BNC connector block	BNC-2110

1	Newport	Micromanipulator	461-XYZ-M
3	Newport	Micro actuators	DM-13B
3	Warner	MP holder	64-1261
1	OZ Optics	Laser source attenuator	BB-500-11-670-4/125-S-40-3S3S-3-0.5
1	OZ Optics	Laser source	FOSS-21-3S-4/125-670-S-0.9
1	OZ Optics	Laser lens	LPF-04-670-4/125-S-1.9-50-18AS-40-3S-3-1
2	ThorLabs	Side camera	DCC1645C
1	Computar	Side camera lens	MLH-10X
1	Warner	micropipette holder	64-0218, Model #MHH-25
1	Analog Devices	Photodiode	AD8251
3	Newport	Micromanipulator	MS-500-XYZ
1	Edmund Optics	Laser Filter	#65-657
2	Unknown (Chinese	XY 30X30mm linear stage	LY30-L
1	Edmund Optics	5mm, Rhomboid Prism, VIS 0 Coated	#47-806
1	PI	Linear piezo electric motor with capacitive feedback	P-753.12C
1	PI	Piezo electric controller	E-509.C1, E-505.00
1	Nikon	Microscope	Diaphot
1	Olympus	LWD Objective	ULWD CDPlan 40PL 0.50 160/0-2

The photodiode board was built in-house. The photodiode itself was purchased from Analog Devices (AD8251) and was selected for its excellent performance in drift, power, noise, and response time. The circuitry of the board itself was designed by Dr. Fang Kong with assistance from the electrical shop at Georgia Institute of Technology (Figure 4). The board itself consists of several components to amplify the signal with adjustable gains.

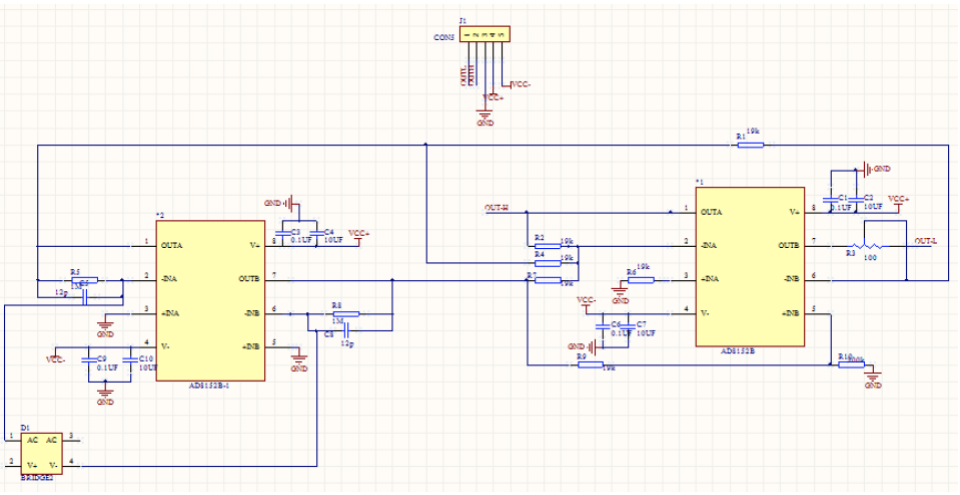

Figure 4. Photodiode board circuitry
Designed by Dr. Fang Kong

A major hindrance to the design of a HAFM is space – a significant number of components must be confined under a microscope. A Solidworks representation of the device was outlined to assist with spatial restrictions and develop machined brackets and the chamber (Figure 5A). The chamber development required several iterations. The laser path penetrates through a Plexiglas piece, referred to as the cantilever mount, which is designed with a slight incline (7.5°) to avoid overlapping laser interference from the two reflective surfaces (air-Plexiglas transition, back of cantilever). For ease of microcantilever placement, a clamp was built-in to hold the microcantilever in place against the cantilever mount and slots were used to slide pieces together. Fasteners for coverslips are made of non-conductive materials for the isolation of metal clamps to heat-conducting glass (used for temperature control) which requires electrical current. A picture of a portion of the completed instrumentation can be seen in Figure 5B.

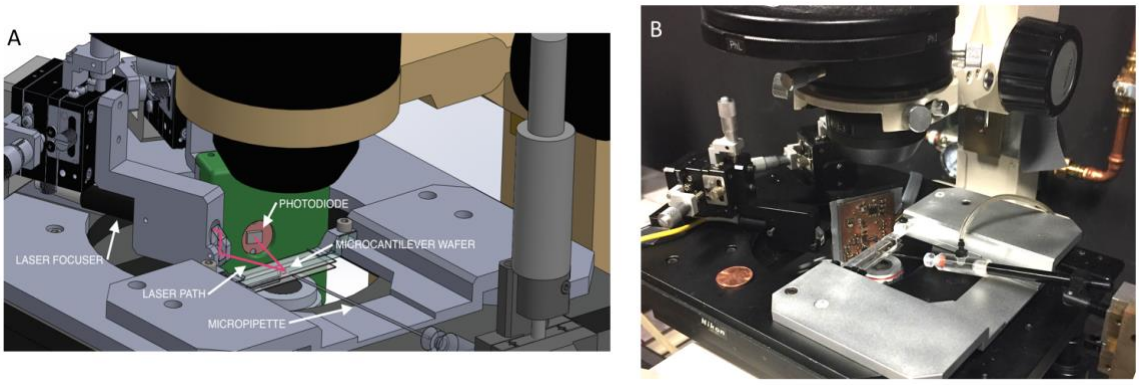

Figure 5. HAFM hardware development requires maximal use of space
(A) Solidworks representation of planned HAFM hardware under microscope. White arrows point to specific components. (B) Picture of completed hardware under microscope. Penny for scale.

4.2.2 Software libraries

Control of the HAFM was developed in Labview with used of State Diagram packages, and analysis was developed in either Matlab or Labview. Programs were written for calibration of photodiode sensitivity, spring constant calibration, micropipette assay, rupture force assay, force clamp assay, and data analysis. More about the outlines of the algorithms will be discussed in the validation section or in Experimental materials and methods.

4.3 Validation of instrumentation

4.3.1 Hallmarks of AFM

HAFM should have the same functional hallmarks as the standard AFM. First, displacement of the microcantilever tip should be linearly proportional to the signal change on the photodiode. Secondly, the power spectrum of thermal noise of a cantilever should have a resonance peak, fitting to the description of it as a simple harmonic oscillator [113].

To test the linear displacement, a stiff polystyrene glass bead was brought into contact with the microcantilever tip using piezo control. Capacitive feedback from the piezo motor simultaneously monitors displacement. Plotting the photodiode voltage against the displacement from the feedback sensor gives a reliable linear response, which is repeatable and consistent at different time intervals (Figure 6A). Examination of the thermal fluctuation power spectrum also gave the characteristic resonant peak (Figure 6B).

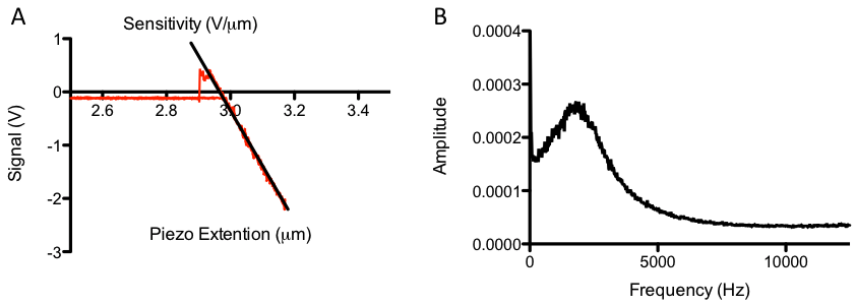

Figure 6. AFM signal hallmarks
(A) Linear voltage vs. displacement response from contacting a glass bead driven by piezo actuation. Red curve is actual signal. Black line represents linear slope for sensitivity calibration. (B) Power spectral density curve of free signal, averaged analysis of 200 runs from 4096 samples at 80000 Hz, showing standard resonance peak for a soft cantilever, used for calculation of spring constant once sensitivity is calibrated.

4.3.2 Micropipette assay

The micropipette assay was developed as a method to determine kinetics of two membrane-bound proteins [123]. In the traditional form of micropipette, a Red Blood Cell (RBC) is coated in the ligand of interest and brought into contact with its receptor for a controlled duration by piezo control. The cells are then separated through retraction of the pipette. If there is a bond at the end of contact, a small deflection is seen at the RBC interface; if there is no bond, a deflection of the RBC is not seen. Repeating this cycle for

many touches across different contact times results in sequences which can be converted into adhesion frequencies, or probabilities of adhesion (P_a), which are reflective of the kinetic characteristics of the receptor-ligand interaction.

There are several limitations to the traditional micropipette assay. First, there exists human error in bond identification. In some receptor-ligand interactions, the bonds are very strong and deflections are easily discerned. However, this is not the case in many interactions which are measured where bonds may be weaker, and there is the possibility of misidentification of events. This can exceptionally difficult when there is more than one bond state and requires significant training and experience.

Secondly, the P_a depends considerably on contact area (amount of area in which the molecules can interact). Because of pipette drift, corrections are required by the user to maintain constant contact area. Additionally, this contact area can vary from user to user depending on preferences, so results are sometimes difficult to compare amongst different users. This can also be rectified by experience and training. However, it is still a source of uncontrollable error in the micropipette assay.

Lastly, it is nearly impossible to maintain a tightly controlled sequence of events. Due to pipette drift and the difficulty of general distractions during the several hours required for the assay, events are not always measured in succession – pauses may be made and events may be missed. This is perfectly acceptable if the sequence of events is Bernoulli which is the case for many receptor-ligand interactions; however, as we will see in CHAPTER 5, sometimes the sequence is Markovian. Additionally, if the user requires

dynamic inputs to the program, these missed events become critical. Analysis of the sequence is therefore disturbed by assay constraints on the user.

The HAFM has the capacity to rectify these problem areas through use of signal recorded bond detection, controlled impact of cell contact, and robustness of the assay performed on the HAFM, respectively. To automate this process, beads coated in the ligand of interest can be adhered to the microcantilever through specific interactions. Several can be loaded for fast transition (see Figure 7 microscope view, up to three beads can be placed simultaneously without signal aberration). The target cell is aspirated by the HAFM micropipette system. Upon initialization of the program, the cell is driven into contact with the ligand-coated bead to a user-inputted signal deflection, i.e. force, through piezo motor control. The surfaces are permitted to interact for a randomly selected contact period defined between a specific interval, then separated to a distance for another randomly selected waiting period between a specifically defined interval. This cycle can be repeated for hundreds of contacts or until an error in the system occurs. Simultaneously, the photodiode signal is recorded at a defined rate, allowing each contact cycle to be analysed at a later point.

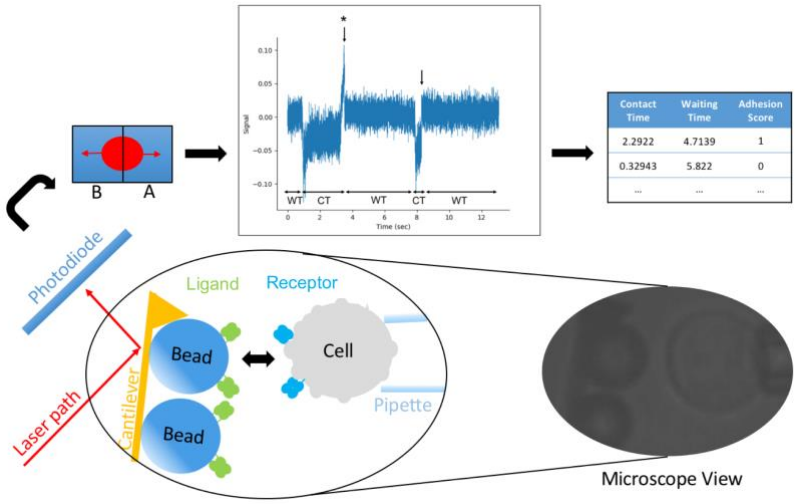

Figure 7. HAFM micropipette assay outline
Beads coated in the ligand of interest are adhered to the microcantilever through specific interactions. A typical microscope view is provided with a cartoon for clarity. The cell and its receptor can be brought into contact with the beads for controlled, automated contact periods. Two example events are shown. Bond events (arrow with *) can be discerned from no-bond (arrow, no *) events through cantilever signal deflection. Contact times (CT) and waiting times (WT) can be randomly selected. The events can be compiled and analyzed in a similar fashion to traditional micropipette data.

This method of micropipette serves to negate the previously described errors associated with traditional micropipette assays. The detection of an event outcome (bond or no bond) is straightforward (Figure 7), even for weak interactions due to the sensitivity of AFM measurements. Unless severe misalignment occurs, the impact force controls a constant contact area over the course of an experiment assuming constant viscoelastic properties of the cell. Lastly, the sequence of events is retained due to automated control of the system and lack of user intervention (Figure 8).

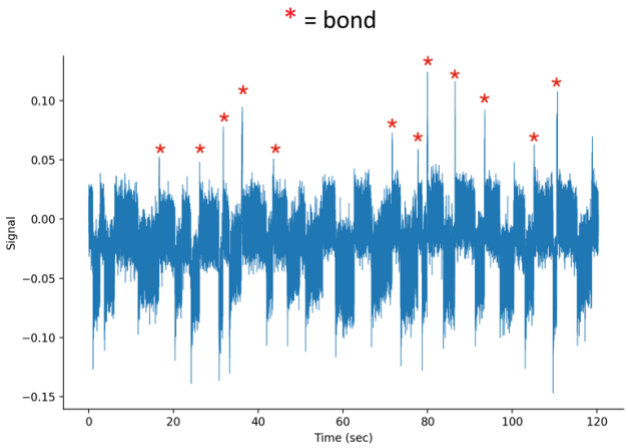

Figure 8. HAFM micropipette data stability
Unfiltered raw data from HAFM. Successive contacts are shown across ~2 minutes. Bonds are marked by red asterisks.

4.3.3 Force clamp and rupture force assays

The force clamp and rupture force assays have been shown to be a powerful tool in understanding the response of cell surface receptors to mechanical stimulation. In the force clamp assay, a single receptor-ligand bond is pulled to a specific force level and permitted to exist until it dissociates. Because these lifetimes are highly stochastic, lifetimes over many different events are compiled for analysis. Rupture force assays are a simple extension of force clamp assays where the force level is set to infinity and the bond is simply pulled until rupture; the output is the force at which the bond dissociates. This is no longer a widely-used technique due to the necessity for pulling at several different force loading rates for significant analysis of the rupture dynamics and the effects of viscous drag forces at high loading rates.

As mentioned previously, there are several instruments which can perform mechanical force assays with purified molecules, but the HAFM has the added advantage

of being able to perform cell-cell force assays. Although many of these systems claim force clamp capabilities, the feedback systems required to clamp at constant force are limited to a distance clamp without closed feedback; the HAFM, due to its fast acquisition rates, is able to provide closed-loop force clamping capabilities to adjust for any disturbances in force level (signal aberrations, cell or molecule relaxation, molecular species changes, cytoskeletal rearrangement, etc.).

To demonstrate these capabilities, we used a Jurkat cell line transfected with 1E6 human TCR against several different pMHC ligands, similar to the setup seen in Figure 3B. A demonstration of the force clamp cycle is shown in Figure 9A where the cell is brought into contact with the bead, permitted to interact for a period of time to allow for bond formation, then retracted to a defined force level which is maintained until bond dissociation. For the duration of a long lifetime bond, the piezo must continuously adjust to maintain force level (Figure 9A, bottom panel). Three different ligands of different potency were tested for their kinetic response to mechanical stimulation through the force clamp assay (Figure 9B-D). Several hundred bond lifetimes across various forces were measured and binned into lifetime vs. force curves. Weak ligand ALW showed a slip-bond, whereas the strong ligands (YQF, RQF-I) had catch bonds. This concept is consistent with previous work [92, 95].

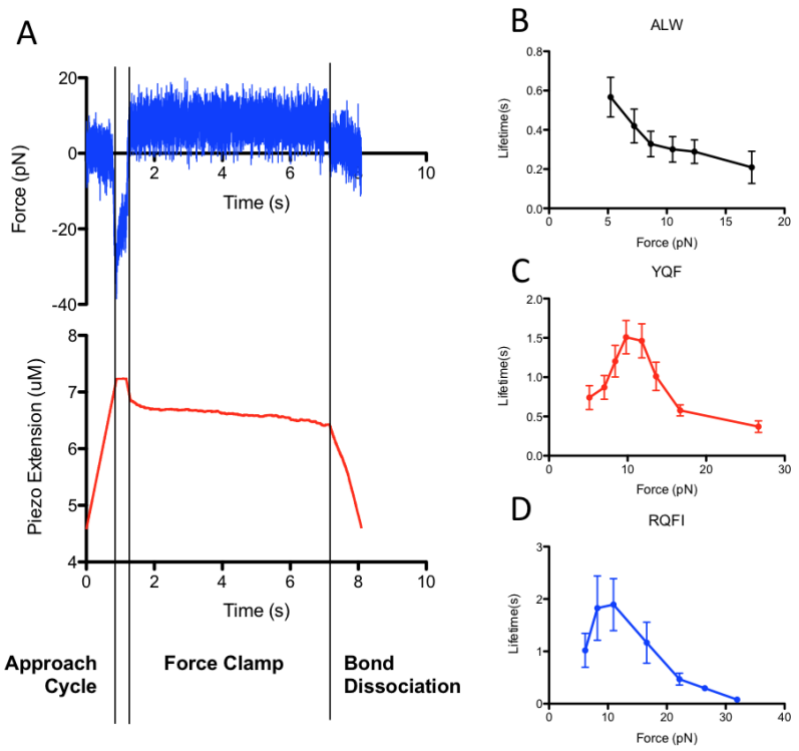

Figure 9. Demonstration of HAFM force clamp assay
(A) Example raw data from the HAFM showing approach, contact, clamp, and dissociation phases of a force clamp assay cycle. (B-D) Compiled data for force-lifetime curves from 1E6 TCR vs. three different ligands (ALW, YQF, RQF-I)

To demonstrate the HAFM modality of cell-cell force experiments, the interaction between CD222 and PD-L1 was tested. The CD222:PD-L1 interaction relies heavily on glycosylation, so it was thought best to examine its interaction kinetics in a native system. Therefore, we mounted a CHO cell transfected with CD222 onto the microcantilever and brought it into contact with a micropipette aspirated HEK cell transfected with CD222 ligand PD-L1; these two cells lines of different species were used to negate some of the background adhesion contributed by other molecules. To examine implications of the receptor-ligand interaction on overall cell-cell adhesion, we performed experiments with

and without the addition of a specific blocking antibody. The cells were brought into contact for either a short or long duration, then pulled until no bonds remained.

Two methods were used to quantify the strength of the intercellular adhesion – rupture energy and peak rupture force. The peak rupture force is the maximum force reached after separation. The rupture energy is how much energy the piezo required to pull the cells apart; this is calculated by integrating the force-extension profile over the entire separation period. An automated process was used to quantify both metrics, with similar results compared to an unbiased human analysis (Figure 10A). As expected, longer contact times permitted more bond formation and therefore stronger intercellular adhesion. However, despite the addition of a blocking antibody inhibiting the interaction, no difference was seen between the two conditions for either contact time or method of quantification (Figure 10B-D).

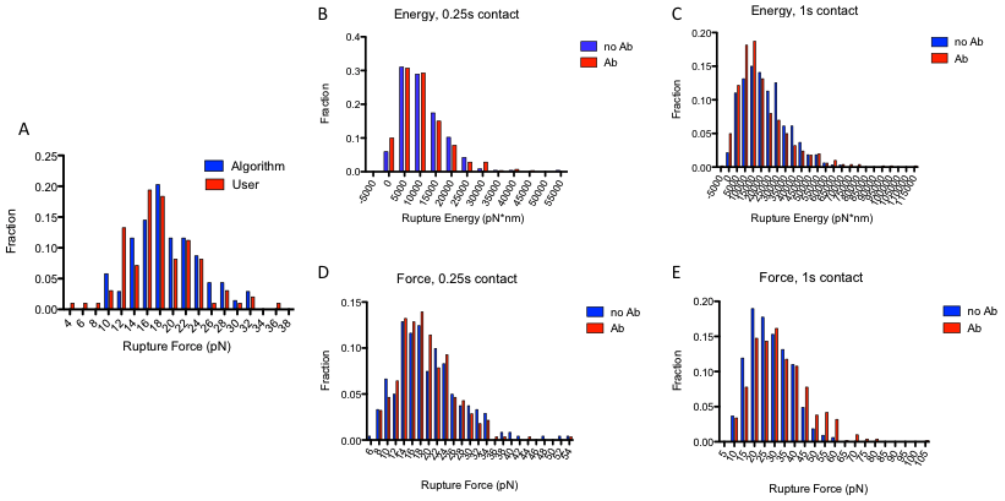

Figure 10. HAFM cell-cell force separation characteristics
HAFM was used to measure the mechanical separation of a CHO cell transfected with CD222 and a HEK cell transfected with ligand PD-L1. (A) Validation between algorithmic and user determination of rupture force. (B,C) Rupture energy required to break cells given 0.25s (B) and 1s (C) contact. (D,E) Maximum rupture force upon cell separation given 0.25s (D) and 1s (E) contact.

There are two possible explanations for the lack of significant differences in the presence of a blocking antibody. First, the PD-L1:CD222 interaction is not well characterized. It is possible that the antibody did not inhibit all interaction sites, although the antibody addition partially blocking tetramer staining. Secondly, we attempted to minimize background adhesion through use of cell lines of different origins, but some still remained. It is likely that the contribution of PD-L1:CD222 was minimal compared to background.

4.4 Discussion and future directions

In this chapter, the HAFM instrumentation was described and demonstrated in several different modalities. There are several components to the device which could be improved. First, although the imaging platform of the microscope is used, very little is utilized at this time. This is in part due to the lack of a filter to isolate only laser-specific passing wavelengths from the microscope light source. Currently, this is due to spatial considerations requiring a custom-designed photodiode board housing. Additionally, due to the size of the microcantilever wafer, the image plane must be approximately 2mm from the bottom of the coverslip. This requires a long working distance objective with low resolution. Decreasing unnecessary wafer thickness by milling could reduce the focal length, but may impact microcantilever function. Secondly, although there is significant manipulation in laser plane, attaching a third dimension of micromanipulation for better control over laser focus would be an improvement; currently it is consigned to slots designed into the housing. Lastly, although the software acquisition rate is ~1000Hz, it could be improved through an optimized parallel data acquisition/processing and refinement of algorithms.

There are several limitations to the HAFM that cannot be overcome through instrument development. First, signal noise is relatively high (Figure 9A) resulting in lower signal resolution. This makes forces below 5pN extremely difficult to maintain, and thermal fluctuation assays for zero force kinetic measurements very difficult. The Biomembrane Force Probe (BFP) or optical trap may be better suited for low force measurements. Additionally, as demonstrated in Section 4.3.3, it is difficult to perform intercellular adhesion to examine the impact of specific receptor-ligand interaction. Background adhesion is very high, and there are limitations to availability of specific blocking antibodies or molecular mutations. Therefore, if these assays are to be developed further, the correct target interaction should be investigated; this limits selection to interactions with a significant impact on intercellular adhesion and adequate reagent availability.

Despite the small improvements that can be made to the instrument, it is highly functional and can perform many different assays. The HAFM micropipette assay itself has many advantages in automation and accuracy over the traditional micropipette. This functionality will be extensively used in the CHAPTER 5 to measure long sequences of adhesions. Additionally, future experiments are suggested to fully develop and validate the model proposed in CHAPTER 6 which rely on the signal stability of the HAFM.

CHAPTER 5. TRANSIENT LIGAND MEMORY IN TCR ANTIGEN RECOGNITION

5.1 Background

It has long been known that T cells utilize their T Cell Receptor (TCR) to identify and promote a response to recognition of antigenic pMHC [9-11]. This process has an uncanny combination of both sensitivity and discrimination, as it is sensitive enough to induce a response to as little as a single antigenic pMHC interaction while still maintaining ample discrimination power from the several magnitudes greater number of self-peptides [51].

The strength of the T cell response has generally correlated very well to the intermolecular affinity of TCR to pMHC with 2D measurements being slightly more sensitive than their 3D counterparts [80]. Models have been envisioned to account for this unique set of abilities, conceptually modeled after kinetic proofreading which heavily relies on the interaction off-rate [79]. With the exception of a few conceptual models [124], binding of TCR to pMHC has been thought to occur with fixed kinetic rates or minimally affected over the course of APC contact. Recent research has shown that kinetic rates may been affected by cholesterol binding [58-60] or over longer periods of time near immunological synapse formation [87, 125], but little emphasis has been put on TCR:pMHC binding during the critical initial triggering phase. A better understanding of these early events will help to understand the complex signaling dynamics at later time points.

Previously, it has been shown that the TCR:pMHC interaction has significantly upregulated periods of adhesion throughout the adhesion frequency assay [126] as quantified by the memory index. This positive memory index is a Markovian process reflective of periods of increased sensitivity to antigen at the molecular level which may play a role in the antigen recognition process. In practice, this value is simply the increase in binding probability following a binding event. However, in a cellular context, this increase in binding probability can be reflective of many different processes, including signaling modifications or cytoskeletal rearrangement. This discovery was largely unnoticed by the TCR field due to the packaging of the paper as a phenomenon of general receptor-ligand interactions with little focus on the TCR itself.

Several methods were applied to determine the presence of ligand memory in TCR binding and its mechanistic origins. To see if the molecules themselves had conformational changes due to binding in the absence of its cellular environment that resulted in this behavior, we analyzed several sets of data from purified TCR:pMHC systems. Additionally, we verified that a positive memory index exists in many different TCR:pMHC systems, both mouse and human. Due to the inherent stochasticity in the adhesion frequency assay and subsequent high variation in the memory index, we also developed a randomized 2D micropipette adhesion frequency approach utilizing the HAFM to measure TCR:pMHC adhesion frequency over an extended period of time (~20-30minutes). This technique was utilized to examine the role of adhesion memory in TCR antigen recognition and the time scales at which it operates. Finally, simulation-based analysis of a mechanism explaining memory will be presented.

5.2 Memory index

As a concept, the memory index arose from the observation that many bonds occurred in series in some micropipette assay experiments, or what was seen as "clusters" of bonds during analysis. In analysis of micropipette experiments for determination of kinetics, each event in the sequence is assumed to be independent and identically distributed (i.i.d.), i.e. the sequence is Bernoulli. Clusters of bonds are not representative of a Bernoulli sequence. If these events are not i.i.d., it was thought that this may be representative of some behavior of the cellular environment or the molecules themselves. Two methods were developed to quantify this "clustering" and termed the memory index [126]. In either method, the exact value of the memory index is defined as the increase in the probability of adhesion if there was a bond in the previous contact versus the case where there was no bond in a previous contact.

The first method was termed the direct method. In this method, the events in an entire sequence of contacts are divided into 4 different cases: n_{00}, n_{01}, n_{10}, n_{11} with the subscripts representing a two sequential contacts with 0 for no bond, 1 for a bond. For example, n_{01} is the total number of events in the sequence where there was no bond followed by a bond; n_{10} is the total number of events where there is a bond followed by no bond, and so forth. The probability of adhesion after a bond would therefore be $p_{11} = n_{11}/(n_{11}+n_{10})$, and similarly, the probability of adhesion after no bond would be $p_{01} = n_{01}/(n_{01}+n_{00})$. The memory index can therefore be calculated as $p_{11}-p_{01}$. If the sequence is Bernoulli, the memory index should be zero.

The second method of memory index quantification is termed the cluster method. In this method, the size of the clusters was fit to a Markovian model. For instance, seven bonds in a row is a cluster of size seven. The total number of clusters of each size were

calculated for an entire sequence. The number of clusters of each size were then fit to the Markovian model.

The direct and cluster methods have been shown to have comparable results in measuring the memory index. More description of the cluster model calculation and comparison between the two can be found in [126]. However, the cluster method has lower resolution; many events are binned into a single point and fit to the model. The direct method is therefore used throughout the rest of the study for the sake of consistency.

5.3 Verification of TCR memory in cellular environment

To determine if this phenomenon results from the TCR in its native cellular environment, we analyzed data from several systems to verify its replicability and validate its presence. Previously, TCR memory had only been demonstrated in a transgenic mouse system (OT-1:OVA TCR:pMHC) [126]. Measurements made by Dr. Jun Huang on a panel of peptides of different potency for the OT-1 system confirmed TCR memory for the strong OVA peptide as well demonstrated memory in weaker peptides (Figure 11A). Additionally, measurements made by Dr. Jin-sung Hong of the 3L2 transgenic TCR mouse system (recognizing a hemoglobin (Hb) peptide fragment bound to MHCII) indicated that TCR memory occurs in class II MHC system (Figure 11B). Contrastingly, the mouse MHC class I and II systems showed different trends of memory index:ligand potency dependence – the 3L2 system showed no dependence on ligand potency, whereas the OT-1 system peaked at a mid-range potency ligand G4 and dropped to zero for very weak ligand R4. This is likely due to the difference in micropipette assay styles of different people (see

discussion in Section 4.3.2), but could also be an artifact of binning data of different contact and waiting times into a single measurement or high variance in the measurement.

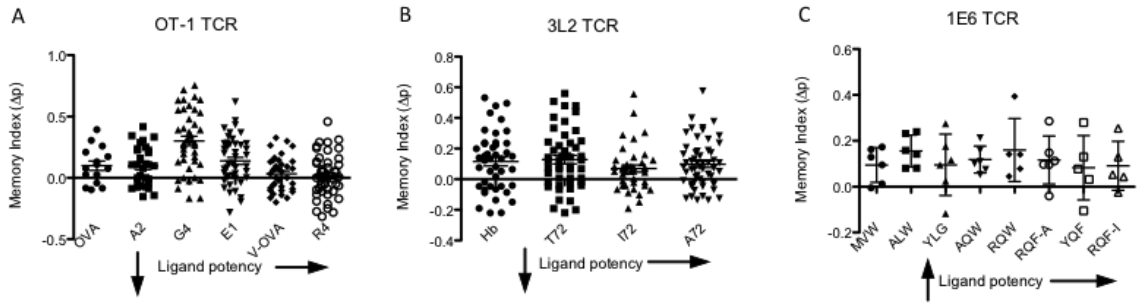

Figure 11. Memory index for several TCR:pMHC systems
(A) Memory index for recombinant OVA Altered Peptide Ligands (APLs) vs. naïve OT-1 T cells. (B) Memory index for recombinant Hb APLs vs. naïve 3L2 T cells, Data are compiled for contact times of 0.1-5seconds, 50 contacts, for A&B. Error bars represent standard error. (C) Memory index of panel of recombinant pMHC against clonally expanded human 1E6 T cells, 100 contacts, 4 seconds. Error bars represent standard deviation.

To limit variance in data collection and test a human system for TCR ligand memory, we performed the micropipette assay with more contacts to decrease memory variance on a clonally expanded 1E6 TCR system against a panel of APLs. The 1E6 TCR recognizes a pre-proinsulin-derived peptide (ALW) loaded onto HLA-A2 pMHC (class I); the cells were isolated from a patient with type I diabetes and a panel of peptides of different potency were gifted from Dr. David Cole [127]. Originally, the reagents were used to make TCR:pMHC affinity measurements. Proper assay development permitted recycling of the experimental data for memory analysis. The memory index had no trend with ligand potency (Figure 11C). The values were not statistically different when compared with a one way ANOVA test.

5.4 Analysis of purified TCR:pMHC systems

The first question to be answered is whether the positive memory index in TCR:pMHC binding is intrinsic to the molecules themselves. Because purification of the extracellular regions or recombinant production is difficult for the TCR, the analyzable systems were limited. Dr. Baoyu Liu provided data he had collected using purified OT-1 TCR vs. ovalbumin peptide fragment OVA. This system previously exhibited positive memory in its cellular context [126]. Memory index across several different contact times was binned to determine any significance, as only one data point can be extracted from a sequence of touches and the calculation itself has high variance. In future sections, it will be shown that the memory index has little dependence on contact time. In the purified system OT-1:OVA system, no memory is seen (Figure 12A). In another data set provided by Muaz Rushdi, E8 TCR recognizing peptide fragment TPI, the purified system did not express positive memory whether or not the streptavidin used for conjugation was divalent or tetravalent (Figure 12B). This implies that clustering of TCR does not influence this effect in the absence of the cellular environment. Neither result is significantly nonzero.

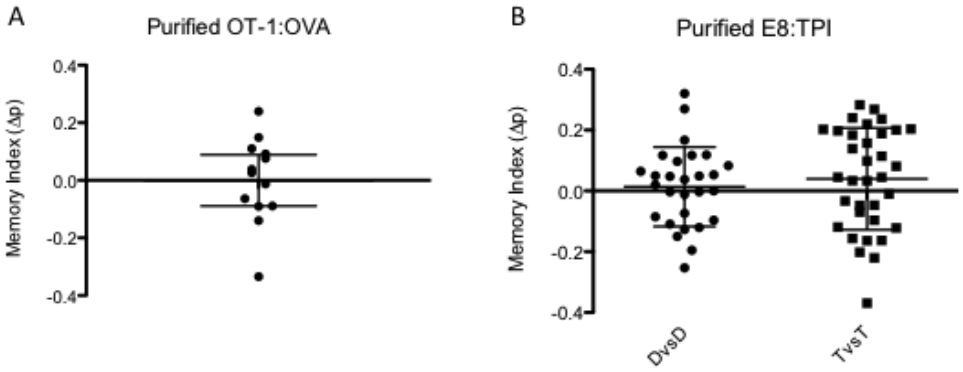

Figure 12. Purified TCR:pMHC memory index
Data are compiled for contact times of 1-10seconds for (A) Memory index for recombinant OVA MHC vs. recombinant OT-1. (B) Memory index for recombinant E8 TCR vs. TPI MHC, Divalent vs. Divalent (DvsD) and Tetravalent vs Tetravalent (TvsT) streptavidin. Error bars represent standard deviation.

5.5 Mechanism exploration by dynamic input micropipette assay

5.5.1 Dynamic input micropipette assay

As seen in Section 5.3, the micropipette assay will not suffice to accurately measure ligand memory or its dynamics for several reasons. First, micropipette methods are subject to high variability due to the inherent stochasticity of the assay and the low number of events. Second, additional variability in the assay introduced through user errors such as 1) misidentification of bonds, 2) time lapses in the process, or 3) user bias 4) pipette drift may lead to misidentified or neglected events which significantly impacts a time series measurement such as the memory index. Lastly, measurements are done with constant contact time over the course of a cell pair and constant time in between contacts. Because we began this study with the intent of studying the time-dependent memory effects, a new method needed to be developed to study it.

It has been shown that using random, unbiased, inputs to a system can better help to understand the inherent dynamics and cell signaling [128]. In this assay, we have two controlled variables: the contact time and time in between contacts, or waiting time; pMHC density can also be controlled, but due to the sensitivity of the memory index, it is best to keep the adhesion frequency around 0.25-0.75 which limits the density variation. Combining the aforementioned issues with variable system inputs makes the process impossible in a practical sense. To overcome these issues, the HAFM automated this process to improve bond identification and record the effects of variable inputs. Otherwise, this assay has the same output as the micropipette assay: a series of events, where 1 denotes a contact period, or event, ending in a bond and 0 denotes an event with no bond.

In the dynamic input micropipette assay, a cell with the receptor of interest (TCR) is brought into contact and allowed to interact with its ligand (pMHC) on the bead surface through piezo control for a randomized period of time (0.25-5s) to an approximate maintained force level. The cell is the separated for a different randomized period of time (0.25-5s). Throughout this process, deflection of the cantilever is translated into a signal through a focused, reflected laser and measured through the photodiode (Figure 7). If a bond exists at the end of the contact period, it can be detected through deflection of the cantilever. This process is repeated several hundred times for a cell and bead pair. This data is then output and analyzed as a series of binding events.

5.5.2 Effects of ligand potency on TCR ligand memory

To study the TCR ligand memory in the context of antigen recognition, we required a stable TCR system with flexibility. We received a TCR-deficient J.RT3-T3.5 Jurkat cell line with a human HLA-A2 restricted 1E6 TCR (1E6-J). This cell line expressed constant TCR expression over several weeks which was necessary to negate the possible impacts of variable receptor expression. Additionally, a panel of pMHCs with different potency were provided for the 1E6 system [127].

The dependence of TCR ligand memory on peptide potency was characterized using the 1E6-J system on a panel of six peptides of different potency. At high or low adhesion frequencies, artifacts may be induced into the calculation of the memory index due to lower sensitivity. Therefore, the average adhesion frequency of each ligand was maintained between 0.4-0.6 by varying the pMHC bead coating density (Figure 13A). However, there was still a significant amount of non-specific adhesion that was not

inherent to the TCR:pMHC interaction as showed by ~10% binding in non-coated bead (SA) or control peptide (CBL-A2). However, it was shown by Monte Carlo simulation that if the non-specific adhesion sequences are Bernoulli, the trends in memory index remain. However, the addition non-specific adhesion leads a sensitivity decrease. At 10% non-specific adhesion, this would lead to an approximately 20% decrease in the calculated memory index (Figure 13B).

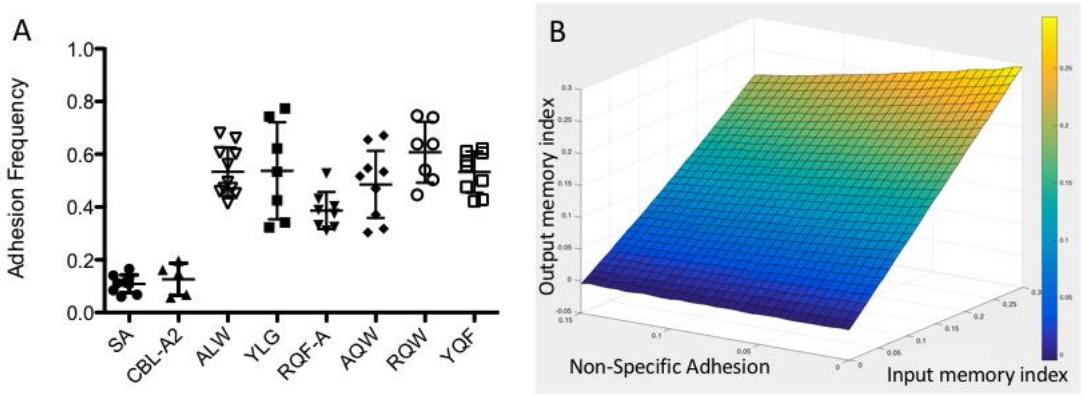

Figure 13. Confirmation of adhesion in different 1E6 TCR ligands
(A) Adhesion frequencies for different ligands tested vs 1E6-J cells. SA is uncoated beads. CBL-A2 is a control peptide. Adhesion frequencies were maintained to a mean of approximately 0.4-0.6 by control of pMHC coating density. (B) Monte Carlo simulations of micropipette adhesion sequences with inputs of the memory index and non-specific adhesion. Baseline adhesion frequency was maintained at 0.3. The output memory index was then calculated from this Monte Carlo sequence and averaged across 10,000 samples.

As the potency of the ligands increased, the TCR ligand memory decreased significantly in a non-linear fashion (Figure 14A). Even with 200-300 contacts for each measurement which should significantly limit data spread, the high variance of the assay is apparent (Figure 14B). There are several possible explanations for this variation. First, cell-to-cell and bead-to-bead variation are a source of error. Receptor and ligand densities

have an inherent level of variance that is extremely difficult to quantify for a single pair. Additionally, the randomized contact and waiting times produce additional variance in this parameter since not all events are based on the same conditions. However, the trend of ligand potency on memory index is apparent.

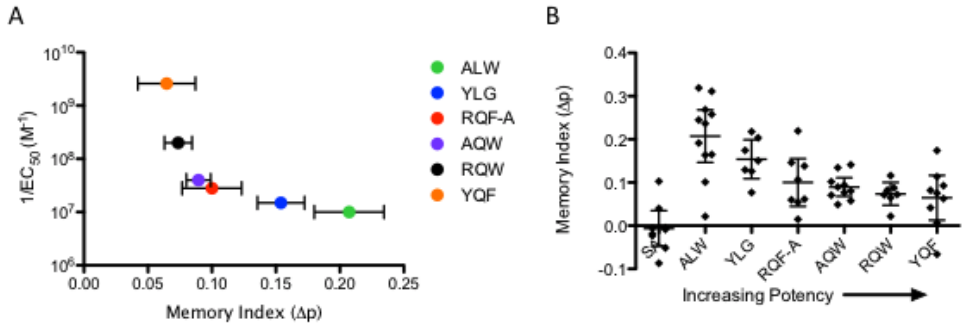

Figure 14. TCR ligand memory dependence on peptide potency
(A) Peptide potency, quantified as peptide concentration required to reach half maximal T cell killing, vs. memory index for 1E6-J cells against a panel of peptides. Error bars represent standard error for memory index calculation. (B) Individual data points from different peptides for same experiment with control of uncoated beads (n = 7-11)

Despite the memory index having an interesting trend with ligand potency, the memory measurement reflects *relative* sensitivity, or sensitivity increase relative to itself. Sensitivity changes in binding, as described in Figure 24, are quantified by the increase in binding relative to the amount of ligand present. Ligands of stronger potency (YQF, RQW) require ~200-400 fold higher coating concentrations to reach the appropriate amount of binding than weaker ligands (ALW, YLG). Therefore, true ligand sensitivity as quantified by the memory index *reverses* trend when normalized by the peptide coating density (Figure 15). Interestingly, ALW peptide, the naturally occurring derivative of insulin related to some forms of type I diabetes, does not fit the trend. Its value increases to

approximately that of 10x stronger peptide RQF-A. However, it should be noted that this normalized value is also not necessarily a better quantification of the change in sensitivity, as this quantity is reflective of a Markovian probability upregulation depending only on the previous bond. If ligand memory last longer than simply two events, which we will show is the case in future sections, this metric will be skewed. More investigation will be required to quantify absolute sensitivity changes.

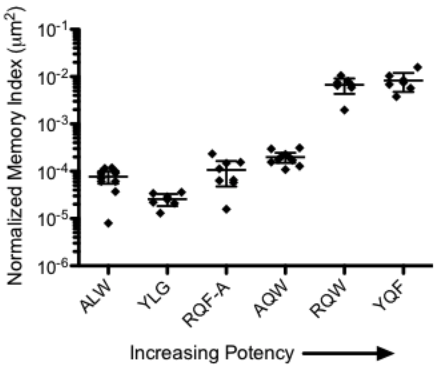

Figure 15. Normalized memory index dependence on ligand potency
Memory index normalized by the coating density of MHC required for adhesion frequency of 0.4-0.6. Error bars represent standard deviation. Arrow denotes direction of increasing potency.

5.5.3 Generalized linear regression model of TCR memory

We analyzed the previous data collected in Section 5.5.2 using a generalized linear regression approach to examine trends with contact and waiting times. It was believed that given enough waiting time, this effect would decay; additionally, given enough contact time for binding/signaling, this trend would increase. In this method, the probability of adhesion was determined using GLR both after a bond, $p_1(ct,wt)$, and after no bond, $p_0(ct,wt)$, using covariates of contact and waiting times controlled in the experiment. The memory index dependency was therefore $p_1(ct,wt)) - p_0(ct,wt))$. Unexpectantly, little to no

dependence was seen on either contact or waiting time for any ligand (Figure 16); some small changes were seen in weaker ligands, but this is most likely due to an artifact of the fitting process. Therefore, the memory index metric is indicative of extended periods of kinetic upregulation longer than the time intervals in this study.

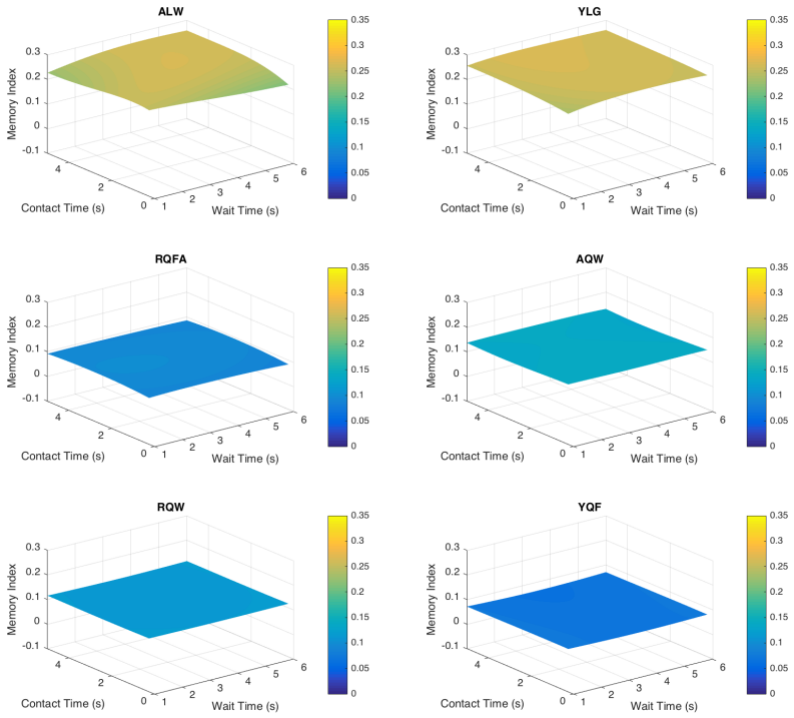

Figure 16. TCR ligand memory dependence on contact and waiting times
A generalized linear regression model was fit to contact times and waiting times in the experimental assay for all 6 ligands in Figure 14. Plots are ordered from weakest ligand top left to strongest ligand bottom right.

5.5.4 Lck assists in triggering long periods of adhesion

When considering a mechanism underlying TCR ligand memory, two aspects of these upregulated binding periods need to be considered. How long are these periods and how are they triggered? As discussed previously in Section 2.2.2, the CD3 subunits associated with TCR become phosphorylated by kinase Lck on the ITAMs upon TCR

activation. Therefore, Lck is a crucial manipulation target for understanding if and how TCR triggering impacts ligand memory. To test the hypothesis that CD3 ITAM phosphorylation impacts TCR ligand memory, we inhibited Lck through an Lck-specific inhibitor which competitively binds the ATP binding site required for activity [61, 129] using the same system as previously described (Section 5.5.2) and the high memory ligand ALW. The adhesion frequency did not significantly change with the addition of addition of Lck inhibitor ($p>0.1$) although it appeared to decrease slightly (Figure 17A). However, Lck inhibition led to a significant decrease in memory showing the unique sensitivity of this measurement over standard micropipette analysis (Figure 17B). Baseline adhesion frequency, that is the adhesion frequency after there was no bond in a previous contact, did not change (Figure 17C), implying that the memory effect is indicative of upregulated binding periods, not downregulation of binding. The memory index was still however significantly above zero, which we found to be counterintuitive. Because the Lck inhibitor can act in a dose-dependent fashion, it was possible Lck was unsaturated and the small fraction of active Lck could maintain some of the memory effect. To confirm this behaviour, we added a much higher level of inhibitor (20μM) to affirm Lck saturation. However, this did not change either the adhesion frequency or memory index (Figure 17).

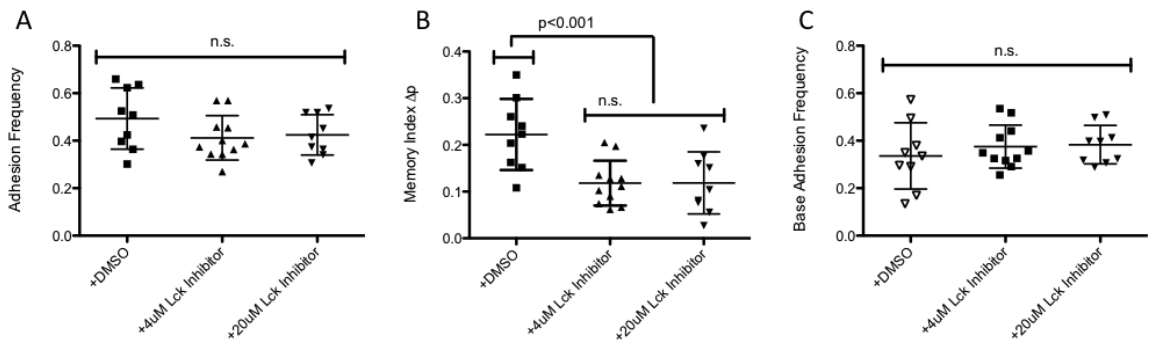

Figure 17. Impact of Lck inhibition on adhesion frequency and ligand memory
(A) Adhesion frequency for Lck inhibition vs DMSO carrier for 1E6-J cells vs. ALW coated beads using dynamic input micropipette assay. (B) Memory index analysis for same data. (C) Adhesion frequency after there was no bond in a previous contact for all cases.

Because the memory index in these experiments was indicative of long, upregulated periods of adhesion (Figure 16), a nonzero level of memory upon inhibition indicated that Lck plays either or both of two roles in TCR ligand memory: 1) Lck assists in maintaining the length of upregulated adhesion periods, thereby leading to more bonds in series and a higher memory index, or 2) Lck assists in triggering the occurrence of upregulated binding periods, thus increasing the probability that these periods occur and increasing memory index. To examine these two roles, we employed a variety of analytical techniques to the data.

To determine if the duration of the upregulated binding periods decreased upon Lck inhibition, we first looked at the average cluster size – that is, how many bonds occur in a row – and normalized this by the average cluster size expected by the adhesion frequency of a Bernoulli sequence. In effect, this normalization would account for the small differences in adhesion frequency seen previously. The normalized cluster size decreased

with the addition of Lck inhibitor (Figure 18A). Additionally, when we looked at the time duration of the clusters – the time from the first bond to the last bond in a sequence – there was no significant difference between the Lck inhibitor and control as their 95% confidence intervals on the mean overlap (Figure 18B-D). However, the non-parametric Dunn's multiple comparison test, used because of non-normality of the data sets, indicated that the median values may be different between the inhibitor and control ($p<0.05$).

There is one major difference which can account for the discrepancy between the two metrics of cluster length. The duration of a cluster (Figure 18B-D) cannot be calculated for clusters of one (i.e. when there is a sequence of no bond, bond, no bond) since there is no length to the cluster; the normalized cluster size can incorporate this data. Therefore, we believed that these clusters of one, or non-triggering events, may be critical to understanding the process. We quantified their relative frequency between the control and Lck inhibitor data sets. Effectively, Lck inhibition leads to a significantly increased fraction of non-triggering events (Figure 18E). This may also explain the contradictory statistical tests on the cluster duration. If low probability multiple triggering events cannot occur as regularly with Lck inhibition, this would lead to a slight shift in the average duration which may not be detectable through some statistical tests. Taken together, these data imply that the role of Lck in TCR ligand memory is to promote the triggering of upregulated binding periods and not to extend their duration.

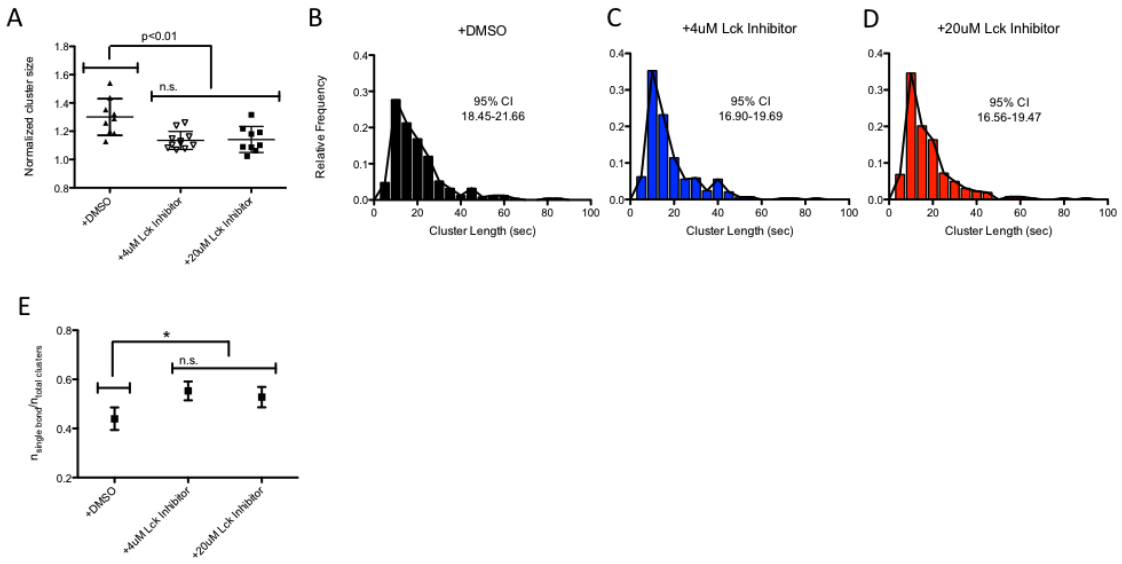

Figure 18. Lck inhibition decreases probability of triggering upregulated adhesion periods
(A) Cluster sizes normalized by the expected value of a cluster size of a Bernoulli sequence of the same adhesion frequency for Lck inhibitor and DMSO carrier. Error bars represent standard deviation. Distributions were checked for normality and significance values were calculated using two-tailed student t-test. (B-D) Relative frequencies of cluster duration for same cases. Confidence intervals on the mean are noted for each panel. (E) Ratio of single bond clusters to total number of clusters. Error bars represent 95% confidence interval.

5.5.5 Cholesterol binding to TCR inhibits ligand memory

Cholesterol and lipid regulation play a significant role in many cellular behaviours [130]. In T cells, lipid rafts on the membrane form dense clusters home to many types of receptors and signalling molecules. The TCR itself primarily resides in such domains in resting cells [45, 54, 57]. Cholesterol is a primary regulator of TCR preclustering. Recent discoveries as to the binding of TCR subunit to cholesterol and its regulation of signalling suggested it may be another target for manipulation of TCR binding [55, 58-60].

To examine the impact of cholesterol on TCR ligand memory, we first treated the 1E6-J cells with cholesterol oxidase. Although oxidation of cholesterol leads to many functional changes in cells, it primarily reduces cell membrane cholesterol content and disperses clustering. Treatment of cells with cholesterol oxidase completely removed memory (Figure 19).

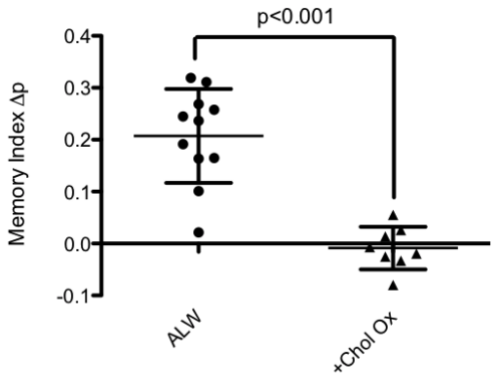

Figure 19. Cholesterol oxidase treatment effects on TCR ligand memory
Memory index for 1E6-J cells vs ALW pMHC with and without cholesterol oxidase treatment. Error bars represent standard deviation.

A recent paper by Wang and colleagues [58] shed light on a naturally occurring analog of cholesterol, cholesterol sulfate, which has been shown to displace naturally occurring cholesterol and bind stronger to the TCR. Interestingly, cholesterol sulfate appeared to decrease binding of tetramer pMHC to TCR. Measurements using divalent and monovalent antibodies for different TCR subunits implied that cholesterol sulfate treatment induced dispersal of TCRs on the membrane. However, it did not rule out changes in the kinetics or affinity.

To test the effects of cholesterol sulfate on memory index, we treated the 1E6-J cells for 1 hour with different concentrations of cholesterol sulfate and performed the

dynamic input micropipette assay against ALW in the continuous presence of cholesterol sulfate or vehicle DMSO. Addition of cholesterol sulfate decreased TCR ligand memory in a dose-dependent fashion. The slope of the fitting was significantly nonzero. Additionally, the baseline adhesion frequency decreased slightly with cholesterol sulfate treatment, implying that cholesterol sulfate addition is changing the kinetic states of the TCR even before priming. Analysis of the cluster duration showed that the duration of the clusters decreased with increasing cholesterol sulfate concentration. The trend in the histograms is apparent as well – as more cholesterol sulfate is added, the relative frequency of shorter clusters increases and the tail begins to disappear.

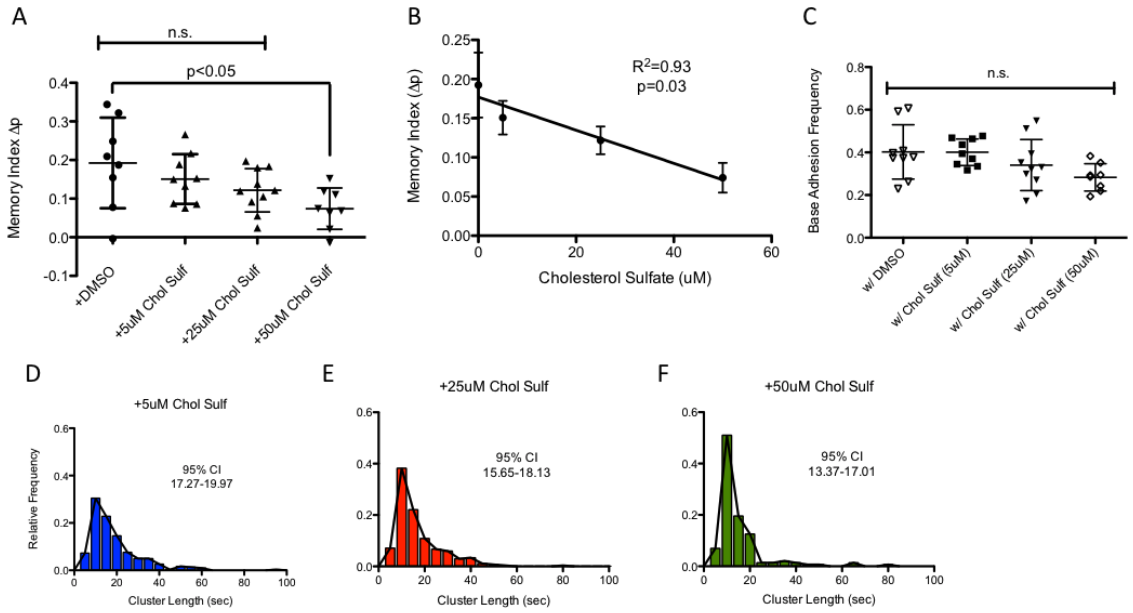

Figure 20. Addition of cholesterol sulfate reduces TCR memory in a dose-dependent fashion.
(A) Memory index for 1E6-J cells vs ALW pMHC with cholesterol sulfate treatment or DMSO vehicle. Error bars represent standard deviation. (B) Correlation of memory index vs cholesterol sulfate dose. Error bars represent standard error. P-value represents likelihood of non-zero slope. (C) Base adhesion frequency for cholesterol sulfate treatments. Error bars represent standard error. (D-F) Duration of cluster histograms for each cholesterol sulfate treatment. Confidence intervals are noted on each panel

5.6 Modeling and simulation of TCR ligand memory

The combination of Lck inhibitor data and cholesterol treatments imply that the mechanism behind TCR ligand memory is under tight control by the molecules most proximal to its function. Several key points concerning the mechanism must be considered.

1) TCR ligand memory is reflective of switching between two dynamically reversible states of kinetically different TCRs – a low affinity binding state whose binding induces a higher affinity binding state. The states must be dynamically reversible or the trend would be towards higher and higher binding frequencies as the assay progresses, which is not the case – the binding appears to come in "waves". It is possible that there are 3+ states, but the dynamic input micropipette assay does not have the refinement capable to discern between 2 or 3+ states. Therefore, we will consider the simplest case of a two-state TCR binding model.
2) Cholesterol binding may be the primary regulator in modulating the two TCR states. A memory index of zero implies that there is only one kinetic state. The effect of cholesterol sulfate on memory index trends toward zero at high concentrations; due to the toxicity of DMSO on cells and low solubility of cholesterol sulfate, higher concentrations were not experimentally feasible. Removal of cholesterol from the membrane also induced no memory and therefore a single state.
3) Lck regulates the ligand memory triggering likelihood. It has been shown that cholesterol binding to TCR sequesters phosphorylation of CD3 ITAMs. However, once phosphorylated, cholesterol is unable to bind to TCR according to recent models. As a consequence, addition of Lck inhibitor would shift the TCR population balance towards cholesterol binding.

4) Signaling for conversion of the two states and regulation of cholesterol binding must be controlled by a mechanism which has not been exclusively identified in this study.

Combining literature and the data presented in this study implies a model of TCR ligand memory where 1) TCR binds pMHC, 2) the TCR:pMHC complex undergoes a modification that induces signaling, and 3) this signaling releases cholesterol from nearby TCRs. Therefore, we simulated this mechanism in its simplest case to see whether or not it could replicate the memory effect.

The mechanism for simulation is outlined in Figure 21. It has been suggested recently that TCR clusters should be considered as their own signaling units; the data collected from the cholesterol sulfate treatment also suggests this may be the case. Therefore, the mechanism is outlined as such. At resting state, TCRs in a cluster are considered to be inactive and have at on and off rate for pMHC, k_r and k_f, which are unique to the resting state. Once TCR and pMHC bind, signaling is induced and the cluster of TCRs undergoes one-step kinetic proofreading described by the parameter k_c. If unsuccessful, nothing happens and the TCR unbinds from MHC. If successful, the cluster of TCRs switches states to an upregulated xTCR state, governed by two new kinetic rates, $k_{f,x}$ and $k_{r,x}$, which are unique to the upregulated state. The cluster of TCRs will then revert back to resting state after a period of time with a specific half-life, t_{half}. This mechanism matches all the points outlined previously.

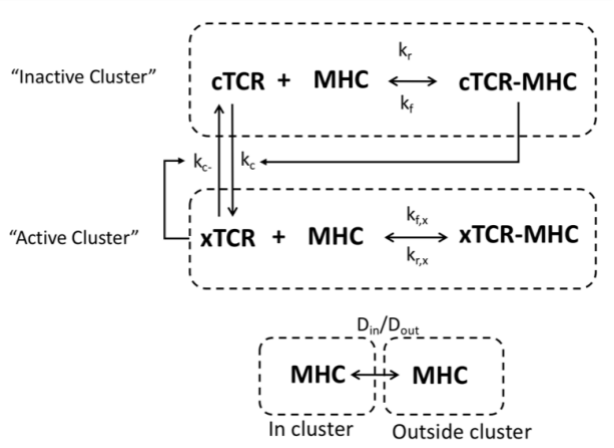

Figure 21. Simulation mechanism outline

Despite the large amount of data collected measuring the presence of bonds at certain periods of time, parameters in this model cannot be directly derived from the acquired data. To estimate the kinetic parameters governing this mechanism, we simulated micropipette sequences using a custom designed algorithm. Each individual TCR cluster across the interface between a cell and bead was simulated for a random contact period in the range of the experiment. TCR clusters were permitted to diffuse for random MHC encounters. The surfaces were then separated. If a bond or bonds were present at the end of contact for any of the TCR clusters, they were broken and a bond event is recorded. A randomized period of waiting time was then applied to replicate experimental conditions. The stochastic simulation algorithm with no approximations was used to solve the equations [131, 132] which relies on the inherent chemical kinetics of the molecules (on/off rate) and characteristic areas of interaction. Parameters used in the simulations are presented in Table 3.

Table 3. Simulation parameters for mechanism investigation

Parameter	Value	Source
Cluster size	7-20 TCR per cluster	Lillemeier, et al. Nat Immunol 2010
TCR density	101 TCR/um^2	measured
MHC density	2700 MHC/um^2	measured
Contact area	1um	estimated
Waiting times	1-6 s	experimental condition
Contact times	0.25-5 s	experimental condition
Diffusion constant	0.001 um^2/s	Stepanek, et al. Cell 2014 says 0.06 for TCR, but no diffusion on bead and cluster moves slower than individual TCRs
Cluster area ratio	0.00077 um/cluster	estimated from Lillemeier, et al. Nat Immunol 2010
Conversion rate from cTCR->xTCR	0.01-100 cluster/s	need to fit
Degrading rate from xTCR->cTCR	0.01-100 cluster/s	need to fit
cTCR:MHC on rate	10^{-8}-10^{-5} um^2/s	need to fit
cTCR:MHC off rate	0.1-10 s^{-1}	need to fit
xTCR:MHC on rate increase	1-10^3	need to fit
xTCR:MHC off rate increase	0.01-100	need to fit

Because there are six unknown parameters and an individual run takes approximately 10 minutes for a ~40 cell pairs, standard methods of parameter estimation would take a significant amount of time. We therefore employed a statistical technique developed by colleague Dr. Chih-Li Sung and colleagues. In this technique, experimental data is fit to a statistical model similar to a logistic regression with the addition of a Gaussian noise term. Monte Carlo scanning of the simulation parameter space using a logarithmic Latin hypercube approach created data sets of simulated data for analysis by the same statistical approach. Error between the two analyses, experimental and Monte Carlo simulations, is minimized converge on approximate values of the unknown parameters. This results in significantly faster convergence.

Simulations were solved through a Stochastic Simulation Algorithm (SSA) approach [131, 132] in MathWorks Matlab (R2015b) using customized algorithms (Figure 22). Each cluster of TCRs was modeled as its own signaling and binding unit, so the number of TCRs, pMHC, and clusters required random selection. In the initialization module, the number of clusters in the interface was determined by dividing the average TCR density on the surface

by the average number of TCRs in a cluster. For each cluster, the number of TCRs within that cluster was derived from a uniform distribution on the specified interval. The initial number of pMHC in each cluster was determined by knowing the average pMHC density. From the cluster area, the average number of pMHC in this area can be calculated. The number of pMHC in the cluster was then randomly selected from the Poisson distribution with the previously calculated average. All other known parameters were initialized.

Unknown parameters were segmented logarithmically along the specified interval by the number of required logarithmic Latin hypercube divisions. These segmented vectors were randomized. The maximum and minimum possible parameter values were estimated from biophysical approximations and adjusted so as to not limit the parameter space resulting in false convergence. The segmented vectors were then randomized, and the simulations iterated through these vectors to solve for the binding sequence. Relevant parameters are outlined in Table 4.

Table 4. TCR ligand memory mechanism simulation parameters

Parameter	Value	Source
Cluster size	7-20 TCR per cluster	Lillemeier, et al. Nat Immunol 2010
TCR density	101 TCR/um^2	measured
MHC density	2700 MHC/um^2	measured
Contact area	1um	estimated
Waiting times	1-6 s	experimental condition
Contact times	0.25-5 s	experimental condition
Diffusion constant	0.001 um^2/s	Stepanek, et al. Cell 2014 says 0.06 for TCR, but no diffusion on bead and cluster moves slower than individual TCRs
Cluster area ratio	0.00077 um/cluster	estimated from Lillemeier, et al. Nat Immunol 2010
Conversion rate from cTCR->xTCR	0.01-100 cluster/s	need to fit
Degrading rate from xTCR->cTCR	0.01-100 cluster/s	need to fit
cTCR:MHC on rate	10^{-8}-10^{-5} um^2/s	need to fit
cTCR:MHC off rate	0.1-10 s^{-1}	need to fit
xTCR:MHC on rate increase	1-10^3	need to fit
xTCR:MHC off rate increase	0.01-100	need to fit

After initialization, each individual cluster's binding was simulated over the contact period randomly selected from the interval 0.25-5s. Once each cluster was simulated, if any of the clusters remained bound after the contact period was completed, the event was marked as a bond and those bonds were broken. If no bonds were present in any of the clusters after that time, no bond was recorded. A waiting time was randomly selected from the uniform interval 1-6s to reflect experimental conditions. This cycle was repeated until the simulation reached the input number of contacts. For calibration of parameter values, 20 cell pairs with 300 contacts were simulated for each set of parameters with a 120-sided hypercube.

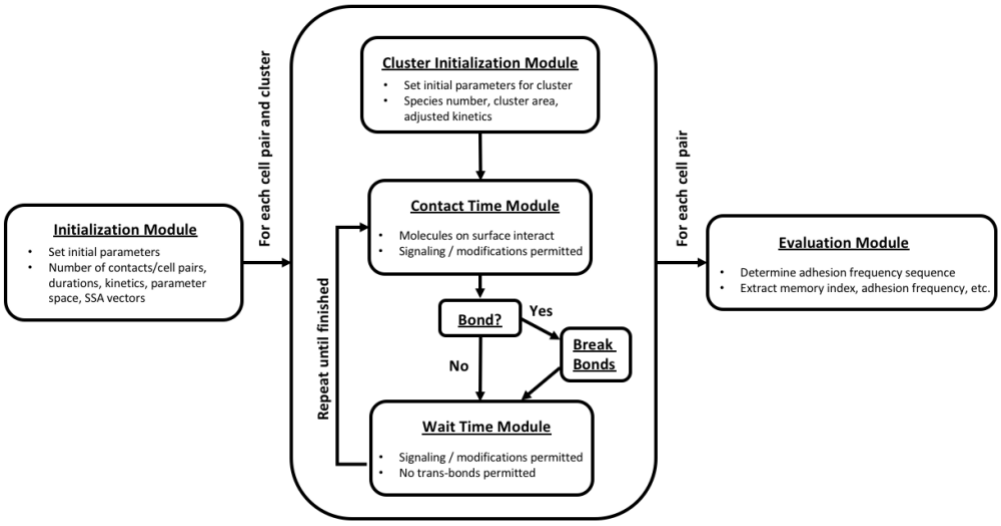

Figure 22. Micropipette simulation algorithm outline

The results of the fitting are seen in (Table 5). Because there may be many different minima in the fitting space and the statistical fitting method may result in artifacts, it is important to consider many different local minima; in this case, we decided to look at the 20 best fitting parameter sets as determined by their statistical cost function, L^2 distance. Upon initial inspection, some of the parameters reached the maximum or minimum of their

simulation intervals. This is not an ideal case, but it still may be an appropriate fit. This required testing.

Table 5. Twenty best parameter fits by statistical model

k_c	k_d	k_{on}	k_{on_x} increase	k_{off}	k_{off_x} increase	L^2 distance
2.624738	10.41196	1.59E-06	24.36661	0.111682	14.9905018	0.02453
0.01	56.615339	1.33E-06	122.3785	1.004167	6.249376	0.0254
28.268174	10.326968	1.32E-06	250.93981	2.212066	17.2322776	0.02597
43.775623	14.520549	2.39E-06	106.00489	1.197712	24.2885719	0.02699
3.659635	69.630037	1.82E-06	1	0.689347	4.6355374	0.02712
32.972703	14.514549	1.06E-06	353.48716	3.554605	14.0725936	0.02724
24.695531	5.292472	7.47E-07	241.2595	4.129003	10.2609748	0.0276
74.754525	24.445556	2.48E-06	247.89286	2.713402	25.9504057	0.0281
53.088692	18.039197	1.04E-06	259.93081	3.20365	13.9056103	0.02835
24.334567	18.801121	1.37E-06	521.70877	4.056436	17.3222686	0.03091
30.212979	2.621739	1.00E-08	114.99589	5.289283	2.4927517	0.0312
37.766224	6.083393	1.00E-08	38.19277	3.316312	0.7809229	0.03132
26.877313	15.202481	6.42E-07	510.52996	6.300568	9.9060103	0.0317
0.01	61.728827	7.82E-07	217.04374	1.767457	15.8594149	0.0345
20.01	17.850216	1.62E-06	580.03039	3.743794	20.4519556	0.03483
0.01	63.411659	8.12E-07	253.67707	1.881208	16.6763332	0.03647
47.217279	21.359865	6.07E-06	1	1.039906	32.3417665	0.03777
33.395661	16.672334	2.30E-06	551.39905	1.282654	33.4626544	0.03878
41.330867	24.170584	2.04E-06	300.95974	2.926351	23.7646243	0.04086
49.916009	24.382562	2.46E-06	247.60315	2.628262	26.6703337	0.04125

Therefore, we performed simulated micropipette assays in the same fashion, but provided the fitted parameters as inputs. The results indicated that there were several artifacts induced by the statistical fitting method (Figure 23). Several parameter sets had zero memory; others had uncharacteristically high adhesion frequencies (Figure 23, blue ovals).

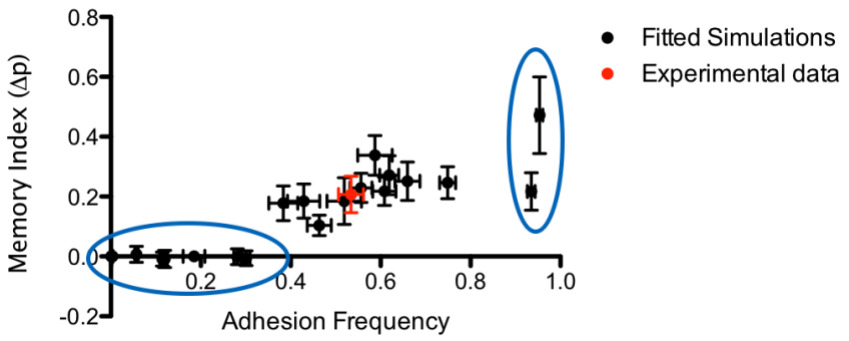

Figure 23. Experimental data vs. simulated parameter fitting using statistical methods
Statistically-fitted parameter sets were used to simulate the micropipette assay using 20 cell pairs, 300 contacts. Their memory index and adhesion frequency were calculated from the simulated adhesion sequence (black circles). This is compared to the experimental data shown by the red circle. Error bars represent standard error for the adhesion frequency and 95% CI for the memory index. Blue ovals indicate outliers.

Therefore, we eliminated these obvious outliers from the parameter fittings. The majority of these outliers were the same parameter sets which contained a parameter that hit the maximum or minimum of the simulated interval. Interestingly, when these outliers were removed, some significant and consistent trends began appeared (Table 6). The upregulated binding periods appear and disappear quickly, as seen by the magnitudes of k_c and k_d, respectively. The on-rate for the upregulated state increased several hundred fold, and the off-rate increased 10-20 fold. These interesting parameter trends indicate that the TCR, upon recognizing antigen, very quickly upregulates the kinetics of nearby TCR to rebind antigen. It releases that antigen soon after for rebinding to another TCR, which again quickly dissociates, allowing another TCR to rebinding. This mechanism would permit several TCRs to interact with the same antigen in quick succession.

Table 6. Best parameter fits by statistical model with outliers removed

k_c	k_d	k_{on}	k_{on_x} increase	k_{off}	k_{off_x} increase	L^2 distance
28.268174	10.326968	1.32E-06	250.93981	2.212066	17.2322776	0.02597
43.775623	14.520549	2.39E-06	106.00489	1.197712	24.2885719	0.02699
32.972703	14.514549	1.06E-06	353.48716	3.554605	14.0725936	0.02724
24.695531	5.292472	7.47E-07	241.2595	4.129003	10.2609748	0.0276
74.754525	24.445556	2.48E-06	247.89286	2.713402	25.9504057	0.0281
53.088692	18.039197	1.04E-06	259.93081	3.20365	13.9056103	0.02835
24.334567	18.801121	1.37E-06	521.70877	4.056436	17.3222686	0.03091
20.01	17.850216	1.62E-06	580.03039	3.743794	20.4519556	0.03483
41.330867	24.170584	2.04E-06	300.95974	2.926351	23.7646243	0.04086
49.916009	24.382562	2.46E-06	247.60315	2.628262	26.6703337	0.04125

5.7 Discussion and future studies

Utilizing a panel of different peptides for a specific TCR and a series of pharmacologic interventions, we show that adhesion memory is the result of a complex process regulated through TCR proximal interactions. Unexpectedly, weaker ligands exhibit higher adhesion memory than stronger ligands for the 1E6-J system. However, analyses of TCR *ex vivo* systems (Figure 11) did not share the same trend, suggesting that this mechanism may be under complex controls and tuned at the thymocyte selection level. Blocking of TCR-proximal signaling molecule Lck slightly decreases the duration of these periods, but significantly impacts the probability of their formation, suggesting a complex role for Lck in this process. Depletion of membrane cholesterol through cholesterol oxidase treatment completely eliminated adhesion memory. Addition of cholesterol sulfate, a naturally occurring analog of cholesterol which disrupts multimer formation and inhibits signaling by binding to the TCR, was shown to deplete adhesion memory in a dose-dependent fashion.

Simulations of this mechanism revealed that the TCR upregulates its binding affinity 10-20 fold to pMHC ALW. This increase is attributed to the interplay between the kinetic on-rate and off-rate – approximately several hundred fold and 10-20 fold, respectively – both of which are important regarding the mechanism influence on antigen recognition. This reflects a very dynamic process. Once a TCR recognizes antigenic pMHC, it communicates to nearby TCRs that an antigen is nearby by the same signaling molecules as the triggering process. That pMHC dissociates, and it remains in the vicinity of TCRs which are primed to quickly recapture it and release it. By this mechanism, several TCR engagements with antigen occur very quickly, fostering more triggered TCRs each binding event. It is a signal amplification mechanism derived from its effects on ligand binding sensitivity. Although not simulated this way, it is likely this signal may spread between TCR clusters, similar to ZAP-70 catch-and-release observations where a signal originates from a single TCR cluster and transitions out to perform its function [133]. Therefore, even a signal antigenic pMHC could induce T cell activation. Despite experimental evidence for TCR kinetic binding upregulation [46-48], this is the first evidence regarding a mechanism which could give rise to this behavior.

However, we must consider that this is not the only possible interaction network; it is quite possible that memory may be induced by other mechanisms which may have different implications. This should not be considered the only possible interpretation of our data. The model we chose was based largely on the pharmacological inhibitions used in experiments and previous knowledge from the literature. We are currently working on developing statistical metrics to compare the validity of different mechanistic models.

Future publications examining the merit of these different possibilities will be critical to interpreting the data.

These upregulated periods of adhesion probability in the micropipette adhesion frequency assay are indicative of changes in the inherent kinetics of the interaction. These changes are unlikely to occur at the single TCR level because the on-rate increase would be outside conceivable ranges. Similarly, a whole cell binding upregulation would require an extremely fast switch-like response and would not be resource efficient considering the cell only has knowledge of the existence of a single antigen. However, if the TCR is able to upregulate its binding kinetics and the kinetics of nearby TCRs in response to previous binding, this process would help to recapture the same antigenic pMHC. As a result, TCR binding induces more TCR binding, leading to further stimulation of the cell. This mechanism is similar to rebinding models [82, 87] where a signal can persist after bond dissociation to propagate signaling and increase antigen sensitivity.

We propose that this positive memory index acts as a measure of ligand sensitivity similar to the Hill coefficient in enzyme kinetics, but with an effect in time rather than concentration, and represents an inherent self-regulation to ligand binding. Hill kinetics moderates reaction velocity in a substrate concentration manner (Figure 24A, top panel), thereby increasing the sensitivity to ligand. This results in a heightened sensitivity window for positive cooperative ligands over traditional kinetics. Similarly, ligand memory shows increased bond formation in time (Figure 24B, top panel). This leads to a heightened sensitivity to ligand in time, followed by a desensitization back to steady-state (Figure 24B, bottom panel). This results in much more dynamic responses to ligands over what was previously considered.

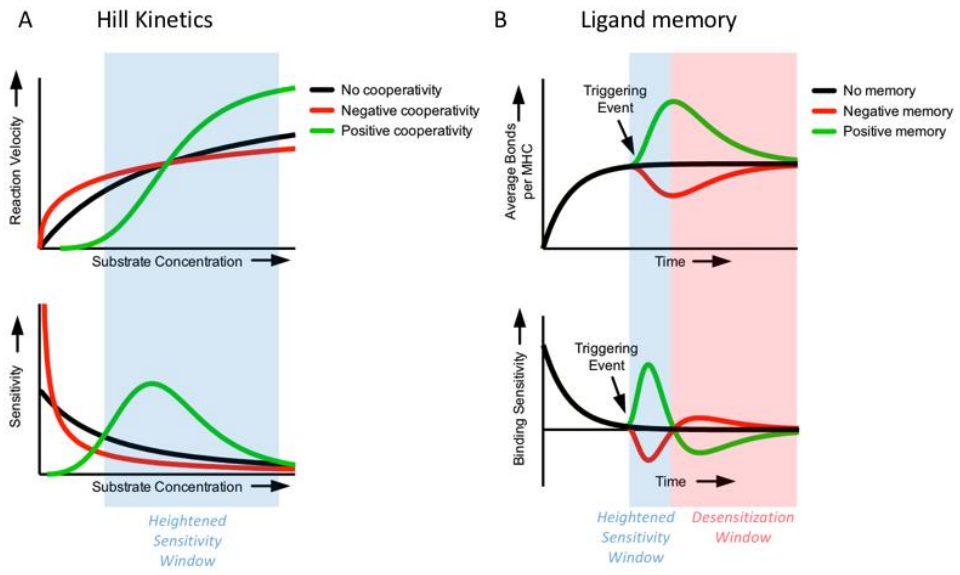

Figure 24. Comparison between Hill coefficient and ligand memory in moderating binding sensitivity

(A) Hill Kinetics reaction velocity (top panel) or sensitivity (bottom panel) vs substrate concentration for cases of no cooperativity, negative cooperativity, and positive cooperativity (black, red, and green curves, respectively). (B) Ligand memory average bonds (top panel) or binding sensitivity (bottom panel) vs. time for cases of no memory, negative memory, and positive memory (black, red, and green curves, respectively)

How does this behavior result from the physical properties of the TCR? At this point, the obvious scapegoat is conformational change to the TCR prompting a more amenable binding interface. A conformational change to TCR or its CD3 subunits has been postulated by several groups [90, 134-137], but it has not been shown to directly affect pMHC interaction kinetics. There is some evidence for this in the survival distributions of lifetime under force which occasionally show multiple dissociation rates, but there is very little supporting structural evidence. In another interpretation, the binding of cholesterol to TCR provides an allosteric effect limiting the range of motion of the distal pMHC binding site. This would directly constrain the effective kinetic on-rate for the interaction. Cholesterol-induced allosteric effects have been known to impact TCR triggering [59], but its effects

on kinetics are unknown. Determining a direct mechanism at the TCR level is an exciting potential direction for future research.

There are many different implications of this study for further research. This enhancement would be intriguing in an *in vivo* context where many different antigenic pMHC are present alongside weaker or self pMHC. For instance, a triggering event may occur for upregulated binding, but that pMHC escapes recapture. However, the cluster of TCRs encounters other, weaker antigens and continues signal persistence for T cell activation. Additionally, the process could occur in the opposite fashion – weaker ligand activation of TCR upregulated binding for strong agonist capture. The complex interplay between ligands of different potency is not studied here, but future studies could examine the impacts of concepts such as antagonism [138] or co-agonism [139], phenotypic explanations for the complex interplay between peptides of different potency, on TCR ligand memory. Models have suggested that this behavior is the result of signaling networks [140, 141], but there is a strong evidence presented in this study that the quality of the peptide impacts the binding of the TCRs.

This new mechanism has implications at many levels of the T cell activation process. We have shown that TCR ligand memory can be tuned by extracellular factors, such as cholesterol sulfate. Likely, this binding enhancement is regulated through a combination of soluble factors, such as hormones and cytokines, impacting membrane cholesterol content and proximal signaling molecule activity prior to APC contact. It has been shown that T cell lineages have differential TCR clustering [142] and Lck activity [112]. Co-stimulatory (CD28) or co-inhibitory (PD-1, CTLA-4) pathways intercede with TCR signaling pathways, adding a layer of regulation once cells have come in contact.

Additionally, although the mechanism presented here is a good candidate for memory induction, it is not the only possible network. Model selection is often a difficult task, and the finest details may be of unique importance. Small modifications to this mechanism, such as adding aspects of force due to pulling of the bond at the end of contact or inducing ligand dissociation upon a state conversion, are critical points to the mechanism which require further investigation. We are currently in the process of developing unique statistical methods to compare the validity of other mechanisms for optimal model section.

Sensitivity changes are typically assayed at the level of T cell activation on a population level, such as increased cytokine secretion or targeted cell killing. However, these metrics are far removed from how the TCR itself produces this behavior in very few binding events. Models have attempted to rectify the unique TCR binding sensitivity and specificity, but are susceptible to undesirable activation [51, 79, 83, 85, 87]. By using a new methodology with a unique metric of sensitivity, we showed that TCR regulates its own binding capacity, and this regulation is under the control of the molecules most proximal to its own triggering. This new mechanism provides a foundation for discoveries influencing the initial binding events leading to full T cell activation.

CHAPTER 6. ROLE OF MECHANICAL FORCE IN CD8 CORECEPTOR BINDING AND ITS IMPACT ON T CELL TOLERANCE

6.1 Introduction

The role of coreceptors in TCR antigen recognition has been debated since their influence on T cell signaling was discovered. As discussed in Section 2.3.5, coreceptors CD4 and CD8 contain an *intracellular* motif which can bind to TCR-proximal signaling molecule Lck; additionally, coreceptors have a low affinity *extracellular* interaction with MHC molecules. Therefore, it is believed that the role of coreceptors is to provide a means for Lck delivery near sights of TCR:pMHC interactions to promote phosphorylation of ITAMs and subsequent TCR activation. Logically, this process seems reasonable and has become a cornerstone of coreceptor influence on T cell immunology. Empirically, there is little evidence to refute it, and this study does not intend to do so.

However, the process of Lck delivery is not exclusive to other mechanisms in the TCR triggering process. In naïve T cells, several mechanisms have been explored as to the role of coreceptors in TCR dynamics [102, 107, 110]. Due to the presence both intracellular and extracellular binding interactions with the TCR(CD3):pMHC complex, coreceptors have been thought to stabilize the TCR:pMHC interaction by "trapping" the molecules in close proximity through this two-pronged binding modality [102]. For example, if the coreceptor unbinds from the complex (TCR:MHC:coreceptor:Lck:CD3, referred to in the future as Pseudo-dimer of dimers or PDD) at its extracellular region, the intracellular

region is still bound at the Lck:CD3 interface. Therefore, rapid rebinding to MHC occurs because the coreceptor is “locked” in place in a beneficial orientation by its intracellular binding. Similarly, if TCR unbinds from MHC, trapping of the MHC by coreceptor extracellular domains and the TCR by its interaction through Lck:CD3 maintains their close proximity, permitting rapid rebinding. In essence, this can significantly extend the lifetime of a TCR interaction with antigen, permitting more time for proofreading of the peptide for TCR triggering. This mechanism was simulated in a simple case and found to be insignificant [110]. However, the results were highly dependent on assumed kinetics, and combined with a lack of experimental evidence, the argument was not strong.

Thymocyte selection was discussed briefly in Section 2.1.1. While in the thymus, thymocytes are presented with “self” ligands to develop two important facets of T cell behavior – tonic signaling and tolerance to self-peptides. Thymocytes which do not respond to self-ligand die by neglect become apoptotic. Thymocytes with TCRs which respond too much to self are also deleted by apoptosis [143]. In effect, this creates a pool of T cells in the periphery which have a specific window of strength to self-pMHC, in which they respond to weaker peptides, but do not elicit a phenotypical response of naïve T cells. This prevents autoimmune disease to self while still maintaining a pool of TCRs which have the chance to recognize foreign pMHC.

The role of coreceptors in the thymocyte selection process has been considered on several occasions [15, 107, 111], but there is no consensus on their role and mechanism. It is likely that mechanisms at the thymocyte level persist into the naïve T cell population. In this study, we will use simulation-based analysis on force-induced bond lifetime data from

an OT-1 thymocyte system to parse mechanisms of CD8's role in binding and thymocyte selection.

6.2 Experimental data

Dr. Jin-sung Hong and Dr. Chenghao Ge initiated a project to understand the role of coreceptors in thymocyte selection. First, they examined the role of coreceptor CD8 in the affinity regulation of a panel of peptides of various potency for OT-1 thymocytes, but saw relatively no difference along the selection region. However, the addition of force with a Biomembrane Force Probe (BFP) created an interesting phenomenon along the selection threshold; this behavior was dependent on CD8. In these BFP experiments, an OT-1 thymocyte was brought into contact with a bead coated in the noted ligand. The bead itself as also adhered to a red blood cell which is used as a force transducer. The bead and thymocyte are then separated, and if a bond is present at the end of contact, the bond is stretched to a predefined force level and held at that force until dissociation. The lifetimes of bonds from several bonds are pooled into a lifetime vs. force curve.

An interesting trend appeared upon analysis. Positively selecting ligands formed slip-bonds with the addition of force, where the average lifetime of a bond decreases exponentially with linearly increasing force (Figure 25E-G, blue labels). Negatively selecting ligands, those which induced apoptosis due to strong signaling, formed a catch-bond which has the counterintuitive response of increasing lifetime with increased force and was followed by slip-bond behavior (Figure 25A-C, red labels). This enhancement relied on the cooperativity of CD8, as antibody blocking of the CD8:MHC interaction or mutant MHC eliminating CD8 binding did not produce this behavior.

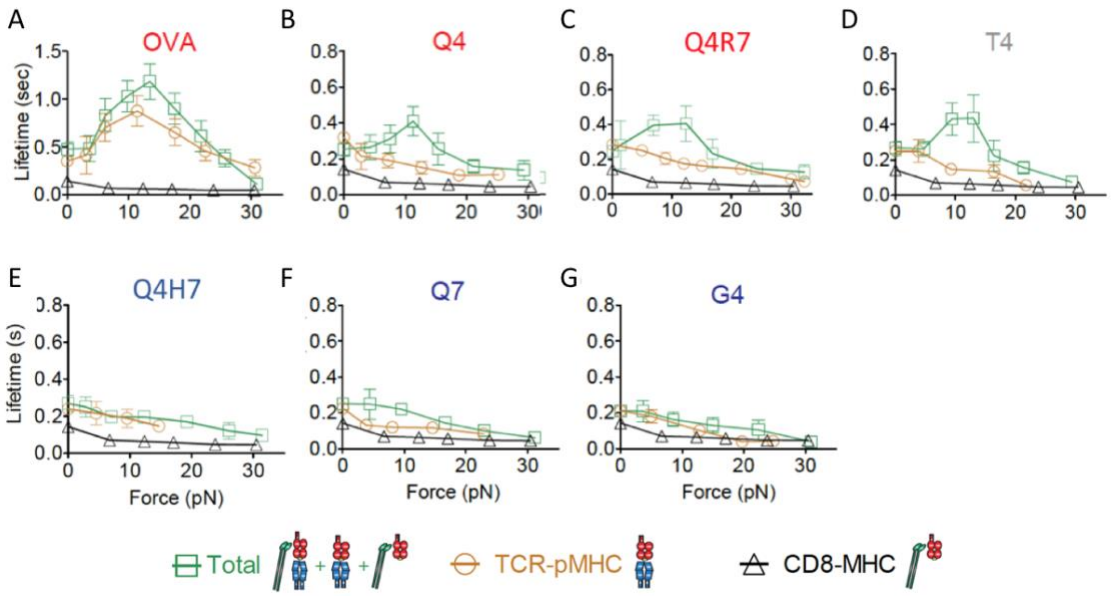

Figure 25. Positively selecting ligands form catch-bonds while negatively selecting ligands form slip bonds in the presence of CD8
Bond lifetime vs. applied force for OT-1 thymocytes vs. a panel of different ligands. Green squares are wild-type pMHC, allowing both CD8 and TCR binding, black triangles for CD8 only, and gold circles for TCR:pMHC binding only. pMHC are noted on the top of the panel, negatively selecting ligands in red, positively selecting ligands in blue. T4 represents a special case in the middle. Error bars represent standard error. Data adapted from submitted manuscript with permission from Dr. Jin-sung Hong.

They next tested another transgenic mouse system that utilized the OT-1 TCR with a modification to CD8 which gave it a CD4 tail which has a higher affinity for Lck (named CD8.4). It was known that this mouse system shifted the threshold for selection slightly, making Q4H7, a previously positively selecting ligand, into a negatively selecting ligand. This modification also turned the slip bond from the Q4H7 to a catch bond (Figure 26C). Additionally, the CD8.4 mutation made negatively selecting ligand Q4R7 into a much stronger catch bond (Figure 26D). Interestingly, these catch bonds could be eliminated

through the addition of an inhibitor for the Lck kinase activity (Figure 26A-D) with the exception of Q4R7 in the CD8.4 system although this data has low confidence. Furthermore, Previous co-immunoprecipitation (co-IP) studies showed that TCR-CD8 or CD4 conjugation through Lck requires ITAM phosphorylation for recruitment of ZAP-70 as an adaptor for Lck intracellular binding to CD3 [144, 145]. In another similar BFP assay where the tyrosines of the CD3ζ ITAMs were mutated to inactive phenylalanines, there was a slight reduction in the catch bond; other ITAMs from non-CD3ζ subunits likely subdued a complete catch-bond elimination. Therefore, Lck phosphorylation of the CD3 tails plays a role in this catch-bond behavior. Overall, this data suggests that the catch-bond criteria is consistent even after shifting the selection threshold by intracellular modifications; additionally, the kinase activity of Lck is critical for this behavior, likely by phosphorylation of CD3 subunits.

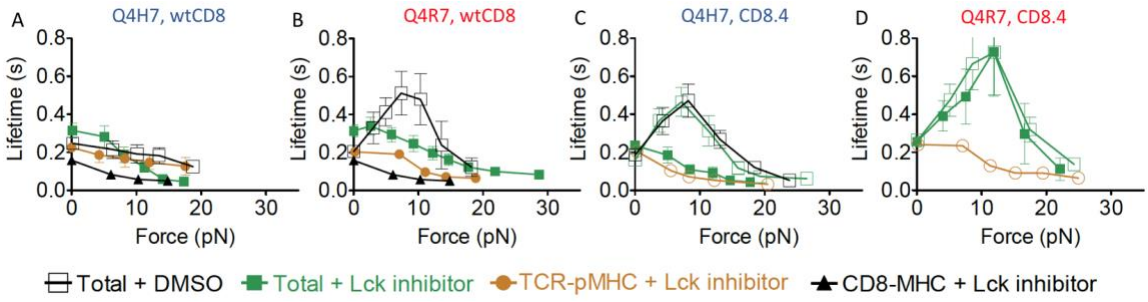

Figure 26. Addition of Lck inhibitor removes catch bond promotion by CD8
Bond lifetime vs. applied force for OT-1 thymocytes vs. Q4H7 (blue) or Q4R7 (red) for wild-type CD8 or CD8.4 thymocytes. Black open squares: DMSO control, solid green squares: addition of Lck inhibitor, gold circles: TCR-pMHC only binding with the addition of Lck inhibitor, solid black triangles: CD8 binding only with the addition of Lck inhibitor, open gold circles: TCR-pMHC binding only, no DMSO. Error bars represent standard error. Data adapted from submitted manuscript with permission from Dr. Jin-sung Hong.

Combining these data sets gives a unique subjective criteria of negative selection – that is, negatively selecting ligands form a catch bond with TCR in the presence of CD8. However, this is not a quantitative metric for selection and the impacts are difficult to comprehend. Several questions arise from this data. What does the catch bond mean in this context? How does increasing conjugation of Lck to CD8, an intracellular interaction, modify the extracellular binding kinetics? And lastly, how does this behavior result in thymocyte selection? In the next few chapters, we will undergo simulation-based analysis on these data sets to explore these questions and suggest a mechanism behind such complex responses.

6.3 Long-lived bond formation is a diffusion limited process

6.3.1 Survival distributions indicate multiple bond states

The measurements presented in lifetime vs. force curves (Figure 25, Figure 26) is very difficult to understand in its current binned form; information is lost in the binning process which can assist in understanding the cause of the behavior. Therefore, it is critical to begin investigation at the data within the bins themselves, each containing many lifetimes acquired at the given force level. The data within an individual bin is classically presented as a survival distribution – the probability of a bond surviving vs. time. A survival distribution for a bond at a given force is an exponential decay function [146], and when plotted on a semi-log axes, should result in a line with slope equivalent to the resulting off-rate for the molecular interaction (Figure 27A). The average bond lifetime can then be found by integrating this curve.

There are unique two possibilities for changes in the survival curve which result in catch-bond behavior. First, the survival distribution may decrease in slope, therefore decreasing the molecular off-rate and increasing bond lifetime (Figure 27B). This is indicative of a single-bond state which is induced by force. Essentially, all bonds respond to force similarly when pulled, and all bonds increase bond lifetime. Secondly, the survival distribution may change to have two or more slopes (Figure 27C). If one of the slopes is small and the population large enough, this results in a small subset of the bonds with long lifetimes which dominate the average bond lifetime. Interpretation of this data can be very difficult, especially in the context of the cellular environment where signaling and membrane dynamics are prevalent. The response of the OT-1 thymocytes in Figure 25 is the second case. There is a new, long-lived bond state induced by force with a ~50x slower off rate than the TCR:pMHC interaction alone (Figure 27D).

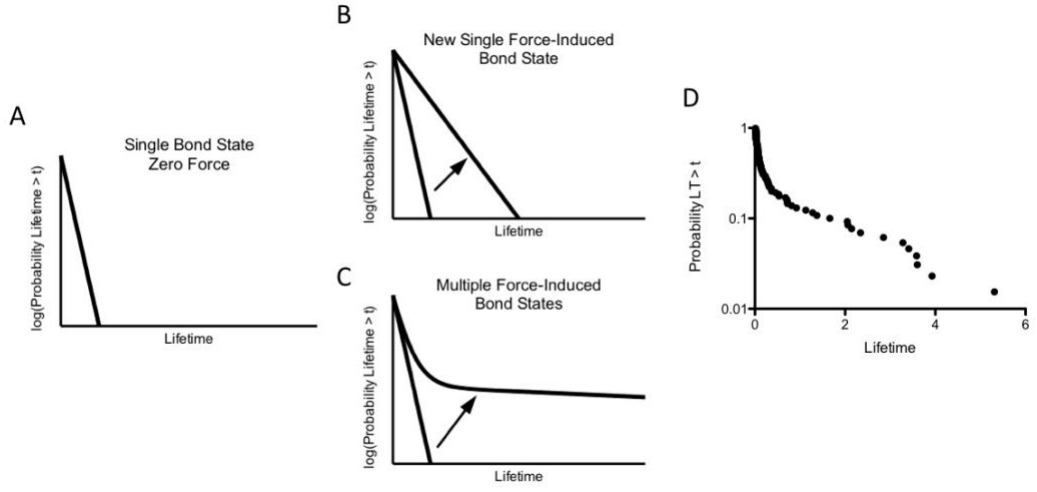

Figure 27. Catch bonds arise from two possible survival distributions
(A) Example survival distribution at zero force contain a single bond state. (B) The application of force may induce a new bond state. The off-rate becomes smaller for all bonds, and the average bond lifetime increases. (C) Application of force may result in formation of multiple bond states, with a population of long-lived bonds (small slope) dominating the average. Arrow points in direction from expected to observed (B,C). (D) Example survival distribution for Q4R7 vs. OT-1 CD8.4 thymocytes, 12pN bin.

Assuming that the long-lived bonds are those which form the full TCR:MHC:CD8:Lck:CD3 complex, or a Pseudo-dimer of dimers (PDD), there are two possible explanations for this behavior. First, there is the possibility of force-induced recruitment. In this mechanism, pulling of one bond species, either TCR:pMHC or CD8:MHC, exposes a binding site in either species which enables binding. For instance, pulling TCR leads to release of CD3 intracellular tails for Lck binding. Secondly, there is the possibility of species deviations. Because the BFP experiment is performed on a single cell for many contacts in a row, there is the possibility that the bonds species change over time due to signaling or membrane perturbations. These two mechanisms will be investigated in the following sections.

6.3.2 Force-induced recruitment models cannot explain data

The concept of force-induced recruitment is outlined in Figure 28. A TCR or CD8 is pulled through the BFP assay. If the second molecule does not diffuse into close proximity with the bond within the recruitment time, the bond breaks and a short lifetime is recorded. However, if the second molecule is recruited, the bond lifetime is extended due to PDD formation. As a consequence, this is primarily a passive, diffusion-based mechanism similar to those previously proposed. Therefore, we simulated both TCR and CD8 pulling to examine whether the second molecule recruitment could explain the data.

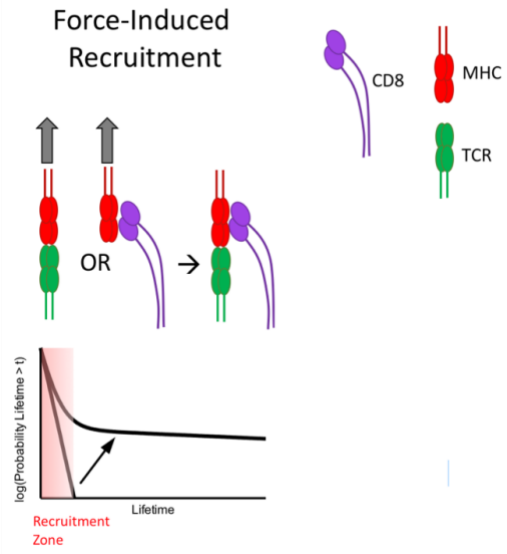

Figure 28. Force-induced recruitment mechanism

If the mechanism is genuine, the experimental fraction of long-lived bonds from the survival distribution should match the simulated fraction. We used a double-exponential fit to determine the fraction of PDD bonds from the experimental data in the 10-15pN range (catch-bond peak) for all pMHC tests except for OVA, since it is a special case. Although there is likely a mixture of TCR/CD8 bonds in the short-lived states, these are similar in off-rate and therefore can be grouped into one parameter. A triple exponential fit resulted in over-fitting of the data. As seen in Figure 29, the off-rate of the PDD bonds is not a perfect fit. Some over-fitting of the data occurs at the short-lived lifetimes to compensate for the time resolution of the BFP assay. However, this is not essential in determining the bond fraction. The double exponential fit adequately predicts the "kink" in the curve of the survival distribution where the dominance of the PDD fraction begins. This "kink" occurs at the fraction of PDD bonds.

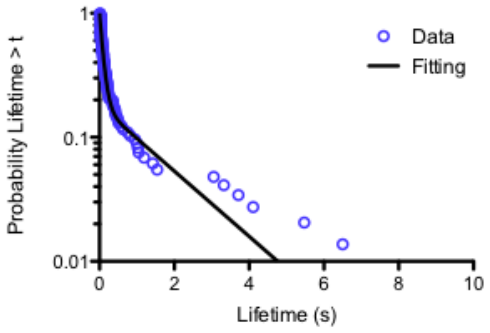

Figure 29. Double exponential fit adequately predicts fraction of PDD bonds

Double exponential decay nonlinear least square fitting using Matlab fit function plotted against survival distribution of wild-type OT-1 thymocytes against Q4R7. Data is binned from the 10-15 pN range.

6.3.2.1 TCR:pMHC force-induced recruitment of CD8 is unlikely

The first case considers if TCR pulling induces recruitment of CD8 bound to Lck. A Markov chain was used to determine the probability of CD8:Lck recruitment over a period of time similar to the approach presented in [111]. Additionally, the probability of a TCR:pMHC bond survival was determined over that same time interval using a Bell model approximation and the experimentally measured TCR:pMHC lifetimes. Plotting the two probabilities against each other and integrating yields the probability of CD8:Lck recruitment before bond dissociation (Figure 30A). As the fraction of CD8:Lck conjugation increased, the probability of CD8:Lck recruitment before dissociation asymptotically approached a value between 0.7-0.9 depending on the TCR:pMHC binding properties (Figure 30B). For reference, the fraction of CD8:Lck has been measured to be ~1.1% and 5.8% in wild-type or CD8.4 OT-1 thymocytes, respectively, [111] but those values have been considered low due to assay limitations.

To bring the experimental and simulation data together, we must consider that there are both CD8:MHC and TCR:pMHC bonds pulled after any contact. Assuming the contact time of 0.1 seconds used in BFP assays, the fraction of TCR:pMHC bonds can be derived from the 2D kinetics of the two molecular interactions (CD8:MHC, TCR:pMHC) and the respective densities of the molecules, which were all measured experimentally. Comparing these two conditions, the probability of pulling a TCR:pMHC bond for most ligands is <0.1 (Figure 30C). Assuming once CD8:Lck is recruited a PDD is formed near-instantaneously, the resultant fraction of PDD bonds is the probability of pulling a TCR bond times the probability of CD8:Lck recruitment before dissociation. If the model fits the data, there should be a 1:1 correlation between the predicted fraction of PDD bonds and the experimental fraction as determined by the double exponential decay fitting. Assuming maximum favorable conditions of 100% CD8:Lck conjugation and fast diffusion kinetics, the experimentally measured fraction of PDD bonds for some ligands remains significantly higher than the predicted fraction (Figure 30D). Despite favorable assumptions, the model cannot explain the experimental data. It is therefore unlikely that pulling of a TCR:pMHC bond can lead to recruitment of CD8:Lck and formation of a long-lived PDD bond.

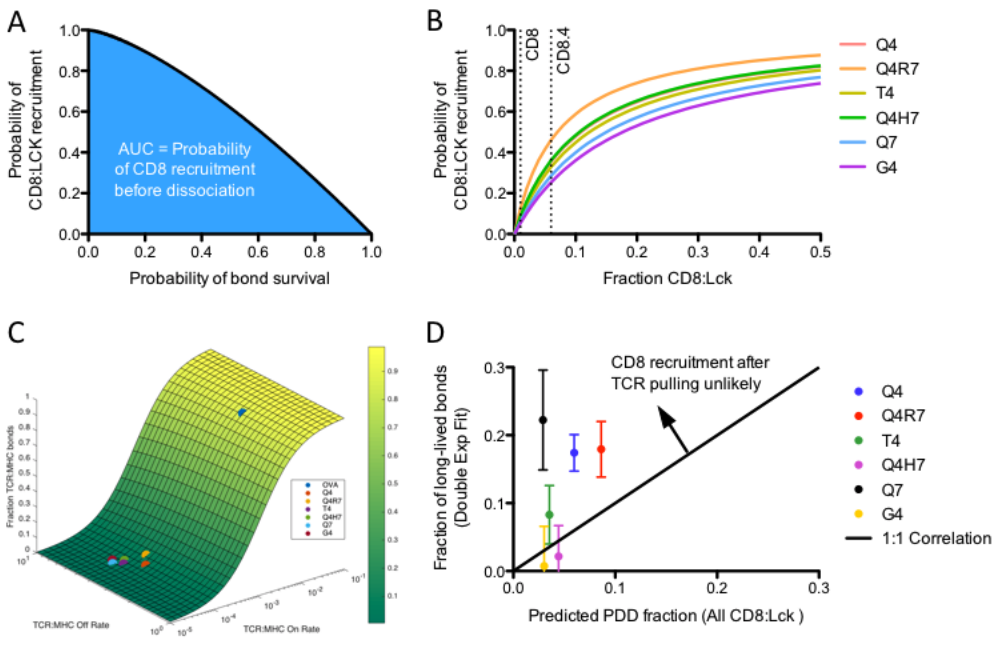

Figure 30. Formation of PDD unlikely after pulling of TCR:pMHC bond
(A) Markov chain prediction of the probability of CD8:Lck recruitment to a pulled TCR:pMHC bond vs. the probability of a TCR:pMHC bond survival. The area under the curve is the probability of CD8 recruitment before the bond breaks. (B) Markov chain prediction of the probability of CD8:Lck recruitment against the fraction of CD8:Lck present on the thymocyte surface (C) Predicted fraction of TCR:pMHC bonds for the BFP assay based on TCR:pMHC kinetics (1-fraction of TCR:pMHC bonds is the fraction of CD8:MHC bonds). The different OT-1 ligands are indicated. (D) Fraction of long-lived bonds determined experimentally against the predicted fraction of PDD assuming 100% CD8:Lck conjugation, near-instantaneous PDD bond formation after CD8:Lck recruitment, and fast diffusion kinetics. Error bars represented 95% confidence interval on the mean. Arrow indicates a region where mechanism is unlikely. Experimental data on the opposite side would imply some assumptions may be too favorable, but the mechanism still possible.

6.3.2.2 CD8:MHC force-induced recruitment of TCR is unlikely

The next mechanism to consider was CD8:MHC force-induced TCR recruitment and subsequent PDD bond formation. As example physical mechanism behind this model, once the CD8:MHC bond is pulled, the binding site for Lck is put in a favorable position, Lck is recruited, and TCR can diffuse to the bond site and bind. In a similar fashion to

Section 6.3.2.1, the probability of TCR recruitment vs. CD8:MHC bond survival was used to calculate the probability of TCR recruitment before bond dissociation for different fractions of CD8:Lck conjugation (Figure 31A,B). Using maximum favorable assumptions, the experimental fraction of long-lived bonds was plotted against the predicted fraction by the Markov chain. Again, this mechanism did not correlate with the data in any fashion (Figure 31C). In fact, the mechanism would result in little to no difference between the ligands.

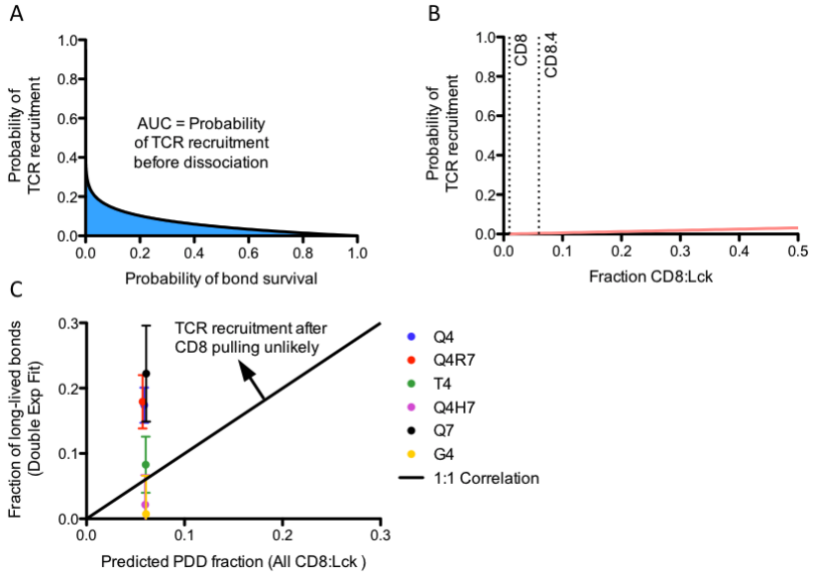

Figure 31. Formation of PDD unlikely after pulling of CD8:MHC bond
(A) Markov chain prediction of the probability of TCR recruitment to a pulled CD8(Lck):MHC bond vs. the probability of a CD8:MHC bond survival. The area under the curve is the probability of CD8 recruitment before the bond breaks. (B) Markov chain prediction of the probability of TCR recruitment against the fraction of CD8:Lck present on the thymocyte surface. (C) Fraction of long-lived bonds determined experimentally against the predicted fraction of PDD assuming 100% CD8:Lck conjugation, near-instantaneous PDD bond formation after CD8:Lck recruitment, and fast diffusion kinetics. Error bars represented 95% confidence interval on the mean. Arrow indicates a region where mechanism is unlikely. Experimental data on the opposite side of this line would imply some assumptions may be too favorable, but the mechanism still possible.

Taken together, these simulation-based analyses converge on several points. The simulations assume that the pulling of one bond leads to recruitment of a second molecule by diffusion. The fast assumed diffusion constant significantly under predicts the formation PDD bonds despite favorable assumptions. Therefore, the formation of PDD bonds is a diffusion-limited process. Additionally, there appears to be little correlation between the experimentally measured fraction of PDD bonds and peptide strength. Therefore, a more complex behavior must be occurring.

6.3.3 Force-induced PDD formation promotes catch-bond response

The different bond types, or species, may deviate from predicted due to a cellular response over time. Because the TCR and CD8 are present in the context of the cellular environment and the BFP assay "tickles" the cell with ligand many times in a row, there is a strong likelihood that signaling and modifications occur to reduce diffusion limitations or promote PDD formation in another manner. Effectively, the molecular environment changes over time, and the sequence violates the i.i.d. assumption used in Section 6.3.2. These environmental changes, provoked by the application of force, result in a survival distribution with many different species (TCR:pMHC, CD8:MHC, etc.) that are not seen in the absence of force (Figure 34).

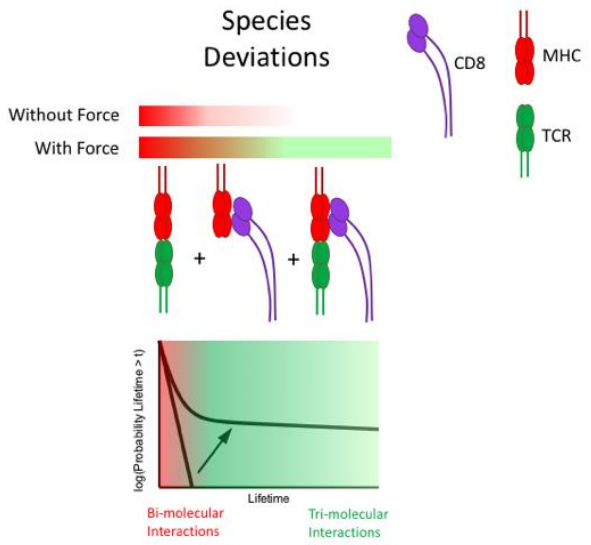

Figure 32. Transient species deviations under force

To understand these changes with the application of force, we examined the changes in PDD fraction with force using a Markov chain survival distribution algorithm which predicts the resulting survival distribution from an input initial species vector (the fraction of the bonds beginning in each state). As a result, there is no time dependency in this analysis. The Markov chain assumes the bond begins a combination of five different species (Figure 33, blue highlighted sections) and can transition between the states based on kinetic constants of the interactions, diffusion, and molecular densities. Bonds with more than one transmembrane interaction (green-filled ovals), such as TCR:CD8:MHC bonds, could not spontaneously unbind and required transition to a single bond state for dissociation. As discussed previously in Section 6.1, rebinding occurs very quickly in the PDD complex (Figure 33, noted by the purple oval). This on-rate increase was calibrated to be approximately ~1500x.

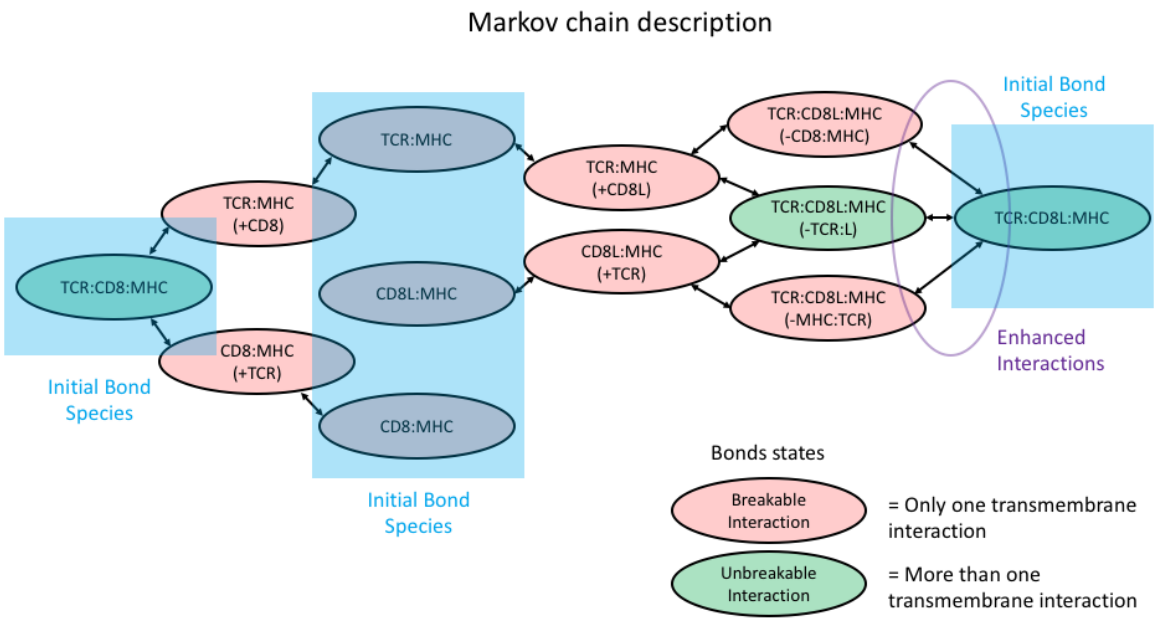

Figure 33. Markov chain connection diagram for determination of survival distribution

Markov chain connection diagram. Bubbles represent species at any given time – red bubbles indicate species that can break, green bubbles indicate species that are unbreakable and require two steps of dissociation. A (+/- molecule) notation represents that the interaction is close, but not currently bound. Bonds begin in any of 5 different states according to interaction kinetics or fit to survival distribution marked in the blue squares. The purple oval highlights the enhanced interactions due to the nature of the PDD complex.

The fraction of PDD bonds is unknown. Therefore, we simulated the survival distribution using the Markov chain approach for each bin in the force-lifetime curves to fit the fraction of PDD bonds (for example, see Figure 34A). The remainder of the bonds were determined by the 2D kinetics of the interactions and their respective densities. To solve the Markov chain, this initial vector of probabilities was solved in time through a system of ordinary differential equations which act at the probabilistic level. The kinetics of probability changes are governed by the chemical master equation, and therefore relate to easily to the inherent “solution” parameters by normalization coefficients such as area

and concentration. The fraction of PDD bonds correlated very well with catch-bond behavior (Figure 34B-I). Because there is significant noise due to the stochasticity of the assay (discussed in future sections), combining the data sets into positively or negatively selecting ligand groups revealed interesting trends. The PDD fraction of slip bond ligands showed a relatively mild response to force (Figure 34J). Interestingly, ligands with catch-bonds showed a more dynamic response (Figure 34K); CD8.4 responses were more pronounced and stronger (Figure 34L).

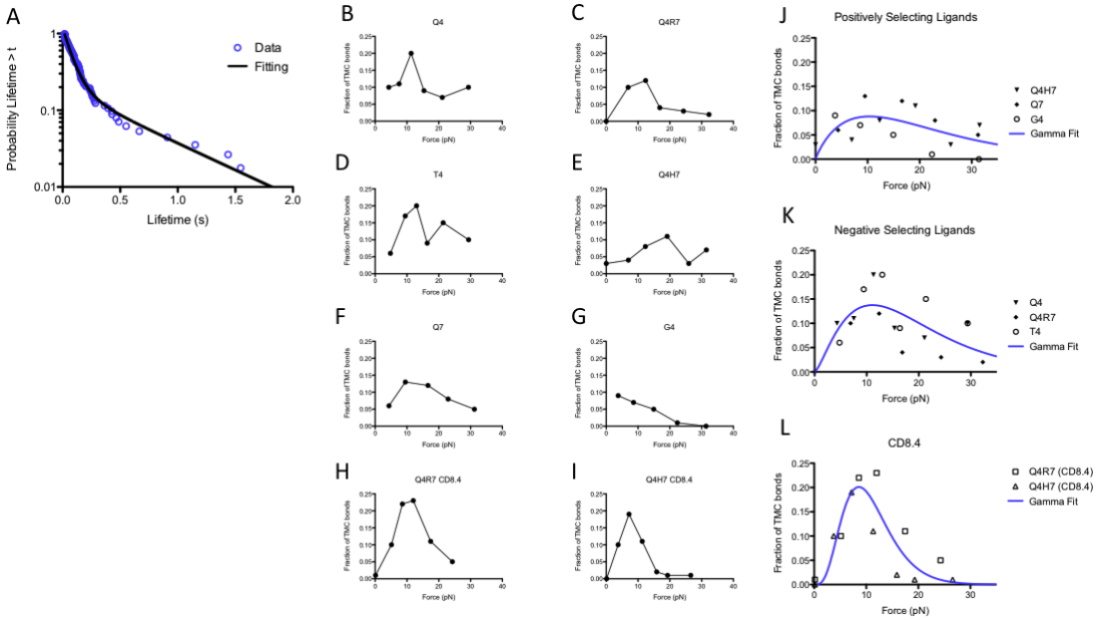

Figure 34. Fraction of PDD bonds correlates with catch-bond behavior.
(A) Markov chain fitting of 12pN bin of Q4H7 vs. CD8.4 OT-1 thymocytes. (B-I) Markov chain prediction of fraction of PDD bonds vs. force for wild-type OT-1 thymocytes against negatively-selecting ligands (B-D), positively-selecting ligands (E-G), and CD8.4 OT-1 thymocytes against negatively selecting ligands (H,I). (J-L) Combined Markov chain fitting data for all positively selecting ligands (J), negatively selecting ligands (K), and CD8.4 thymocytes vs. negatively selecting ligands (L). Fit with a Gamma distribution to show apparent trend (blue line).

6.4 Model and simulations on proposed mechanism explain experimental data

6.4.1 Proposed mechanism for catch-bond behaviour in thymocyte selection

Previous analyses suggest that force provokes PDD bond formation; it is not a passive response governed through diffusive processes. For several reasons outlined below, we believe that TCR and CD8 may form complexes, one or more CD8s conjugating to a single TCR, on the surface of T cells over time. For the sake of simulation and conceptual simplicity, we will refer to this complex as a heterodimer or dimer. This heterodimer is the result of TCR mechanotransduction.

1) The application of mechanical force on TCR triggers signaling [88, 90-93].
2) TCR is especially responsive when pulled to a force of approximately 10pN [92]. Interestingly, this coincides with the PDD fraction peak (Figure 34J-L).
3) Lck is a proximal signaling kinase in TCR signaling [61]. Lck inhibitor blocked catch-bond formation in negatively-selecting ligands.
4) Coreceptors are initially separated from TCR islands which converge with TCRs upon TCR stimulation [109, 147]. This separation changes as T cells mature to increase sensitivity [148]. This effect would decrease the diffusion limitations outlined in Section 6.3 over time.
5) CD8 showed increased FRET signaling with CD3 upon APC stimulation [109], suggesting that CD8 and CD3(TCR) come in close contact after T cell stimulation. Additionally, CD3 antibody stimulation indicated stimulation-induced association of CD8/CD4 coreceptors to TCR by co-IP [144, 145].

Therefore, we suggest the following model to explain the catch-bond behavior in thymocyte negative selection, outlined in Figure 35. The thymocyte begins at an initial

state where TCR and CD8 are separated on the cell surface and the CD3 tails for Lck binding are buried in the membrane. If there is no force on a TCR bond or a CD8 bond is pulled, no signaling occurs (Figure 35A, No Signaling path) and the cell maintains the initial state. However, if a TCR is pulled, signaling occurs (summarized in Figure 35B), tails of nearby CD3 molecules are released from the membrane and phosphorylated, and TCR forms TCR:CD8 dimers through the interaction of Lck with CD3 (Figure 35A, Signaling path). It then has the ability to overcome diffusion limitations and form periods of upregulated bond lifetimes in the BFP assay through PDD formation.

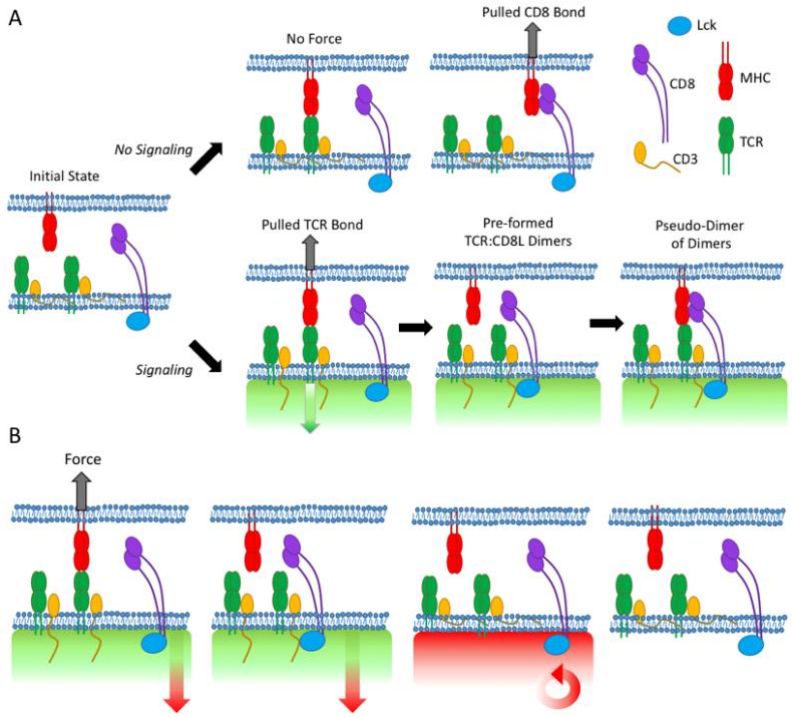

Figure 35. Proposed mechanism for catch-bond behavior in thymocyte negative selection

(A) Thymocyte membrane interactions. Thymocytes activate signaling upon TCR pulling which promotes release of CD3 tails into cytosol. These tails bind to Lck on the CD8 tails, leading to pre-formed TCR:CD8(Lck) dimers which have the capacity to for PDD bonds. (B) Signaling interactions. Once TCR is pulled by a pMHC interaction, signaling occurs proximal to the TCR in the form of Lck (green shading). Additionally, the release of the tails promotes generic phosphatase activity (red shading) which builds to suppress Lck kinase activity, resulting in thymocyte reversion to initial state.

This proposed mechanism corresponds with the outcomes of the data analyses and the literature. It combines aspects of TCR mechanotransduction, proximal signaling, and transient species deviations. In the next section, we will simulate this behavior and compare its results to the BFP data to explain the mechanism behind catch bonds in thymocyte negative selection.

6.4.2 Simulations on proposed mechanism

First, an algorithm was developed to simulate the results of the BFP assay. BFP is a unique assay in that there is a significant element of stochasticity to bond formation – different bonds can be pulled, at different times, for different durations – measured sequentially to output the static representation of a lifetime vs. force curve. The algorithm is outlined in Figure 36. It begins by initializing the two surfaces – thymocyte and bead – with their respective molecular densities, kinetics, and other inputs. The simulation models the contact between cell and bead by permitting transmembrane interactions for a period of time. After the contact period, the simulation determines presence, or lack, of a bond and its species. If the bond does not survive pulling or there is no bond, no lifetime is recorded and the system transitions to a waiting time module where signalling and modifications are permitted, but no transmembrane interactions can be formed (i.e. no binding to MHC). If the bond survives pulling, a lifetime is selected from the survival distribution for that bond and recorded. The thymocyte may signal during this time to modify the TCR for CD8 binding and activate Lck or phosphatase. After the bond time is finished, the simulation returns to the waiting time model. This can be repeated many times to create a sequence of bond lifetimes for a single cell-bead pair. In essence, this reflects the process of approach-contact-pull-clamp-wait cycle of the BFP force-clamp assay.

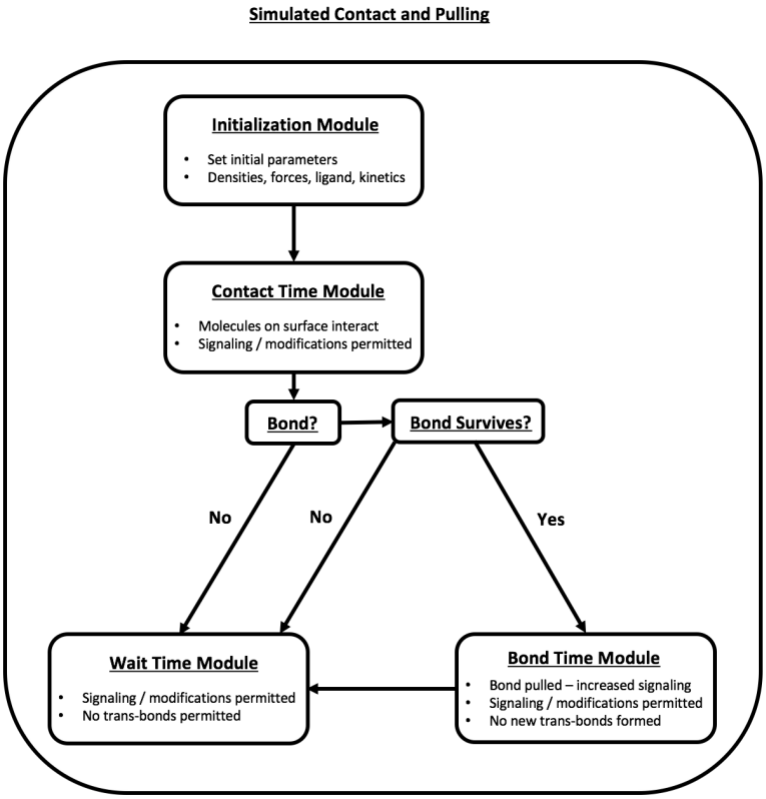

Figure 36. BFP simulation algorithm flow diagram
The algorithm begins at the initialization module and proceeds in the direction indicated by the arrows. Each module is outlined in a rectangle. This can be repeated many times in sequence to replicate the experimental conditions of the micropipette assay.

Several different methods are used to evaluate the modules presented in the algorithm. The contact time, waiting time, and bond time modules are solved through a system of ordinary differential equations (ODEs) representing the first or second order interactions outlined in Figure 37 and solved with the ode45 function in Mathworks Matlab (R2015b). The probability of bond formation at the end of contact is determined from the total average number of bonds from the ODE system and assuming a Poisson model of the number of binding events [123]. The bond type is governed by weighted random selection from the relative fractions of bonds at the end of contact. Bond pulling survival probability was determined by integrating the expression for the rupture probability distribution at a

given ramping rate [149] to the clamping force. The bond lifetime was selected from the Markov chain (Figure 33) by setting the appropriate initial species vector. The kinetics of individual interactions under force were determined through fitting to the Bell model [146].

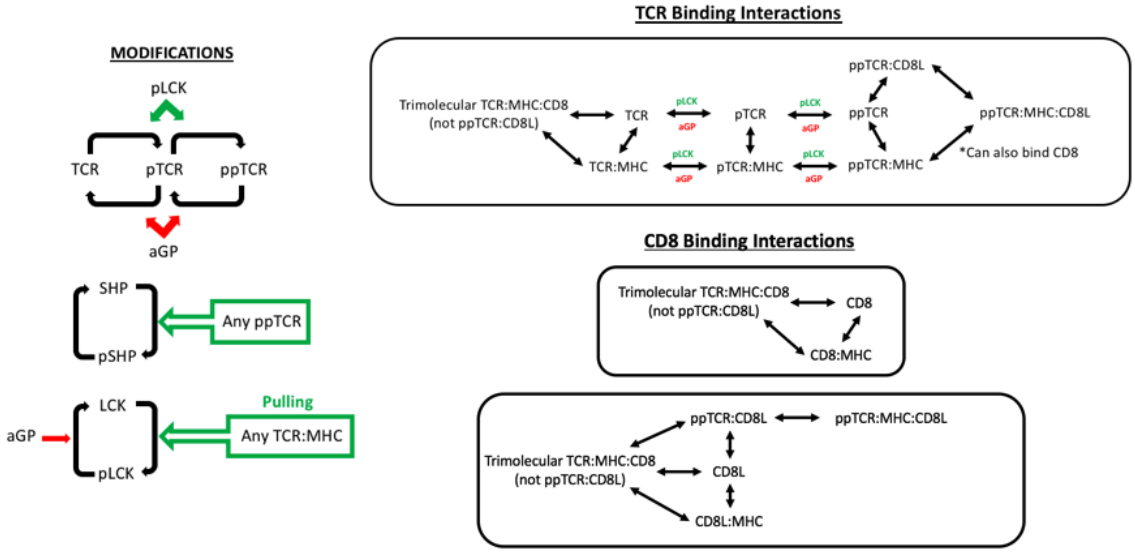

Figure 37. Outline of system interactions

Parameters for the model are outlined in Table 7. Most the values are experimental conditions or measured by other assays. Others were selected from the appropriate literature or estimated.

Table 7. Simulation parameters for CD8 thymocyte binding mechanism

Parameter	Value	Source
Number of contacts	200	experimental condition estimation - can vary
Contact time	0.1 s	experimental condition
Waiting time	0.25 s	experimental condition estimation - can vary slightly
Initial adhesion frequency	0.2	experimental condition estimation, used to calculate MHC density
Contact Area	1 um^2	experimental condition estimation
Pulling rate	200 pN/s	measured
TCR density	8 TCR/um^2	measured
MHC density	311 CD8/um^2	measured
Lck density	20 Lck/um^2	from Altan-Bonnet, et al. Plos Bio 2005, naïve cells
GP density	530 molec/um^2	from Shp Altan-Bonnet, et al. Plos Bio 2005
Fraction CD8:Lck	n/a	varies depending on condition
On rate CD8:MHC	$4x10^{-5}$ um^2/s	measured
Off rate CD8:MHC	7.84 s^{-1}	measured
Nominal force (Bell model) for CD8:MHC	21.9pN	measured
On rate TCR:MHC	n/a	measured, varies depending on condition
Off rate TCR:MHC	n/a	measured, varies depending on condition
Nominal force (Bell model) for TCR:MHC	n/a	measured, varies depending on condition
On rate Lck:CD3	10^{-3} um^2/s	estimated high affinity from Li, et al. PNAS 2017
Off rate Lck:CD3	0.1 s^{-1}	estimated slow off rate from Li, et al. PNAS 2017
Phosphorylation CD3 by Lck	0.03 um^2/s	estimated to fit lifetime data
Activation of GP by fully active TCR	0.01 um^2/s	estimated very fast
Deactivation of GP (CD3/Lck)	0.01 um^2/s	estimated very fast
Avidity binding enhancement (TCR:CD8 dimers)	100	estimated
Trapping ehancement (CD8/TCR bound, binding of other)	10	estimated
Proximity rebinding enhancement (TCR:CD8:MHC:Lck)	1500	estimated to fit survival data

The TCR signaling capacity requires a force-induced response. To estimate an appropriate function for this response, we looked to the catch-bond-like shape of the fraction of PDD bonds with force. The response fit very well to a gamma distribution (Figure 34). Additionally, several studies have indicated that T cells have a specific cellular response to force through their TCR [92, 93]. An optimal force is required on the TCR through the MHC to produce adequate downstream calcium flux; forces falling outside this range, whether higher or lower, do not signal. For these reasons, we decided to use the gamma function to approximate TCR mechanotransduction. The activation of Lck was given a response governed by the force on the TCR:pMHC bond (Figure 38). Other parameters were either measured, taken from literature, estimated, governed by assay conditions, or fit to data trends (see Experimental materials and methods, Table 7).

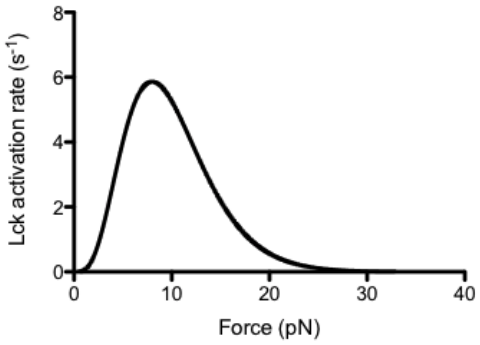

Figure 38. TCR:pMHC force induced Lck activation function

To examine the trends of the simulations on catch bond behavior, we focused on two ligands on the edges of the selection threshold for the wild-type OT-1 system, Q4H7 (positively selecting ligand) and Q4R7 (negatively selecting ligand). Simulation trends matched the experimental data trends very well (Figure 39). With low amounts of CD8:Lck conjugation (wild-type OT-1 thymocytes) Q4H7 simulations showed a slip bond, while Q4R7 simulations showed a catch bond behavior. If the only the fraction of CD8:Lck conjugation was increased while all other parameters remained the same, Q4H7 shifted its behavior to a catch bond, and Q4R7 made a much stronger catch bond (Figure 40). This is consistent with the experimental data.

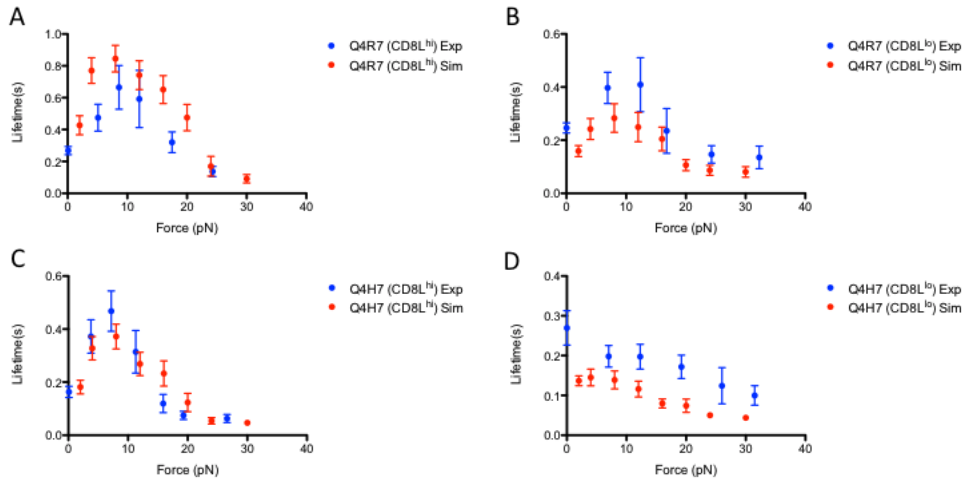

Figure 39. Simulated vs. Experimental thymocyte lifetime vs. force
Experimental (blue circles, error bars represent standard error) vs. Simulation (red circles, error bars represent 95% CI) force vs. lifetime curves for high Q4R7 with high (A, CD8.4) or low (B, wild-type CD8) CD8:Lck conjugation, and Q4H7 with high (C, CD8.4) or low (D, wild-type CD8) CD8:Lck conjugation.

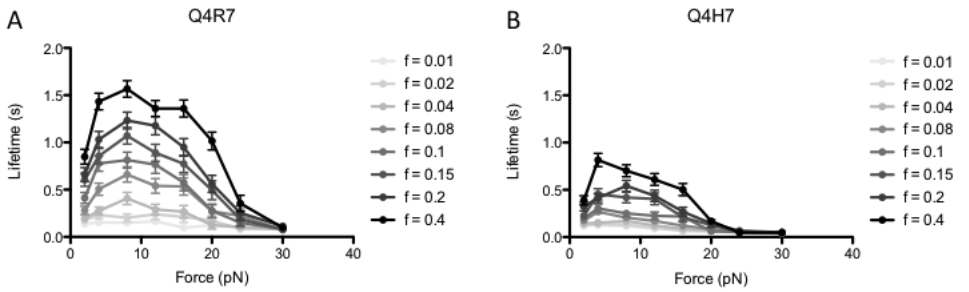

Figure 40. Simulated BFP data indicates high Q4R7 sensitivity to mechanism
BFP data was simulated varying the CD8:Lck conjugation fraction (f) for Q4R7 (A) and Q4H7 (B). Gradient towards black indicates direction of increasing f. Error bars represent 95% CI.

6.5 Discussion and future studies

Significant technical constraints limit the interpretation of BFP data in the context of multiple-bond interactions such as in the CD8-TCR-MHC system. This difficulty begins with the fact that many different bonds can be formed, and any bond under force could be

one of many different species, even switching between states after the bond is clamped. Because the assay only measures bond lifetime and force levels, the type of bond, whether it be TCR:MHC, CD8:MHC, trimolecular, etc., cannot be determined. Compiling the data into lifetime vs. force curves provides some interpretation of the system mechanisms, but binning data loses a significant portion of information. Basic intuition reasons that force increases bond lifetime, thereby permitting more time for signal processing by the cell. However, due to the complexity of multiple bond types, this type of analysis falls short. By including some of this lost information in the form of survival distribution analysis, we have revealed a new mechanism in the TCR:CD8:MHC system and elucidated the origins of the thymocyte catch-bond behavior.

The situation of antigen presentation in the thymus is much different from the BFP assay. For example, the BFP assay limits pMHC density to maintain a low binding frequency; this maintains single bond pulling. Only a single bond is pulled at a time whilst other TCR:pMHC interactions are not permitted. Only one pMHC species is present in the assay. In contrast, thymic antigen presentation allows multiple TCR:pMHC interactions to occur simultaneously with many different pMHC species, random or differential waveforms in mechanical bond loading, interactions with cytokines and other receptors, and all the additional complexities of *in vivo* cell-cell interactions. Nevertheless, the high resolution and control afforded by the BFP assay provides a unique platform for highly-controlled probing of the cell, resulting in insights into thymic TCR antigen recognition otherwise unattainable through conventional approaches.

The analysis on the BFP data presented in this chapter implicates TCR:pMHC forced-induced binding of CD8:Lck to TCR for longer lifetimes and antigen processing

(Figure 35). This new mechanism has many implications in thymic selection. Most coreceptor mechanism research has relied on non-thymocytes, but the mechanisms occurring at the thymocyte level are likely similar. In support of this mechanism, similar coreceptor CD4 (also conjugated to Lck) became more proximal to TCR after stimulation in primary T cell blasts [147]. Similarly, different ligands recruit CD8 to the immunological synapse with different time delays, with weaker ligands taking longer than stronger ligands, but approximately to the same level [150]. Casas and colleagues showed CD3 and CD8 increased FRET signaling after T cell hybridoma stimulation by APCs [109]. Interestingly, they showed that this proximity change relied on CD8:Lck conjugation, as mutants removing the binding site eliminated the increase. However, the coreceptor-scanning concept, that a TCR:pMHC bond must last long enough to "scan" coreceptors for one bound to Lck for efficient signaling transmission, has gathered wide support [111, 112]. Figure 30 indicates this mechanism is unlikely to explain the BFP data. The mechanism presented in this study was not previously fathomable due to the nature of the assays, but it is still consistent with their experimental data. The analysis presented here does not exclude coreceptor scanning from contributing, albeit to a lesser degree.

There are several implications of the proposed mechanism, outlined below.

1) CD8:Lck conjugation regulates antigen sensitivity by TCR:CD8 conjugation capacity. In the BFP assay, conjugation controls the capacity of TCR and CD8:Lck to form dimers independent of direct pMHC contact. *In vivo*, the situation would be similar. Weak bonds would not elicit much response, but once a strong bond is pulled, CD8 and TCR would begin dimerization. A higher CD8:Lck fraction would allow more TCR-CD8 dimerization, increased pMHC sampling and higher

likelihood of rebinding that same antigen. It has previously been shown that this fraction varies between T cell subtypes [101, 148]. This indicates a control point for antigen sensitivity amplification.

2) Control over the non-kinase binding of Lck to TCR(CD3) is critical. Phosphorylation of ITAMs by Lck modifies their charge and negates membrane sequestration of the tails which contain a basic residue sequence for Lck unique domain motif binding [49, 151]. Because this is a recently discovered interaction, control mechanisms are currently unknown, but Lck conformational states changes by phosphorylation or modifications due to CD8 binding are likely candidates. There is also significant evidence that CD3 ITAM-bound ZAP-70 mediates the interaction with Lck(CD8) [144, 145, 152]. The nature of the simulations does not preclude this interaction – Lck activation of TCRs could lead to ZAP-70 recruitment, which would require one additional linear TCR modification to the model and therefore not change the outcome. Dissemination of these two possibilities could be a focal point for future research.
3) Intracellular signaling dynamics controls CD3 tail stabilization and TCR-CD8 dimerization. Lck is a likely candidate for stabilization due to its kinase activity. However, the generic phosphatase presented in the model is unknown. Likely candidates include Shp-1 or Shp-2 [52, 83, 84]. The interaction networks for these phosphatases are tightly controlled systems regulated by many different receptors and other signaling molecules [153].
4) The proposed mechanism results in periods of TCR-CD8 dimerization, followed by dissociation and desensitization due to low bond number and lack of continuous

stimulation during the BFP assay. There is some evidence for this from the BFP data, but the data is not conclusive and more statistical analyses are required. *In vivo*, it would likely manifest as a stochastic and fast increase in dimerization which, depending on the amount of antigen present, may not contain a desensitization period if there is sufficient stimulation.

5) This mechanism produces a second layer of regulation to the initial TCR triggering process. In effect, the TCR triggering occurs first, followed by TCR:CD8 dimerization. This process induces an upregulated binding state for antigen recapture, similar to rebinding models discussed in Section 2.3.3. Therefore, a single TCR-pMHC interaction can trigger the response, but more TCR interactions are likely necessary for prolonged signaling and full T cell activation.

There are several limitations to the simulation-based analysis presented in this chapter. First, it is difficult to control aspects of membrane organization in simulations due to computational resource constraints. This analysis does not preclude the possibility of membrane spatial control – i.e. if TCR force dynamics result in changes to the spacing between TCR and CD8, decreasing the effective binding rates. However, there must be some control over either there spacing or kinetics which is induced by force on a TCR:pMHC bond. In the simulations, this mechotransduction was produced through Lck activity, and is the most likely candidate at this time. Lck activity upregulates after TCR simulation, possibly through kinetic segregation methods (Section 2.3.2), but the exact mechanism is not known at this time. Additional studies are required to elucidate more about this mechanotransduction mechanism. Secondly, there are many parameters drawn from relevant literature, but the model was fit exclusively to two parameters – the interplay

between TCR-induced Lck activation and the generic phosphatase rates. Small changes to these parameters results in significant changes to the magnitude of the response. Therefore, it is important to note that the simulation results are indicative of larger trends resulting from the mechanism rather than a definitive quantitative description.

In this chapter, we have presented the first evidence that mechanical forces on TCRs by pMHC can trigger a second level of antigen sensitivity regulation by inducing TCR and CD8 to dimerize through Lck:CD3 conjugation in thymocytes. Future studies will focus on validating this mechanism either by evidence of periods long-bond formation using the HAFM in its force-clamp capacity or direct evidence of CD8-TCR proximity changes after TCR mechanotransduction using FRET techniques and/or super-resolution microscopy cross-correlation analyses.

CHAPTER 7. CONCLUSIONS AND FUTURE DIRECTIONS

Fixed kinetic rates are considered in nearly every analysis of TCR triggering and activation [71, 79-83, 85, 111]. In this study, we have shown several pieces of evidence that indicate that the kinetics governing the TCR antigen recognition process are much more complicated than originally conceived. In the absence of sustained force, TCRs upregulate their kinetics for fast intervals upon initial antigen recognition. Pharmacological intervention revealed that the most proximal TCR signaling molecules, Lck and cholesterol, play a significant role in regulating these periods. Additionally, mechanical force exerted on the TCR through pMHC recruits CD8 to proximal TCRs, inducing further sensitivity changes over time. This mechanism increases antigen capture as well as extends lifetime for proofreading.

Although not studied directly in this work, these two mechanisms intersect on many levels. Both mechanisms involve Lck signaling and specific membrane organization. Both mechanisms develop in response to initial antigen recognition. Both mechanisms increase sensitivity for antigen recapture, both while maintaining ample discrimination capabilities. There are many basic questions that come from these mechanisms: At what level are these mechanisms controlled – DNA, microenvironment, other receptors? Is ligand memory impacted by mechanical forces similar to CD8? Which mechanism is more dominant during which stages of antigen recognition? These questions expose important challenges in informing therapeutic treatments. For instance, if we understand how these mechanisms controlling sensitivity are modulated in the human body, we can develop therapeutics targeting control points for either enhanced or suppressed T cell activation – an effect that

can be critical for pathogen clearance or limiting autoimmune damage, respectively. Additionally, a better understanding of these mechanisms would lead to more informed treatments. If TCR ligand memory is critical at the tonic signaling level, suppression would lead to cell death; however, if TCR force-induced CD8 recruitment follows, then suppression of this mechanism, while not affecting TCR ligand memory, would allow for cell survival but decreased TCR sensitivity. The sequencing of these mechanisms and their respective interactions is therefore critical for translational research and should be a focus of future studies.

This work directly couples with antigen recognition in T cells; however, it also revealed the possibility of new mechanisms underlying other ligand-receptor binding interactions. Although not shown in these studies, several other receptor-ligand systems showed a positive memory index, and others exhibited changes to binding quality over time due to mechanotransduction. The unique assays used to parse these mechanisms are tedious and require extensive training, unlike many standardized techniques available today, such as flow cytometry and blotting techniques. Therefore, it is unlikely that all receptor-ligand interactions can be probed at this level; even the studies presented here provide an incomplete picture. However, these mechanisms should be considered in the interpretation of systems requiring high sensitivity and discrimination; they likely rely on multiple layers of regulation originating from the first few binding events, and not wholly on signaling pathways.

APPENDIX A. MATLAB CODE FOR SIMULATION OF TCR MEMORY MECHANISM

A.1 Code for cholesterol binding model

```
% Simulate the micropipette binding assay
% Create files outputting the adhesion frequency for each cluster over
time
% Written by William Rittase

clearvars; close all

%% Inputs
n_times = 20; % number of cell pairs to simulate
n_touches = 300; % number of touches per cell pair
s = 120; % number of Latin hypercube divisions
export_folder = 'insert folder string';

%% Input necessary folders
functionPath = 'insert folder string';

addpath(functionPath)

%% Micropipette conditions
tc = [0.25,5]; % contact time min and max
tw = [1,6]; % waiting time min and max
Ac = 1; % simulation contact area

mT = 108; % density TCR
mM = 2700; % density MHC

n_clusters_to_sim = round(mT*Ac/13.5); % number of clusters in each
cell pair

%% Cluster probability distribution
minClustSize = 7;
maxClustSize = 20; % maximum cluster size from Davis paper
clust_area_ratio = 0.07;
r_t_ratio = pi*clust_area_ratio^2/maxClustSize; % maximum cluster area
from Davis paper, 70nm radius (assume 20 TCRs)

%% Binding Parameters

D = 0.001; % diffusion constant in um^2/s

% Scanning parameters (to be fit from statistical model)

kt_f_norand = logspace(-8,-5,s); % on rate for TCR:MHC binding
```

```
kt_r_norand = logspace(-1,1,s); % off rate for TCR:MHC binding

ktx_r_norand = logspace(-2,2,s); % off rate for xTCR:MHC binding

ktx_f_norand = logspace(0,3,s); % on rate for xTCR:MHC binding

kd_norand = logspace(-2,2,s); % transformation constant -> reversion
from xTCR to TCR cluster

kc_norand = logspace(-2,2,s); % conversion rate for cluster TCR -> xTCR

%% Inport v and R vectors
v = xlsread('v_6.xlsx');
R_start = xlsread('R_6.xlsx');

%% Species vector (m)
% 1: TCR, unbound low affinity TCR
% 2: TCRx, unbound higher affinity TCR
% 3: TCR:MHC, bound TCR:MHC, no phos
% 4: TCRx:MHC, bound TCR:MHC, phos
% 5: MHC, unbound MHC
% 6: Placeholder, always 1: used for diffusion of MHC, conversion of
% cluster (reactions 5 and 6)

% Get from get_molec_species_modelx

bonds = logical([0,0,1,1,0,0]); % which species are bonds

%% Kinetic vector (k)
% 1: TCR:MHC binding
% 2: TCR:MHC unbinding
% 3: TCRx:MHC binding
% 4: TCRx:MHC unbinding
% 5: Conversion coefficient (coverting cluster TCR->xTCR)
% 6: Degrading coefficient (coverting cluster xTCR->TCR)
% 7: MHC diffusion out
% 8: MHC diffusion in

% Get from get_kinetics_parameters_modelx

%% Randomize parameters
kt_r_scan = kt_r_norand(randperm(length(kt_r_norand)));
kt_f_scan = kt_f_norand(randperm(length(kt_f_norand)));
kc_scan = kc_norand(randperm(length(kc_norand)));
ktx_f_scan = ktx_f_norand(randperm(length(ktx_f_norand)));
ktx_r_scan = ktx_r_norand(randperm(length(ktx_r_norand)));
kd_scan = kd_norand(randperm(length(kd_norand)));

for i = 1:s % for each scanning condition
    kt_r = kt_r_scan(i);
    kc = kc_scan(i);
    kd = kd_scan(i);
    kt_f = kt_f_scan(i);
```

```
    ktx_f = ktx_f_scan(i)*kt_f;
    ktx_r = kt_r*ktx_r_scan(i);

    for n1 = 1:n_times

        af = zeros(n_clusters_to_sim,n_touches);
        ct = (tc(2)-tc(1))*rand(1,n_touches)+tc(1);
        wt = (tw(2)-tw(1))*rand(1,n_touches)+tw(1);

        tic

        for n2 = 1:n_clusters_to_sim % for each cluster

            [m,A_clust] = get_molec_species_model6(mM, minClustSize,
maxClustSize, r_t_ratio);
            [k_on,k_off] = get_kinetic_parameters_model6(mM, kt_f,
kt_r, ktx_f, ktx_r, kc, kd, D, A_clust);

            R = R_start;

            m_start = m;

            for n3 = 1:n_touches
                % contact time
                m_on = one_touch_model6(m,k_on,ct(n3),R,v);
                % if there was a bond
                if sum(m_on(bonds)) > 0
                    af(n2,n3) = 1;
                    % break bonds
                    m = m_on;
                    m(1) = m(1)+m(3);
                    m(2) = m(2)+m(4);
                    m(3) = 0;
                    m(4) = 0;
                    m(5) = m(3)+m(4)+m(5);
                else
                    m = m_on;
                end
                % waiting time
                m = one_touch_model6(m,k_off,wt(n3),R,v);
            end
        end

        % export data to folder
        folder_now = [export_folder,'/Condition ',num2str(i),'/','Cell
Pair ',num2str(n1),'/'];

        if ~isdir(folder_now)
            mkdir(folder_now)
        end

        csvwrite([folder_now,'af'],af)
        csvwrite([folder_now,'ct'],ct)
```

```
        csvwrite([folder_now,'wt'],wt)

        disp(['s = ',num2str(i)])
        disp([num2str(n1),' of ',num2str(n_times),' Runs Completed.'])
        disp(['Time Elapsed = ',num2str(toc)])

    end

end

all_scanned_parameters = [kt_r_scan; kt_f_scan; ktx_r_scan; ktx_f_scan;
kc_scan; kd_scan];

csvwrite([export_folder,'/all variables'],all_scanned_parameters)
```

A.2 Code for get kinetic parameters function

```
function [k_on,k_off] = get_kinetic_parameters_model6(mM, kt_f, kt_r,
ktx_f, ktx_r, kc, kd, D, A_clust)
% use this function to output the kinetic parameters vector for solving
the
% SSA

% Output kinetics format (k_on or k_off where on = cells in contact,
off =
% cells not in contact)
% 1: TCR:MHC binding
% 2: TCR:MHC unbinding
% 3: TCRx:MHC binding
% 4: TCRx:MHC unbinding
% 5: Conversion coefficient (coverting cluster TCR->xTCR)
% 6: Degrading coefficient (coverting cluster xTCR->TCR)
% 7: MHC diffusion out
% 8: MHC diffusion in

%% k_on

    k_on = zeros(1,8);

    k_on(1) = kt_f/A_clust;
    k_on(2) = kt_r;
    k_on(3) = ktx_f/A_clust;
    k_on(4) = ktx_r;
    k_on(5) = kc;
    k_on(6) = kd;

    Mavg = mM*A_clust; % average MHC in cluster

    k_on(7) = D/A_clust; % diffusion rate out

    k_on(8) = k_on(7)*Mavg; % diffusion rate in

%% k_off
```

```
    k_off = zeros(1,8);

    k_off(1) = 0;
    k_off(2) = 0;
    k_off(3) = 0;
    k_off(4) = 0;
    k_off(5) = 0;
    k_off(6) = kd;

    Mavg = mM*A_clust; % average MHC in cluster

    k_off(7) = D/A_clust; % diffusion rate out

    k_off(8) = k_on(7)*Mavg; % diffusion rate in

end
```

A.3 Code for one touch function

```
function m_out = one_touch_model6(m,k,t_max,R,v)
% simulate one touches using input vectors and kinetics for time t
% m = species vector
% k = kinetics vector
% t_max = contact/waiting time
% R = proportions required for ssa evalulation
% v = species change vector

t = 0;
stop = 0;

n = 0;

while stop == 0

    n = n+1;

    [m_new,dt,rxn] = ssa_model6(m,v,k,R);

    if t+dt > t_max % if time is exceeded, stop and output
        m_out = m;
        stop = 1;
    elseif (t+dt < t_max) && (rxn ~= 5) && (rxn ~= 6)
        m = m_new;
        t = t+dt;
    elseif rxn == 5 % if conversion of cluster from TCR to xTCR
        m(2) = m(1);
        m(1) = 0;
        m(4) = m(3);
        m(3) = 0;
        R(6,end) = 1; % need to change R so that degrading is in
    elseif rxn == 6 % if conversion of cluster from xTCR to TCR
        m(1) = m(2);
```

```
        m(2) = 0;
        m(3) = m(4);
        m(4) = 0;
        R(6,end) = 0; % need to change R so that degrading is out
    end

end

end
```

A.4 Code for SSA function

```
function [Xnew,dt,iEvent] = ssa_model6(X,v,k,R)
% Perform the stochastic simulation algorithm from Gillepsie and output
new
% species vector and rate constant vector
% X is species vector
% k is kinetics vector
% v is change of species vector
% R is species vector for propensities determination

P = zeros(size(k));

for i = 1:length(k)
    Ri = R(i,:);
    ri = Ri > 0;

    if sum(ri)>0

        P(i) = k(i) * prod(X(ri).*Ri(ri));

    end
end

Psum = cumsum(P);
dt = - log(rand)/Psum(end); % time step for next reaction
r = rand*Psum(end);
iEvent = length(Psum(Psum<r))+1; % choose reaction that fires

Xnew = X + v(iEvent,:);

end
```

A.5 Code for model evaluation script

```
% Use the outputs from cholester binding model to determine the
adhesion
% frequency
% Make sure to change data_folder to export_folder from cholesterol
binding
% model
```

```
clearvars

%% Inputs
n_cond = 120;
n_times = 20;
n_clusters_to_sim = 8;

%% Necessary folders

data_folder = 'insert folder string';

%% Begin af evaluation for each condition
for i = 1:n_cond
    af_all = [];
    wt_all = [];
    ct_all = [];

    current_folder = [data_folder,'Condition ',num2str(i),'/'];

    for j = 1:n_times
        current_folder_cp = [current_folder,'Cell Pair
',num2str(j),'/'];

        % read simulation data files from current folder cp (cell pair
        % designation)

        af_now = csvread([current_folder_cp,'af']); % adhesion
frequency for each cluster
        wt_cp = csvread([current_folder_cp,'wt']); % wating times for
cell pair
        ct_cp = csvread([current_folder_cp,'ct']); % contact times for
cell pair

        % Determine actual adhesion frequency for cell pair based on
all
        % the clusters - if one cluster is bound, then a binding event
        % occurred

        afs_now = sum(af_now,1);
        af_cp = afs_now>0; % cell pair adhesion frequency

        % Put together data sets
        af_all = [af_all;af_cp];
        wt_all = [wt_all;wt_cp];
        ct_all = [ct_all;ct_cp];

    end

    csvwrite([current_folder,'af_all'],af_all)
    csvwrite([current_folder,'ct_all'],ct_all)
    csvwrite([current_folder,'wt_all'],wt_all)

end
```

A.6 Code for memory index evaluation and plotting script

```
% Evaluate the adhesion frequency from model_evaluation_af to extract
% memory index
% Make sure to change the data_folder to contain output from model
% evalulation

clearvars

%% Inputs
n_cond = 120;
n_times = 20; % equivalent to n cell pairs
af_plot = 0; % if plotting distribution for adhesion frequency
dp_plot = 0; % if plotting distribution
af_vs_dp_plot = 1;

%% Necessary folders

data_folder = 'insert folder string';

%% Storage

dp = zeros(n_cond,n_times);
af = zeros(n_cond,n_times);

%% Go condition by condition
for i = 1:n_cond
    % Import data
    current_folder = [data_folder,'Condition ',num2str(i),'/'];
    af_folder = csvread([current_folder,'af_all']);

    % Go cell pair by cell pair
    for j = 1:n_times
        af_now = af_folder(j,:);
        % for each touch after the first,
        n11 = 0;
        n10 = 0;
        n01 = 0;
        n00 = 0;
        for k = 2:length(af_now)

            if af_now(k) == 1
                if af_now(k-1) == 0
                    n01 = n01+1;
                else
                    n11 = n11+1;
                end
            elseif af_now(k) == 0
                if af_now(k-1) == 0
                    n00 = n00+1;
                else
                    n10 = n10+1;
                end
            end
```

```
        end

        p11 = n11/(n10+n11);
        p01 = n01/(n01+n00);

        dp(i,j) = p11-p01;

        af(i,j) = mean(af_now);

    end

end

dp = dp';
af = af';

csvwrite([data_folder,'dp_all'],dp)
csvwrite([data_folder,'af_all'],af)

dp_mean = mean(dp,1);
af_mean = mean(af,1);

scanned_parameters = csvread([data_folder,'all variables']);

if dp_plot == 1
    subplot(3,2,1)
    scatter(scanned_parameters(1,:),dp_mean)
    title('kT_r')
    a = gca;
    a.XScale = 'log';

    hold all

    subplot(3,2,2)
    scatter(scanned_parameters(2,:),dp_mean)
    title('kT_f')
    a = gca;
    a.XScale = 'log';

    subplot(3,2,3)
    scatter(scanned_parameters(3,:),dp_mean)
    title('kTx_r')
    a = gca;
    a.XScale = 'log';

    subplot(3,2,4)
    scatter(scanned_parameters(4,:),dp_mean)
    title('kTx_f')
    a = gca;
    a.XScale = 'log';

    subplot(3,2,5)
    scatter(scanned_parameters(5,:),dp_mean)
```

```
    title('k_c')
    a = gca;
    a.XScale = 'log';

    subplot(3,2,6)
    scatter(scanned_parameters(6,:),dp_mean)
    title('k_d')
    a = gca;
    a.XScale = 'log';
end

if af_plot == 1
    subplot(3,2,1)
    scatter(scanned_parameters(1,:),af_mean)
    title('kT_r')
    a = gca;
    a.XScale = 'log';

    hold all

    subplot(3,2,2)
    scatter(scanned_parameters(2,:),af_mean)
    title('kT_f')
    a = gca;
    a.XScale = 'log';

    subplot(3,2,3)
    scatter(scanned_parameters(3,:),af_mean)
    title('kTx_r')
    a = gca;
    a.XScale = 'log';

    subplot(3,2,4)
    scatter(scanned_parameters(4,:),af_mean)
    title('kTx_f')
    a = gca;
    a.XScale = 'log';

    subplot(3,2,5)
    scatter(scanned_parameters(5,:),af_mean)
    title('k_c')
    a = gca;
    a.XScale = 'log';

    subplot(3,2,6)
    scatter(scanned_parameters(6,:),af_mean)
    title('k_d')
    a = gca;
    a.XScale = 'log';
end

if af_vs_dp_plot == 1
    scatter(af_mean,dp_mean)
    xlabel('Adhesion Frequency')
    ylabel('Memory Index')
```

```
end
```

APPENDIX B. MATLAB CODE FOR MARKOV CHAIN SURVIVAL DISTRIBUTION FITTING

B.1 Code for fitting algorithm

```
% Run best fit for species holding kenh constant
% Assume it starts in variable state
% Fit distribution, not average lifetime

% Written by William Rittase
% January 23, 2018

% Important outputs:
% fracTMC_best: best fitting fraction of PDD bonds, fracTMC_best is a
cell
% vector with fracTMC_best{i} containing the best fit solutions for
% file{i}. See scan_model_check_hold_kenh function for contents of
% fracTMC_best{i}
% pBest: best survival distributions probabilities, pBest is a cell
vector
% with pBest{i} containing the best fit solutions for file{i}. See
% scan_model_check_hold_kenh
% tBest: best survival distributions times, pBest is a cell vector
% with pBest{i} containing the best fit solutions for file{i}. See
% scan_model_check_hold_kenh

clearvars; close all

%% Add data and function paths
dataPath = 'input folder for data';
functionPath = 'input folder for functions';
scriptsPath = 'input folder for scripts';

addpath(dataPath)
addpath(functionPath)
addpath(scriptsPath)

%% Inputs (starting probabilities vector)

numCond = 8;
fracTMC_best = cell(numCond,1);
tBest = cell(numCond,1);
pBest = cell(numCond,1);
F = cell(numCond,1);
names = cell(numCond,1);

n = 0;

%% wQ4
```

```
file = 'wQ4';
n = n+1;
[F{n},~,~,~,~,~,~] = readData_v3(file);

% Kinetic rates (force-free)
kf_tm = 0.0000899378/6;
kr_tm = 4.22;
f_T = 30.2;
% Initial condition
fracTMC_ic = repmat(0.2,length(F{n}),1);

[fracTMC_best{n},pBest{n},tBest{n}] =
scan_model_check_hold_kenh(kr_tm,kf_tm,f_T,file,fracTMC_ic);
names{n} = file;

%% wQ4R7
file = 'wQ4R7';
n = n+1;
[F{n},~,~,~,~,~,~] = readData_v3(file);

% Kinetic rates (force-free)
kf_tm = 0.000135225/6;
kr_tm = 3.45;
f_T = 72.3;
% Initial condition
fracTMC_ic = repmat(0.2,length(F{n}),1);

[fracTMC_best{n},pBest{n},tBest{n}] =
scan_model_check_hold_kenh(kr_tm,kf_tm,f_T,file,fracTMC_ic);
names{n} = file;

%% wT4
file = 'wT4';
n = n+1;
[F{n},~,~,~,~,~,~] = readData_v3(file);

% Kinetic rates (force-free)
kf_tm = 0.0000592144/6;
kr_tm = 2.75;
f_T = 13;
% Initial condition
fracTMC_ic = repmat(0.2,length(F{n}),1);

[fracTMC_best{n},pBest{n},tBest{n}] =
scan_model_check_hold_kenh(kr_tm,kf_tm,f_T,file,fracTMC_ic);
names{n} = file;

%% Run wQ4H7
file = 'wQ4H7';
n = n+1;
[F{n},~,~,~,~,~,~] = readData_v3(file);

% Kinetic rates (force-free)
kf_tm = 0.0000706784/6; % fit from other data
kr_tm = 4.15; % fit from other data
```

```
f_T = 30.8;
% Initial condition
fracTMC_ic = repmat(0.2,length(F{n}),1);

[fracTMC_best{n},pBest{n},tBest{n}] =
scan_model_check_hold_kenh(kr_tm,kf_tm,f_T,file,fracTMC_ic);
names{n} = file;

%% wQ7
file = 'wQ7';
n = n+1;
[F{n},~,~,~,~,~,~] = readData_v3(file);

% Kinetic rates (force-free)
kf_tm = 0.0000457382/6;
kr_tm = 6.72;
f_T = 46.3;
% Initial condition
fracTMC_ic = repmat(0.2,length(F{n}),1);

[fracTMC_best{n},pBest{n},tBest{n}] =
scan_model_check_hold_kenh(kr_tm,kf_tm,f_T,file,fracTMC_ic);
names{n} = file;

%% wG4
file = 'wG4';
n = n+1;
[F{n},~,~,~,~,~,~] = readData_v3(file);

% Kinetic rates (force-free)
kf_tm = 0.0000542196/6;
kr_tm = 3.63;
f_T = 11.9;
% Initial condition
fracTMC_ic = repmat(0.2,length(F{n}),1);

[fracTMC_best{n},pBest{n},tBest{n}] =
scan_model_check_hold_kenh(kr_tm,kf_tm,f_T,file,fracTMC_ic);
names{n} = file;

%% wQ4R7
file = 'wQ4R7_8p4';
n = n+1;
[F{n},~,~,~,~,~,~] = readData_v3(file);

% Kinetic rates (force-free)
kf_tm = 0.000135225/6;
kr_tm = 3.45;
f_T = 72.3;
% Initial condition
fracTMC_ic = repmat(0.2,length(F{n}),1);

[fracTMC_best{n},pBest{n},tBest{n}] =
scan_model_check_hold_kenh(kr_tm,kf_tm,f_T,file,fracTMC_ic);
names{n} = file;
```

```
%% Run wQ4H7
file = 'wQ4H7_8p4';
n = n+1;
[F{n},~,~,~,~,~,~] = readData_v3(file);

% Kinetic rates (force-free)
kf_tm = 0.0000706784/6; % fit from other data
kr_tm = 4.15; % fit from other data
f_T = 30.8;
% Initial condition
fracTMC_ic = repmat(0.2,length(F{n}),1);

[fracTMC_best{n},pBest{n},tBest{n}] =
scan_model_check_hold_kenh(kr_tm,kf_tm,f_T,file,fracTMC_ic);
names{n} = file;

close all

save('bestFit_model_check_hold_kenh_var_weight')
```

B.2 Code for gathering data function

```
function [F,LT,var_LT,stderr_LT,Fstore,LTstore,pLT] =
readData_v3(dataFile)
% Read data from file dataFile and output it into a cell array
% dataFile: string with name of file
% F: F(i) is the mean force for bin i
% lt: lt(i) is the average lifetime for bin i
% var_lt: lt_var(i) is the variance of lifetime for bin i
% Fstore = cell array where Fstore{i} = forces for bin i
% LTstore = cell array where LTstore{i}(j) = lifetimes for force from
%   Fstore{i}(j)
% pLT = cell array where pLT{i}(j) = survival probability for LT{i}(j),
% ln(LT>t)


addpath('input folder for matlab data')

dataAll = load(dataFile);

dataAll = dataAll.data;

[~,y] = size(dataAll);

numForces = y/4;

F = zeros(numForces,1);
LT = zeros(numForces,1);
var_LT = zeros(numForces,1);
stderr_LT = zeros(numForces,1);
Fstore = cell(numForces,1);
LTstore = cell(numForces,1);
```

```
pLT = cell(numForces,1);

for i = 1:numForces
    istart = (i-1)*4 + 2;
    dataNow = dataAll(:,istart);

    n = length(dataNow(dataNow>0));
    data = [dataAll(1:n,istart-1),dataAll(1:n,istart)];

    F(i) = mean(data(:,1));
    LT(i) = mean(data(:,2));
    stderr_LT(i) = std(data(:,2))/sqrt(n);
    var_LT(i) = mean(data(:,2).^2) - mean(data(:,2))^2;
    Fstore{i} = data(:,1);
    LTstore{i} = data(:,2);

    pLT{i} = zeros(1,n);
    for j = 1:n
        pLT{i}(j) = (n-j)/n;
    end
end
```

B.3 Code for scanning parameter space

```
function [fracTMC_best,pBest,tBest] =
scan_model_check_hold_kenh(kr_tm,kf_tm,f_T,file,fracTMC_ic)

%% This function runs the parameter scan for PDD bond fraction
% Scans peptide data file string to find best fit for PDD bond fraction
% coefficient
% January 22, 2018
% uses readData_v3, fitres_dist_model_check_hold_kenh, errorfx_v9,
deqC_fs_Dinv3, mainsimulation_fs_Din_v5, deqC_fs_Din_v3
% Inputs:
% kr_tm = off rate for tcr-mhc interaction
% kf_tm = on rate for tcr-mhc interaction
% f_T = nominal force for TCR:MHC interaction in Bell model
% file = file name (in folder dataPath)
% fracTMC_ic = best fit initial conditions for fitting fraction of PDD
% bonds
% Outputs:
% fracTMC_best: best fitting fraction of PDD bonds for each force
% pBest: best fitting simulation probabilities for survival
distribution,
% cell vector where pBest{i} corresponds to force F(i)
% tBest: best fitting simulation times for surival distribution, cell
% vector where tBest{i} corresponds to force F(i)

%% Load data
[F,~,~,~,~,LTstore,pLT] = readData_v3(file);
n = length(F); % number of forces
errorType = 4; % way to calculate error (errorfx_v9)

folder_path = 'input folder for figures export';
```

```
%% Q4R7
% Kinetic rates (force-free)
kr_mc = 7.84; % CD8:MHC off rate
kf_mc = 0.00004/6; % CD8 MHC on rate
kr_tl = 0.1; % Lck:TCR off rate
kf_tl = 1e-3; % Lck:CD8 on rate

f_C = 21.9; % nominal force for Bell model

t = 0:0.0001:10; % recording times for simulation
t = t';

D = 0.08; % from Chakraborty/Palmer model

% Densities
mT = 8; % TCR density
mC = 311; % MHC density

f = 0.05; % fraction of CD8:Lck conjugation

% Contact rate coefficients
mC_0 = mC*(1-f); % unconjugated CD8 fraction
mC_L = mC*f; % Lck conjugated CD8 fraction

D_T = mT*D*pi; % TCR contact rate
D_C0 = mC_0*D*pi; % CD8 null contact rate
D_CL = mC_L*D*pi; % CD8:Lck contact rate

kenh = 1500; % enhancement coefficient for rebinding

fracTMC_best = fracTMC_ic;

% Storage
pBest = cell(n,1);
tBest = cell(n,1);

% Initial plot to be updated later
semilogy(t,zeros(size(t)),LTstore{1},pLT{1},'o');
h = gcf;
drawnow
axesObj = get(h, 'Children');  %axes handles
dataObj = get(axesObj, 'Children');

for j = 1:n % for each force condition
    %% Run fitting around initial condtion until fitting condition is
met, coarse scan
    res_fracTMC = 0.1;
    stop = 0;
    run = 0;
    errorLast = inf;

    set(dataObj(1),'XData',LTstore{j}','YData',pLT{j})
```

```
    drawnow

    while stop == 0
        [fracTMC_best(j),run,stop,errorLast,pBest{j},tBest{j}] =
fitres_dist_model_check_hold_kenh(res_fracTMC,kenh,fracTMC_best(j),stop
,run,F(j),LTstore{j},pLT{j},errorType,errorLast,t,f,kr_tm,kf_tm,kr_mc,k
f_mc,kr_tl,kf_tl,f_T,f_C,D,D_T,D_C0,D_CL,dataObj);
        axesObj.XLim = [0,max(LTstore{j})];
        axesObj.YLim = [pLT{j}(end-1),1];
        drawnow
        disp(strcat('Run number',{' '},num2str(run),'|| Best Fit Now
=',{' '},num2str(fracTMC_best(j))))
    end

    %% Run fitting around initial condtion until fitting condition is
met, fine scan
    res_fracTMC = 0.01;
    stop = 0;
    run = 0;
    errorLast = inf;

    while stop == 0
        [fracTMC_best(j),run,stop,errorLast,pBest{j},tBest{j}] =
fitres_dist_model_check_hold_kenh(res_fracTMC,kenh,fracTMC_best(j),stop
,run,F(j),LTstore{j},pLT{j},errorType,errorLast,t,f,kr_tm,kf_tm,kr_mc,k
f_mc,kr_tl,kf_tl,f_T,f_C,D,D_T,D_C0,D_CL,dataObj);
        axesObj.XLim = [0,max(LTstore{j})];
        axesObj.YLim = [pLT{j}(end-1),1];
        drawnow
        disp(strcat('Run number',{' '},num2str(run),'|| Best Fit Now
=',{' '},num2str(fracTMC_best(j))))
    end

    file_path = strcat([file,'_',num2str(round(F(j)))]);
    fig_path = [folder_path,file_path];
    savefig(fig_path)

end

disp(strcat('bestFit',{' '},file,{' '},'complete'))

end
```

B.4 Code for running the different cases and finding lowest residual function

```
function [fracTMC_out,run,stop,errorLast,pAllBest,t_now] =
fitres_dist_model_check_hold_kenh(res_fracTMC,kenh,fracTMC,stop,run,F,L
Tstore,pLT,errorType,errorLast,t,f,kr_tm,kf_tm,kr_mc,kf_mc,kr_tl,kf_tl,
f_T,f_C,D_out,D_T,D_C0,D_CL,dataObj)

% Inputs come from scan_model_check_hold_kenh
% res_fracTMC: resolution of fitting
% kenh: enhancement coefficient
% stop: marker to stop fitting
```

```
% run: run number, how many times this has run
% F: force bins level
% LTstore: lifetimes in force bin
% pLT: probabilities in force bin
% errorType: used for errorfx_v9
% errorLast: error from last run
% t: times to simulated survival distribution
% f: fraction of CD8:Lck conjugation
% kf/kr_tm: on and off rates for TCR:MHC binding
% kf/kr_cm: on and off rates for CD8:MHC binding
% f_C/T: nominal force for Bell model for CD8/TCR:MHC
% D_out: diffusion out of the contact zone
% D_T/C0/Cl: diffusion into contact zone for TCR,CD8null,CD8:Lck
% dataObj: handle for figure

% Outputs
% fracTMC_out: best fitting PDD fraction
% run: how many runs it took
% stop: marker for checking completion
% errorLast: error from last run
% pAllBest: probabilities for survival distribution best fit
% t_now: times for best fit survival distribution

% January 22, 2018
% Uses errorfx_v9, mainSimulation_fs_Din_v5, deqC_fs_Din_v3

    run = run+1;

    fracTMC_fit = round([fracTMC-
res_fracTMC,fracTMC,fracTMC+res_fracTMC],2);

    gt0_fracTMC = fracTMC_fit>=0 & fracTMC_fit<=1; % res cannot pull
out negative values

    pAll = cell(3,1);

    errorBest = inf;

    mT = 8;
    mC = 311;

    for i = 1:3

        if gt0_fracTMC(i) > 0

            kenh_now = kenh;
            fracTMC_now = fracTMC_fit(i);

            mstart = zeros(12,1);
            mstart(1) = fracTMC_now;
            pT = kf_tm/kr_tm*mT;
            pC = kf_mc/kr_mc*mC*(1-f);
            pCL = kf_mc/kr_mc*mC*f;
            sumAll = pT+pC+pCL;
```

```
            mstart(6) = (1-fracTMC_now)*pT/sumAll;
            mstart(7) = (1-fracTMC_now)*pC/sumAll;
            mstart(8) = (1-fracTMC_now)*pCL/sumAll;

            mstore =
mainSimulation_fs_Din_v5(mstart,t,F,kr_tm,kf_tm,kr_mc,kf_mc,kr_tl,kf_tl
,kenh_now,f_T,f_C,D_out,D_T,D_C0,D_CL);

            mstore_now = sum(mstore,2);
            LTstore = round(LTstore,4);
            mstore_now2 = mstore_now(t>=min(LTstore));
            t_now = t(t>=min(LTstore));
            pAll{i} = mstore_now2/mstore_now2(1);

            errorNow = errorfx_v9(pAll{i},pLT(1:end-
1),t_now,LTstore(1:end-1),errorType);    %
errorfx_v2(pAllSim,pAllExp,tAllSim,tAllExp,errorType)

            if i == 1
                errorBest = errorNow;
                fracTMC_out = fracTMC_fit(i);
                iBest = i;
            elseif errorNow < errorBest
                errorBest = errorNow;
                fracTMC_out = fracTMC_fit(i);
                iBest = i;
            end

        end

    end

    if errorBest >= errorLast
        fracTMC_out = fracTMC_fit(2);
        pAllBest = pAll{2};
        stop = 1;
    else
        errorLast = errorBest;
        pAllBest = pAll{iBest};
        set(dataObj(2),'XData',t_now,'YData',pAllBest)
        drawnow
    end

end
```

B.5 Code for simulating a single Markov chain function

```
function mstore =
mainSimulation_fs_Din_v5(mstart,t,F,kr_tm,kf_tm,kr_mc,kf_mc,kr_tl,kf_tl
,k_increase,f_T,f_C,D_out,D_T,D_C0,D_CL)

%% Simulation to analyze pseudo-dimer of dimers pulling experiment
% Note: diffusion of molecules back in allowed
% Same as v4 but faster due to no globalization of k
```

```
%% Inputs
% mstart: initial species probabilities vector
% t: time vector for lifetime (should be relatively fine resolution)
% F: vector for forces to evalulate lifetime
% kr_tm: unbinding tcr-mhc (zero force)
% kf_tm: rebinding tcr-mhc
% kr_mc: unbinding mhc-cd8 (zero force)
% kf_mc: rebinding mhc-cd8
% kr_tl: unbinding tcr-lck (zero force)
% kf_tl: rebinding tcr-lck
% k_increase: enhanced rebinding due to pdd
% f_T: Bell model nominal force for TCR
% f_C: Bell model nominal force for CD8
% D_out: Diffusion constant input (in um^2/s)
% D_C0: Contact rate for CD8 without LCK
% D_CL: Contact rate for CD8 with LCK
% D_T: Contact rate for TCR
%% Outputs
% mstore: m-by-1 cell vector with each cell containing n-by-p vector
where
%   mstore{m}(n,p) is the probability of species p existing at time
t(n)

%% Inputs
% f = 10; % nominal force for Bell model, added as model input

% Which bond
kf_enhance = k_increase;

L = 0.01; % length of confinement/"close" zone

%% Normalization
A = L^2; % area of confinement zone
kf_tm_norm = kf_tm/A;
kf_mc_norm = kf_mc/A;
kf_tl_norm = kf_tl/A;
D_norm = D_out/A;

%% Storage
mstore = cell(size(F)); % store markov results

for i = 1:length(F)
    kr_tm_now = kr_tm*exp(F(i)/f_T);
    kr_mc_now = kr_mc*exp(F(i)/f_C);

    kr_tm_fs = kr_tm*exp(F(i)/2/f_T);
    kr_mc_fs = kr_mc*exp(F(i)/2/f_C);

    k = [kf_tm_norm;...
        kr_tm_now;...
        kf_mc_norm;...
        kr_mc_now;...
        kf_tl_norm;...
        kr_tl;...
        kf_enhance;...
```

```
        D_norm;...
        D_norm;...
        D_norm;
        kr_tm_fs;...
        kr_mc_fs;...
        D_CL;...
        D_C0;...
        D_T];

    m = mstart;

    % species by ratio of affinities

    % run to steady state
    options = odeset('RelTol',1e-5,'AbsTol',1e-
7);%,'OutputFcn',@odewbar);

    % run sim
    [~,mo] = ode45(@(t,m)deqC_fs_Din_v3(t,m,k),t,m,options);

    mstore = mo;

end
```

B.6 Code for finding error residuals function

```
function [errorOut] =
errorfx_v9(pAllSim,pAllExp,tAllSim,tAllExp,errorType)
% Find error between simulation and experimental data

% Inputs
% pAllSim: simulated probability of lifetime for survival distribution
% pAllExp: experimental probability of lifetime for survival
distribution
% tAllSim: simulated times for probability (pAllSim(i) corresponds to
% tAllSim(i))
% tAllExp: experimental times for probability (pAllExp(i) corresponds
to
% tAllExp(i))
% errorType = 1 for weight LS, 2 for chi-square, 3 for alternate LS, 4
for

% Outputs
% errorOut: error from fitting based on error type

% variance based fitting
tAllSim = round(tAllSim,4);
tAllExp = round(tAllExp,4);
%% Weighted^2 Least squares error
if errorType == 1
    errorOut = 0;
    for i = 1:length(pAllExp)
        findi = length(tAllSim(tAllSim<=tAllExp(i))); % index of
lifetimes in simulated data less than experimental lifetime (i)
```

```
        errorOut = errorOut + tAllSim(findi)^2*(pAllSim(findi)-
pAllExp(i))^2;
    end
end
%% Pearson's chi-square
if errorType == 2
    errorOut = 0;
    for i = 1:length(pAllExp)
        findi = length(tAllSim(tAllSim<=tAllExp(i))); % index of
lifetimes in simulated data less than experimental lifetime (i)

        errorOut = errorOut + (pAllSim(findi)-
pAllExp(i))^2/pAllSim(findi);
    end
end
%% Weighted Least squared error
if errorType == 3
    errorOut = 0;
    for i = 1:length(pAllExp)
        findi = length(tAllSim(tAllSim<=tAllExp(i))); % index of
lifetimes in simulated data less than experimental lifetime (i)

        errorOut = errorOut + tAllSim(findi)*(pAllSim(findi)-
pAllExp(i))^2;
    end
end
%% Variance-based weighting
if errorType == 4
    weights = zeros(size(pAllExp));
    errorOut = 0;
    variance_measurement = 0.1;
    % find weights
    for i = 1:length(pAllExp)
        weights(i) = 1/(variance_measurement*pAllExp(i))^2;
    end

    norm_weights = weights./mean(weights);

    for i = 1:length(pAllExp)
        findi = length(tAllSim(tAllSim<=tAllExp(i))); % index of
lifetimes in simulated data less than experimental lifetime (i)

        errorOut = errorOut + norm_weights(i)*(pAllSim(findi)-
pAllExp(i))^2;
    end
end
```

B.7 ODE equations for Markov transition

```
function dm = deqC_fs_Din_v3(t,m,k)
%% Differential equations for Markov chain evaluating Pseudo-dimer of
dimers (pdd) model
```

```
% Enhancement of binding occurs to both TCR and CD8 and LCK under
force, TCR and CD8 equally
% share load when bound to MHC
%% Kinetic parameter vector
    % Single-molecule interactions
    % 1: TCR:MHC binding
    % 2: TCR:MHC unbinding
    % 3: CD8:MHC binding
    % 4: CD8:MHC unbinding
    % 5: TCR:LCK binding
    % 6: TCR:LCK unbinding
    % 7: Rebinding enhancement if close
    % 8: CD8:LCK diffuse out
    % 9: CD8 diffuse out (no Lck)
    % 10: TCR diffuse out
    % 11: TCR:MHC unbinding (with force share)
    % 12: CD8:MHC unbinding (with force share)
    % 13: CD8:LCK diffuse in
    % 14: CD8 diffuse in
    % 15: TCR diffuse in
%% Species vector
    % 1: TCR-MHC-CD8-LCK
    % 2: TCR-MHC-LCK (CD8 close)
    % 3: MHC-CD8-LCK (TCR close, bound LCK)
    % 4: TCR-MHC-CD8 (LCK close)
    % 5: TCR-MHC-CD8 (no LCK)
    % 6: TCR-MHC (CD8 diffused away)
    % 7: MHC-CD8 (no LCK) (TCR diffused away)
    % 8: MHC-CD8-LCK (TCR diffused away)
    % 9: TCR-MHC (CD8 close, no Lck)
    % 10: TCR-MHC (CD8 close, with Lck)
    % 11: CD8-MHC-LCK (TCR close, unbound to anything)
    % 12: CD8-MHC (TCR close, unbound, no LCK)


%% equations
% Notes: m = [m1,m2...], kinetics = [k1,k2...]

    dm = zeros(size(m));

    dm(1) = -k(11)*m(1) - k(12)*m(1) - k(6)*m(1) + k(1)*k(7)*m(3) +
k(3)*k(7)*m(2) + k(5)*k(7)*m(4); % TCR unbinds, CD8 unbinds, LCK
unbinds, TCR rebinds, CD8 rebinds, LCK rebinds,
    dm(2) = -k(3)*k(7)*m(2) - k(6)*m(2) - k(2)*m(2) + k(12)*m(1) +
k(5)*m(10); % CD8 rebinds, LCK unbinds, TCR unbinds, CD8 rebinds (CD8
unbinds m1, LCK rebinds when close)
    dm(3) = -k(1)*k(7)*m(3) - k(4)*m(3) - k(6)*m(3) + k(11)*m(1) +
k(5)*m(11);
    dm(4) = -k(5)*k(7)*m(4) - k(11)*m(4) - k(12)*m(4) + k(6)*m(1) +
k(3)*m(10) + k(1)*m(11); %TCR-MHC-CD8 (LCK close)
    dm(5) = -k(11)*m(5) - k(12)*m(5) + k(1)*m(12) + k(3)*m(9);
    dm(6) = -k(2)*m(6) + k(9)*m(9) + k(8)*m(10) - k(13)*m(6) -
k(14)*m(6);
    dm(7) = -k(4)*m(7) + k(10)*m(12) - k(15)*m(7);
    dm(8) = -k(4)*m(8) + k(10)*m(11) - k(15)*m(8);
```

```
    dm(9) = -k(9)*m(9) - k(2)*m(9) - k(3)*m(9) + k(12)*m(5) +
k(14)*m(6);
    dm(10) = -k(2)*m(10) - k(3)*m(10) - k(5)*m(10) - k(8)*m(10) +
k(12)*m(4) + k(6)*m(2) + k(13)*m(6);
    dm(11) = -k(1)*m(11) - k(4)*m(11) - k(5)*m(11) - k(10)*m(11) +
k(11)*m(4) + k(6)*m(3) + k(15)*m(8);
    dm(12) = -k(1)*m(12) - k(4)*m(12) - k(10)*m(12) + k(11)*m(5) +
k(15)*m(7);

end
```

APPENDIX C. MATLAB CODE FOR SIMULATION OF CD8 CATCH-BOND MECHANISM

C.1 Code to run BFP assay for one ligand, several CD8:Lck fractions

```
% Scan fraction of CD8:Lck conjugation, several runs of bfp assay and
output lifetime results
% Written by William Rittase

% Requires inputs of number of runs, ligand, and the force/fraction of
% CD8:Lck conjugation

clearvars

%% Q4R7 runs

num_runs = 40; % number of cell pairs to simulation
ligand = 'wQ4R7'; % which ligand to simulate
force = [2,4,8,12,16,20,24,30]; % different force clamping levels (pN)
num_forces = length(force);
f = [0.01,0.02,0.04,0.08,0.1,0.15,0.2,0.4]; % fraction Lck conjugation
to CD8

for k = 1:length(f)

    lifetimes = cell(num_runs,num_forces); % cell matrix to store
lifetimes
    start_times = cell(num_runs,num_forces); % cell matrix to store
time at which lifetime was measured

    for j = 1:num_forces

        for i = 1:num_runs

            [~,~,lifetime_store,lifetime_start_time] =
tcr_lck_shp_switch_force_dependence_function_v4(force(j),ligand,f(k));
% simulate assay for one cell pair, one force

            lifetimes{i,j} = lifetime_store;
            start_times{i,j} = lifetime_start_time;

            disp([num2str(j),',',num2str(i)])

        end

    end

    folder_path = 'input folder string';
```

```
    file_path = ['workspace_wq4r7_',num2str(f(k)),'.mat'];

    full_path = [folder_path,file_path];

    save(full_path) % save workspace for future analysis

end
```

C.2 Code to determine bond lifetimes for one cell and pair function

```
function [m_store,t_store,lifetime_store,lifetime_start_time] =
tcr_lck_shp_switch_force_dependence_function_v4(force,ligand,f)

% Simulation of TCR pulling-stimulation induced CD8 conjugation through
% activation of Lck and single phos of TCR. Shut down by GP (ppTCR
% activated)
tic
functionPath = 'input folder string';
addpath(functionPath)

% Inputs
num_touches = 200; % number of contacts in BFP assay
contact_time = 0.1; % contact time (how long the cell and bead are in
contact)
waiting_time = 0.25; % waiting time (how long the cell and bead are
separated after bond ends or there is no bond)
dt = 0.001; % recording interval
initial_af = 0.2; % adhesion frequency at the beginning of the assay
pulling_rate = 200; % bond pulling rate up to clamping force in pN/s

%% Densities
mT = 8; % TCR density
mC = 300; % CD8 density
mC_L = f*mC; % CD8:Lck fraction
mC_null = (1-f)*mC; % CD8 without Lck fraction
mL = 20; % estimate from Germain PLoS Comp Bio 2005 (1um^2 area, 25nm
depth)
mGP = 80/3*mL; % as SHP from Germain 2005

%% Peptide independent kinetics
% Kinetic rates (force-free)
kr_mc = 7.84; % CD8:MHC off rate
kf_mc = 0.00004/6; % CD8:MHC on rate
f_C = 21.9; % nominal force of CD8:MHC interaction under Bell model
kr_tl = 0.1; % LCK:TCR estimated based on measurements by Chenqi Xu,
high affinity, low off rate
kf_tl = 1e-3; % LCK:TCR on rate

k_pL_pulled = get_kpL_v4(force); % activation rate of Lck by pulled TCR
k_phos_lck_by_ptcr = 0; % activation of Lck by partially activated TCR
k_phos_tcr_by_lck = 0.03; % activation of TCR by active Lck
k_phos_gp_by_pptcr = 0.01; % activation of generic phosphotase by fully
active TCR
```

```
k_gp_tcr = 0.01; % deactivation rate of TCR by GP
k_gp_lck = k_gp_tcr; % deactivation rate of Lck by GP
k_dephos = 0.1; % passive dephosphorylation

k_enh_avidity = 100; % enhanced binding of MHC by TCR:CD8 dimers
k_enhance_trapping = 10; % trapping enhancement of binding (doesn't
really matter)
k_enhance_rebinding = 1500/0.01^2; % Approximate fit to survival curve
-
% 0.01^2 is approximate grid area
% 1500 could mean restrition in area to 0.5% or 1.8 degrees of
% restriction, or grid area change to 0.005nm^2 (length of 0.0707nm)

%% Peptide dependent kinetics
% Import values
[kr_tm,kf_tm,f_T,mM] = get_kinetics(ligand,initial_af,contact_time,1);

%% Kinetic vectors
k_all = [k_pL_pulled;...
    k_phos_lck_by_ptcr;...
    k_phos_gp_by_pptcr;...
    k_phos_tcr_by_lck;...
    k_gp_lck;...
    k_gp_tcr;...
    k_dephos;...
    kf_tl;...
    kr_tl;...
    kf_tm;...
    kr_tm;...
    kf_mc;...
    kr_mc;...
    k_enh_avidity;...
    k_enhance_trapping;...
    k_enhance_rebinding];

k_no_pull = [0;k_all(2:end)];
k_pull = k_all;

global k

%% Initial Species vector
m_start = zeros(24,1);
m_start(1) = mT;
m_start(4) = mC_L;
m_start(6) = mL;
m_start(8) = mGP;
m_start(10) = mM;
m_start(11) = mC_null;

%% Simulation

options = odeset('RelTol',1e-5,'AbsTol',1e-7);%,'OutputFcn',@odewbar);

t_contact = dt:dt:contact_time;
t_wait = dt:dt:waiting_time;
```

```
m = m_start;

bond_types = zeros(num_touches,1);

t_store = [];
m_store = [];
accum_lifetime = [];

bond = [];
lifetime_store = zeros(num_touches,1);
lifetime_start_time = zeros(num_touches,1);
n = 0;

for i = 1:num_touches

    % Run contact time
    k = k_no_pull;
    [t_c,m_c] = ode45(@deq_switch,t_contact,m,options);

    % remove all bonds (CD8:MHC,TCR:MHC)
    m = m_c(end,:);
    m(1) = m(1) + m(12) + m(17) + m(20);
    m(2) = m(2) + m(13) + m(18) + m(21);
    m(3) = m(3) + m(14) + m(19);
    m(4) = m(4) + m(16) + m(20) + m(21);
    m(5) = m(5) + m(22) + m(23) + m(24);
    % m6-9 stay the same
    m(10) = 0;
    m(11) = m(11) + m(15) + m(17) + m(18) + m(19);
    % m10-end become zero
    for j = 12:24
        m(j) = 0;
    end

    % Pulling time
    r = rand;

    prob_adhesion = 1-exp(-sum(m_c(end,12:24)));

    if r < prob_adhesion % if bond

        % Determine type of bond being pulled
        bonds = m_c(end,12:24);
        bonds_p = cumsum(bonds/sum(bonds));
        r = rand;
        which_bond = sum(bonds_p<r)+1+11;
        % determine if pulled bond survives and for how long it lasts
        if which_bond >= 12 && which_bond <= 14 % if TCR-MHC bond

            % determine if bond survives pulling
            p_rup =
prob_of_rupture_b4_clamp_v3(force,kr_tm,f_T,pulling_rate);
            r = rand;
```

```
            if p_rup > r
                % pull bond lifetime from distribution
                pulled_T = 1;
                bond = 'TCR:MHC';
                lifetime = get_lifetime(bond,ligand,force);
                t_bond = 0:dt:lifetime;
                bond_types(i) = 1;

                n = n+1;
                lifetime_store(n) = lifetime;
                if ~isempty(t_store) % if first contact
                    lifetime_start_time(n) = t_store(end)+contact_time;
                end
            else
                pulled_T = 0;
                t_bond = 0;
            end

        elseif which_bond == 15 || which_bond == 16 % if CD8-MHC bond

            % determine if bond survives pulling
            p_rup =
prob_of_rupture_b4_clamp_v3(force,kr_mc,f_C,pulling_rate);
            r = rand;

            if p_rup > r
                % pull bond lifetime from distribution
                pulled_T = 0;
                bond = 'MHC:CD8';
                lifetime = get_lifetime(bond,ligand,force);
                t_bond = 0:dt:lifetime;
                bond_types(i) = 2;

                n = n+1;
                lifetime_store(n) = lifetime;
                if ~isempty(t_store) % if first contact
                    lifetime_start_time(n) = t_store(end)+contact_time;
                end
            else
                pulled_T = 0;
                t_bond = 0;
            end

        elseif which_bond >= 17 && which_bond <=21 % if trimolecular,
not pdd
            % pull bond lifetime from distribution
            pulled_T = 1;
            bond = 'TCR:MHC:CD8';
            lifetime = get_lifetime(bond,ligand,force);
            t_bond = 0:dt:lifetime;
            bond_types(i) = 3;

            n = n+1;
            lifetime_store(n) = lifetime;
```

```
            if ~isempty(t_store) % if first contact
                lifetime_start_time(n) = t_store(end)+contact_time;
            end

        else % pdd bond
            % pull bond lifetime from distribution
            pulled_T = 1;
            bond = 'TCR:MHC:CD8L';
            lifetime = get_lifetime(bond,ligand,force);
            t_bond = 0:dt:lifetime;
            bond_types(i) = 4;

            n = n+1;
            lifetime_store(n) = lifetime;
            if ~isempty(t_store) % if first contact
                lifetime_start_time(n) = t_store(end)+contact_time;
            end

        end

        % Simulate the system for the duration of the bond
        % Immediately follow by simulating the waiting time in between
        % contacts
        if pulled_T == 1
            k = k_pull;
            if length(t_bond) >= 2
                [t_b,m_b] = ode45(@deq_switch,t_bond,m,options);

                k = k_no_pull;
                [t_w,m_w] =
ode45(@deq_switch,t_wait,m_b(end,:),options);
            else
                t_b = [];
                m_b = [];

                k = k_no_pull;
                [t_w,m_w] = ode45(@deq_switch,t_wait,m,options);
            end
        elseif pulled_T == 0
            if length(t_bond) >= 2
                k = k_no_pull;
                [t_b,m_b] = ode45(@deq_switch,t_bond,m,options);

                k = k_no_pull;
                [t_w,m_w] =
ode45(@deq_switch,t_wait,m_b(end,:),options);
            else
                t_b = [];
                m_b = [];

                k = k_no_pull;
                [t_w,m_w] = ode45(@deq_switch,t_wait,m,options);
            end
        else
            disp('We have a problem in the pulling species')
```

```
        end
    else
        m_b = [];
        t_b = [];
        k = k_no_pull;

        [t_w,m_w] = ode45(@deq_switch,t_wait,m,options);

    end

    % add contact time
    [t_store,m_store,accum_lifetime] =
add_stuff(0,t_store,m_store,accum_lifetime,t_c,m_c);
    % add pulling time
    [t_store,m_store,accum_lifetime] =
add_stuff(1,t_store,m_store,accum_lifetime,t_b,m_b);
    % add waiting time
    [t_store,m_store,accum_lifetime] =
add_stuff(0,t_store,m_store,accum_lifetime,t_w,m_w);

    % Bring MHC back in and start over
    m = m_w(end,:);
    m(10) = mM;

end

toc

% Shorten matrices
lifetime_store = lifetime_store(1:n);
lifetime_start_time = lifetime_start_time(1:n);

toc
```

C.3 Code for get kinetics function

```
function [kr_tm,kf_tm,f_T,mM] =
get_kinetics(ligand,initial_pa,contact_time,get_mM)
% Get kinetics for defined ligand
% assume contact area = 1um^2
% Inputs:
% ligand = ligand string name
% initial_pa = initial adhesion frequency for calculation of MHC
density
% contact_time = how long the cells are in contact during BFP assay
% get_mM = 1 or 0, 1 if you want to calculate the MHC density

% kf_tm = on rate for interaction
% kr_tm = off rate for interaction
% f_T = nominal force from Bell model fitting
% all parameters were calibrated from exerimental data
```

```
if strcmp(ligand,'wQ4')

    kf_tm = 0.0000899378/6;
    kr_tm = 4.22;
    f_T = 30.2;

elseif strcmp(ligand,'wQ4R7')

    kf_tm = 0.000135225/6;
    kr_tm = 3.45;
    f_T = 21.72; % this is baoyu's data, jin's data = 72.3;

elseif strcmp(ligand,'wT4')

    kf_tm = 0.0000592144/6;
    kr_tm = 2.75;
    f_T = 13;

elseif strcmp(ligand,'wQ4H7')

    kf_tm = 0.0000706784/6; % fit from other data
    kr_tm = 4.15; % fit from other data
    f_T = 30.8;

elseif strcmp(ligand,'wQ7')

    kf_tm = 0.0000457382/6;
    kr_tm = 6.72;
    f_T = 46.3;

elseif strcmp(ligand,'wG4')

    kf_tm = 0.0000542196/6;
    kr_tm = 3.63;
    f_T = 11.9;

else

    disp('Error in get_kinetics.m: No ligands match kinetics')

end

if get_mM == 1
    mT = 8;
    mC = 300;
    kr_mc = 7.84; % CD8:MHC
    kf_mc = 0.00004/6; % CD8:MHC
    avg_num_bonds_T_over_MHC = (mT*kf_tm/kr_tm)*(1-exp(-
kr_tm*contact_time));
    avg_num_bonds_C_over_MHC = (mC*kf_mc/kr_mc)*(1-exp(-
kr_mc*contact_time));
    avg_num_bonds_over_MHC = avg_num_bonds_T_over_MHC +
avg_num_bonds_C_over_MHC;
```

```
    mM = -log(1-initial_pa)/avg_num_bonds_over_MHC;
else
    mM = 0;
end

end
```

C.4 Code to determine the probability of rupture before clamp function

```
function p = prob_of_rupture_b4_clamp_v3(f,k_0,f_b,rf)
% calculates the approximate probability of bond rupture before
clamping
% based on the clamping force (f), zero force off rate (k_0), scale
% force(f_b), and ramping rate (rf)

df = 0.01;

if f > df

    force = 0:df:f;

    % probability that
    pdf = k_0/rf*exp(force/f_b).*exp(-k_0*f_b/rf*(exp(force/f_b)-1)); %
based on Eq 23 from Effects of cellular viscoelasticity in lifetime
extraction of single receptor-ligand bonds

    p = 1-trapz(force,pdf);

else

    p = 0;

end

end
```

C.5 Code to select a lifetime function

```
function [lifetime] = get_lifetime(bond,ligand,force)

folder_path = 'input folder string';
file_path = strcat([folder_path,'/',ligand,'/',num2str(force)]);
data = csvread(file_path);

t = data(:,5);

if strcmp(bond,'TCR:MHC')
    m = data(:,1);

elseif strcmp(bond,'MHC:CD8')
    m = data(:,2);
```

```
elseif strcmp(bond,'TCR:MHC:CD8')
    m = data(:,3);

elseif strcmp(bond,'TCR:MHC:CD8L')
    m = data(:,4);

end

% Interpolate
p = rand; % probability
index_gt = sum(m>p)+1;
index_lt = index_gt-1;

if index_gt > length(m)
    lifetime = t(end);
else
    lifetime = (p-m(index_lt))/(m(index_gt)-m(index_lt)) *
(t(index_gt)-t(index_lt)) + t(index_lt);
end

end
```

C.6 Code to compile data function

```
function [t_store_out,m_store_out,accum_bond_lifetime_out] =
add_stuff(is_bond,t_store_in,m_store_in,accum_bond_lifetime_in,t,m)
% Append matrices and adjust things

if is_bond == 0 % if there is no bond
    if isempty(accum_bond_lifetime_in) % if first run
        accum_to_add = zeros(size(t));
        t_to_add = t;
    else
        accum_to_add = repmat(accum_bond_lifetime_in(end),size(t));
        t_to_add = t + t_store_in(end);
    end

    accum_bond_lifetime_out = [accum_bond_lifetime_in;accum_to_add];
    t_store_out = [t_store_in;t_to_add];
    m_store_out = [m_store_in;m];
else

    t_to_add = t + t_store_in(end);
    accum_to_add = accum_bond_lifetime_in(end) + t;

    accum_bond_lifetime_out = [accum_bond_lifetime_in;accum_to_add];
    t_store_out = [t_store_in;t_to_add];
    m_store_out = [m_store_in;m];
end

end
```

C.7 Code to plot lifetimes and extract data from workspace script

```
% Plot lifetime curves or distributions for a specific ligand across
% several CD8:Lck fractions
% Input the workspace file
% Requires changing folder_path/workspace_name to reflect several runs
% inputs for directory to correct matlab workspace file

clearvars
close all

f = [0.01,0.02,0.04,0.08,0.1,0.15,0.2,0.4];
n = length(f);

folder_path = 'input folder string';
workspace_name = ['workspace_wq4h7_',num2str(f(1)),'.mat'];

full_path = [folder_path,workspace_name];

load(full_path)

lifetimes_in_force_bin = cell(num_forces,n); % lifetimes in each bin
mean_lifetime = zeros(num_forces,n); % average lifetime in bin
stderr_lifetime = zeros(num_forces,n); % standard error of lifetime in
bin
n_lifetime = zeros(num_forces,n); % number of lifetimes in each bin
stdev_lifetime = zeros(num_forces,n); % standard deviation of lifetimes
in each bin

for index = 1:n

    folder_path = '/Users/williamrittase/Dropbox (GaTech)/Simulations
in development/Switch/Lck-Shp change bond lifetime/workspaces/v5
scan/h7/';
    workspace_name = ['workspace_wq4h7_',num2str(f(index)),'.mat'];

    full_path = [folder_path,workspace_name];

    load(full_path)

    % important variables: lifetimes, start_times, force,
    % num_forces, num_runs

    for i = 1:num_forces

        lifetimes_all = [];

        for j = 1:num_runs

            lifetimes_now = lifetimes{j,i}(lifetimes{j,i}<10 &
lifetimes{j,i}>0.002);
```

```
            lifetimes_all = [lifetimes_all;lifetimes_now];

        end

        mean_lifetime(i,index) = mean(lifetimes_all);
        stderr_lifetime(i,index) =
std(lifetimes_all)/sqrt(length(lifetimes_all));
        lifetimes_in_force_bin{i,index} = lifetimes_all;
        n_lifetime(i,index) = length(lifetimes_all);
        stdev_lifetime(i,index) = std(lifetimes_all);

    end

    % Plot lifetimes
    scatter(force,mean_lifetime(:,index))
    hold on

errorbar(force,mean_lifetime(:,index),stderr_lifetime(:,index),'LineSty
le','none')
    xlabel('Force (pN)')
    ylabel('Average Lifetime (sec)')

    a = gcf;
    a.Color = [1,1,1];
    a.Children.Children(1).LineWidth = 2; % set error bar size
    a.Children.Children(2).LineWidth = 2; % set dot size
    a.Children.Children(2).SizeData = 80;
    a.Children.Children(2).CData = [0.8500 0.3250 0.0980];

end
```

REFERENCES

1. Gest, H., *The discovery of microorganisms by Robert Hooke and Antoni Van Leeuwenhoek, fellows of the Royal Society.* Notes and records of the Royal Society of London, 2004. **58**(2): p. 187-201.

2. Mazzarello, P., *A unifying concept: the history of cell theory.* Nature cell biology, 1999. **1**(1): p. 5.

3. Schultz, M., *Rudolf Virchow.* Emerging Infectious Diseases, 2008. **14**(9): p. 1480-1481.

4. Sahl, S.J., S.W. Hell, and S. Jakobs, *Fluorescence nanoscopy in cell biology.* Nat Rev Mol Cell Biol, 2017. **18**(11): p. 685-701.

5. Mahmood, T. and P.-C.C. Yang, *Western blot: technique, theory, and trouble shooting.* North American journal of medical sciences, 2012. **4**(9): p. 429-434.

6. Krutzik, P.O., et al., *Analysis of protein phosphorylation and cellular signaling events by flow cytometry: techniques and clinical applications.* Clinical immunology (Orlando, Fla.), 2004. **110**(3): p. 206-221.

7. Schreiber, G., *Kinetic studies of protein-protein interactions.* Current opinion in structural biology, 2002. **12**(1): p. 41-47.

8. Kitano, H., *Computational systems biology.* Nature, 2002. **420**(6912): p. 206-210.

9. Allison, J.P., B.W. McIntyre, and D. Bloch, *Tumor-specific antigen of murine T-lymphoma defined with monoclonal antibody.* Journal of immunology (Baltimore, Md. : 1950), 1982. **129**(5): p. 2293-2300.

10. Haskins, K., et al., *The major histocompatibility complex-restricted antigen receptor on T cells. I. Isolation with a monoclonal antibody.* The Journal of experimental medicine, 1983. **157**(4): p. 1149-1169.

11. Meuer, S.C., et al., *Clonotypic structures involved in antigen-specific human T cell function. Relationship to the T3 molecular complex.* The Journal of experimental medicine, 1983. **157**(2): p. 705-719.

12. Blum, J.S., P.A. Wearsch, and P. Cresswell, *Pathways of Antigen Processing.* Annual review of immunology, 2013. **31**(1): p. 443-473.

13. *Janeway's Immunobiology.* taylorfrancis, 2016.

14. Anderson, G., et al., *Cellular interactions in thymocyte development.* Annual review of immunology, 1996. **14**: p. 73-99.

15. Singer, A., S. Adoro, and J.-H.H. Park, *Lineage fate and intense debate: myths, models and mechanisms of CD4- versus CD8-lineage choice.* Nature reviews. Immunology, 2008. **8**(10): p. 788-801.

16. Robey, E. and B.J. Fowlkes, *Selective Events in T Cell Development.* Annual Review of Immunology, 1994. **12**(1): p. 675-705.

17. Myers, D.R., J. Zikherman, and J.P. Roose, *Tonic Signals: Why Do Lymphocytes Bother?* Trends in Immunology, 2017. **38**(11): p. 844-857.

18. Klein, L., et al., *Positive and negative selection of the T cell repertoire: what thymocytes see (and don't see).* Nature Reviews Immunology, 2014. **14**(6): p. 377-391.

19. Grakoui, A., et al., *The immunological synapse: a molecular machine controlling T cell activation.* Science (New York, N.Y.), 1999. **285**(5425): p. 221-227.

20. Qi, S.Y., J.T. Groves, and A.K. Chakraborty, *Synaptic pattern formation during cellular recognition.* Proceedings of the National Academy of Sciences of the United States of America, 2001. **98**(12): p. 6548-6553.

21. Irvine, D.J., et al., *Direct observation of ligand recognition by T cells.* Nature, 2002. **419**(6909): p. 845-849.

22. Lee, K.-H., et al., *The immunological synapse balances T cell receptor signaling and degradation.* Science (New York, N.Y.), 2003. **302**(5648).

23. Harris, N.L., et al., *Differential T Cell Function and Fate in Lymph Node and Nonlymphoid Tissues.* The Journal of Experimental Medicine, 2002. **195**(3): p. 317-326.

24. Sallusto, F., J. Geginat, and A. Lanzavecchia, *Central memory and effector memory T cell subsets: function, generation, and maintenance.* Annual review of immunology, 2004. **22**: p. 745-763.

25. Bluestone, J.A., et al., *The functional plasticity of T cell subsets.* Nature reviews. Immunology, 2009. **9**(11): p. 811-816.

26. Gao, G.F., Z. Rao, and J.I. Bell, *Molecular coordination of αβ T-cell receptors and coreceptors CD8 and CD4 in their recognition of peptide-MHC ligands.* Trends in Immunology, 2002. **23**(8): p. 408-413.

27. Marti, L., et al., *Lymphocyte Updates - Cancer, Autoimmunity and Infection.* intech, 2017.

28. Golubovskaya, V. and L. Wu, *Different Subsets of T Cells, Memory, Effector Functions, and CAR-T Immunotherapy.* Cancers, 2016. **8**(3): p. 36.

29. Mosmann, T.R. and S. Sad, *The expanding universe of T-cell subsets: Th1, Th2 and more.* Immunology Today, 1996. **17**(3): p. 138-146.

30. Jonuleit, H. and E. Schmitt, *The Regulatory T Cell Family: Distinct Subsets and their Interrelations.* The Journal of Immunology, 2003. **171**(12): p. 6323-6327.

31. Zhang, H., et al., *Subsets of regulatory T cells and their roles in allergy.* Journal of Translational Medicine, 2014. **12**(1): p. 1-11.

32. Ueno, H., *T follicular helper cells in human autoimmunity.* Current Opinion in Immunology, 2016. **43**: p. 24-31.

33. Mori, L., M. Lepore, and G. De Libero, *The Immunology of CD1- and MR1-Restricted T Cells.* Annual review of immunology, 2016. **34**: p. 479-510.

34. Godfrey, D.I., et al., *The burgeoning family of unconventional T cells.* Nature immunology, 2015. **16**(11): p. 1114-1123.

35. Chien, Y.-h., C. Meyer, and M. Bonneville, *γδ T Cells: First Line of Defense and Beyond.* Immunology, 2014. **32**(1): p. 121-155.

36. Laydon, D.J., C.R.M. Bangham, and B. Asquith, *Estimating T-cell repertoire diversity: limitations of classical estimators and a new approach.* Phil. Trans. R. Soc. B, 2015. **370**(1675): p. 20140291.

37. Miles, J.J., D.C. Douek, and D.A. Price, *Bias in the αβ T-cell repertoire: implications for disease pathogenesis and vaccination.* Immunology and Cell Biology, 2011. **89**(3): p. 375.

38. Arstila, P.T., et al., *A Direct Estimate of the Human αβ T Cell Receptor Diversity.* Science, 1999. **286**(5441): p. 958-961.

39. *Major histocompatibility complex*. [cited 2018 April 24]; Available from: https://en.wikipedia.org/wiki/Major_histocompatibility_complex.

40. Garcia, K.C., et al., *An alphabeta T cell receptor structure at 2.5 A and its orientation in the TCR-MHC complex.* Science (New York, N.Y.), 1996. **274**(5285): p. 209-219.

41. Wucherpfennig, K.W., et al., *Structural biology of the T-cell receptor: insights into receptor assembly, ligand recognition, and initiation of signaling.* Cold Spring Harbor perspectives in biology, 2010. **2**(4).

42. Davis, M.M. and P.J. Bjorkman, *T-cell antigen receptor genes and T-cell recognition.* Nature, 1988. **334**(6181).

43. Rossjohn, J., et al., *T Cell Antigen Receptor Recognition of Antigen-Presenting Molecules.* Annual review of immunology, 2014.

44. Birnbaum, M.E., et al., *Molecular architecture of the αβ T cell receptor-CD3 complex.* Proceedings of the National Academy of Sciences of the United States of America, 2014. **111**(49): p. 17576-17581.

45. Smith-Garvin, J.E., G.A. Koretzky, and M.S. Jordan, *T cell activation.* Annual review of immunology, 2009. **27**: p. 591-619.

46. O'Donoghue, G.P., et al., *Direct single molecule measurement of TCR triggering by agonist pMHC in living primary T cells.* eLife, 2013. **2**.

47. Huang, J., et al., *A single peptide-major histocompatibility complex ligand triggers digital cytokine secretion in CD4(+) T cells.* Immunity, 2013. **39**(5): p. 846-857.

48. Sykulev, Y., et al., *Evidence that a single peptide-MHC complex on a target cell can elicit a cytolytic T cell response.* Immunity, 1996. **4**(6): p. 565-571.

49. Xu, C., et al., *Regulation of T cell receptor activation by dynamic membrane binding of the CD3epsilon cytoplasmic tyrosine-based motif.* Cell, 2008. **135**(4): p. 702-713.

50. Shi, X., et al., *Ca2+ regulates T-cell receptor activation by modulating the charge property of lipids.* Nature, 2013. **493**(7430): p. 111-115.

51. Chakraborty, A.K. and A. Weiss, *Insights into the initiation of TCR signaling.* Nature Immunology, 2014. **15**(9): p. 798807.

52. Wang, H., et al., *ZAP-70: an essential kinase in T-cell signaling.* Cold Spring Harbor perspectives in biology, 2010. **2**(5).

53. Au-Yeung, B.B., et al., *The structure, regulation, and function of ZAP-70.* Immunological reviews, 2009. **228**(1): p. 41-57.

54. Lillemeier, B.F., et al., *TCR and Lat are expressed on separate protein islands on T cell membranes and concatenate during activation.* Nature immunology, 2010. **11**(1): p. 90-96.

55. Molnár, E., et al., *Cholesterol and sphingomyelin drive ligand-independent T-cell antigen receptor nanoclustering.* The Journal of biological chemistry, 2012. **287**(51): p. 42664-42674.

56. Bray, D., M.D. Levin, and C.J. Morton-Firth, *Receptor clustering as a cellular mechanism to control sensitivity.* Nature, 1998. **393**(6680): p. 85-88.

57. Castro, M., et al., *Receptor Pre-Clustering and T cell Responses: Insights into Molecular Mechanisms.* Frontiers in immunology, 2014. **5**: p. 132.

58. Wang, F., et al., *Inhibition of T cell receptor signaling by cholesterol sulfate, a naturally occurring derivative of membrane cholesterol.* Nature immunology, 2016. **17**(7): p. 844-850.

59. Swamy, M., et al., *A Cholesterol-Based Allostery Model of T Cell Receptor Phosphorylation.* Immunity, 2016. **44**(5): p. 1091-1101.

60. Schamel, W.W.A., et al., *The Allostery Model of TCR Regulation.* The Journal of Immunology, 2017. **198**(1): p. 47-52.

61. Hui, E. and R.D. Vale, *In vitro membrane reconstitution of the T-cell receptor proximal signaling network.* Nature structural & molecular biology, 2014.

62. Chen, L. and D.B. Flies, *Molecular mechanisms of T cell co-stimulation and co-inhibition.* Nature reviews. Immunology, 2013.

63. Ghosh, S. *T Cell Receptor Signaling Interactive Pathway*. July 2014 [cited 2018 April 25]; Available from: https://www.cellsignal.com/contents/science-cst-pathways-immunology-and-inflammation/t-cell-receptor-signaling-interactive-pathway/pathways-tcell.

64. Maupin-Furlow, J., *Proteasomes and protein conjugation across domains of life.* Nature Reviews Microbiology, 2011. **10**(2): p. 100-111.

65. Rudensky, A., et al., *Sequence analysis of peptides bound to MHC class II molecules.* Nature, 1991. **353**(6345).

66. *The Mode of Action of Drugs on Cells.* Journal of the American Medical Association, 1933. **101**(16): p. 1260-1261.

67. Schmid, D.A., et al., *Evidence for a TCR affinity threshold delimiting maximal CD8 T cell function.* Journal of immunology (Baltimore, Md. : 1950), 2010. **184**(9): p. 4936-4946.

68. Tian, S., et al., *CD8+ T Cell Activation Is Governed by TCR-Peptide/MHC Affinity, Not Dissociation Rate.* The Journal of Immunology, 2007. **179**(5): p. 2952-2960.

69. Corse, E., R.A. Gottschalk, and J.P. Allison, *Strength of TCR–Peptide/MHC Interactions and In Vivo T Cell Responses.* The Journal of Immunology, 2011. **186**(9): p. 5039-5045.

70. Racioppi, L., et al., *Peptide-major histocompatibility complex class II complexes with mixed agonist/antagonist properties provide evidence for ligand-related differences in T cell receptor-dependent intracellular signaling.* The Journal of Experimental Medicine, 1993. **177**(4): p. 1047-1060.

71. Alam, M.S., et al., *T-cell-receptor affinity and thymocyte positive selection.* Nature, 1996. **381**(6583): p. 616-620.

72. Cole, D.K., et al., *T-cell Receptor (TCR)-Peptide Specificity Overrides Affinity-enhancing TCR-Major Histocompatibility Complex Interactions.* Journal of Biological Chemistry, 2014. **289**(2): p. 628-638.

73. van der Merwe, P.A., et al., *Cytoskeletal polarization and redistribution of cell-surface molecules during T cell antigen recognition.* Seminars in Immunology, 2000. **12**(1): p. 5-21.

74. Furlan, G., et al., *Phosphatase CD45 Both Positively and Negatively Regulates T Cell Receptor Phosphorylation in Reconstituted Membrane Protein Clusters.* The Journal of biological chemistry, 2014.

75. Cordoba, S.-P.P., et al., *The large ectodomains of CD45 and CD148 regulate their segregation from and inhibition of ligated T-cell receptor.* Blood, 2013. **121**(21): p. 4295-4302.

76. James, J.R. and R.D. Vale, *Biophysical mechanism of T-cell receptor triggering in a reconstituted system.* Nature, 2012. **487**(7405): p. 64-69.

77. Purbhoo, M.A., et al., *T cell killing does not require the formation of a stable mature immunological synapse.* Nature Immunology, 2004. **5**(5): p. 524.

78. Kersh, G.J., et al., *Structural and functional consequences of altering a peptide MHC anchor residue.* Journal of immunology (Baltimore, Md. : 1950), 2001. **166**(5): p. 3345-3354.

79. McKeithan, T.W., *Kinetic proofreading in T-cell receptor signal transduction.* Proceedings of the National Academy of Sciences of the United States of America, 1995. **92**(11): p. 5042-5046.

80. Huang, J., et al., *The kinetics of two-dimensional TCR and pMHC interactions determine T-cell responsiveness.* Nature, 2010. **464**(7290): p. 932-936.

81. Liu, B., et al., *2D TCR-pMHC-CD8 kinetics determines T-cell responses in a self-antigen-specific TCR system.* European journal of immunology, 2014. **44**(1): p. 239-250.

82. Dushek, O., R. Das, and D. Coombs, *A role for rebinding in rapid and reliable T cell responses to antigen.* PLoS computational biology, 2009. **5**(11).

83. Altan-Bonnet, G. and R.N. Germain, *Modeling T cell antigen discrimination based on feedback control of digital ERK responses.* PLoS biology, 2005. **3**(11).

84. Lipniacki, T., et al., *Stochastic effects and bistability in T cell receptor signaling.* Journal of theoretical biology, 2008. **254**(1): p. 110-122.

85. Mukhopadhyay, H., et al., *Systems model of T cell receptor proximal signaling reveals emergent ultrasensitivity.* PLoS computational biology, 2013. **9**(3).

86. Voisinne, G., et al., *T Cells Integrate Local and Global Cues to Discriminate between Structurally Similar Antigens.* Cell reports, 2015.

87. Dushek, O. and P.A. van der Merwe, *An induced rebinding model of antigen discrimination.* Trends in immunology, 2014. **35**(4): p. 153-158.

88. Ma, Z., P.A. Janmey, and T.H. Finkel, *The receptor deformation model of TCR triggering.* FASEB journal : official publication of the Federation of American Societies for Experimental Biology, 2008. **22**(4): p. 1002-1008.

89. Kim, S.T., et al., *The alphabeta T cell receptor is an anisotropic mechanosensor.* The Journal of biological chemistry, 2009. **284**(45): p. 31028-31037.

90. Ma, Z. and T.H. Finkel, *T cell receptor triggering by force.* Trends in immunology, 2010. **31**(1): p. 1-6.

91. Kim, S.T., et al., *TCR Mechanobiology: Torques and Tunable Structures Linked to Early T Cell Signaling.* Frontiers in immunology, 2012. **3**: p. 76.

92. Liu, B., et al., *Accumulation of dynamic catch bonds between TCR and agonist peptide-MHC triggers T cell signaling.* Cell, 2014. **157**(2): p. 357-368.

93. Feng, Y., et al., *Mechanosensing drives acuity of αβ T-cell recognition.* Proceedings of the National Academy of Sciences, 2017. **114**(39).

94. Evans, E., *Probing the relation between force--lifetime--and chemistry in single molecular bonds.* Annual review of biophysics and biomolecular structure, 2001. **30**: p. 105-128.

95. Das, D.K., et al., *Force-dependent transition in the T-cell receptor β-subunit allosterically regulates peptide discrimination and pMHC bond lifetime.* Proceedings of the National Academy of Sciences of the United States of America, 2015.

96. Hui, K.L., et al., *Cytoskeletal forces during signaling activation in Jurkat T-cells.* Molecular biology of the cell, 2015. **26**(4): p. 685-695.

97. Li, L., et al., *Lipid rafts enhance the binding constant of membrane-anchored receptors and ligands.* Soft matter, 2017. **13**(23): p. 4294-4304.

98. Wyer, J.R., et al., *T cell receptor and coreceptor CD8 alphaalpha bind peptide-MHC independently and with distinct kinetics.* Immunity, 1999. **10**(2): p. 219-225.

99. Xiong, Y., et al., *T Cell Receptor Binding to a pMHCII Ligand Is Kinetically Distinct from and Independent of CD4.* The Journal of biological chemistry, 2001. **276**(8): p. 5659-5667.

100. Veillette, A., et al., *The CD4 and CD8 T cell surface antigens are associated with the internal membrane tyrosine-protein kinase p56lck.* Cell, 1988. **55**(2): p. 301-308.

101. Bachmann, M.F., et al., *Developmental regulation of Lck targeting to the CD8 coreceptor controls signaling in naive and memory T cells.* The Journal of experimental medicine, 1999. **189**(10): p. 1521-1530.

102. Wooldridge, L., et al., *Interaction between the CD8 coreceptor and major histocompatibility complex class I stabilizes T cell receptor-antigen complexes at the cell surface.* The Journal of biological chemistry, 2005. **280**(30): p. 27491-27501.

103. Li, Y., Y. Yin, and R.A. Mariuzza, *Structural and biophysical insights into the role of CD4 and CD8 in T cell activation.* Frontiers in immunology, 2013. **4**: p. 206.

104. Pecht, I. and D.M. Gakamsky, *Spatial coordination of CD8 and TCR molecules controls antigen recognition by CD8+ T-cells.* FEBS Letters, 2005. **579**(15): p. 3336-3341.

105. Li, Q.-J.J., et al., *CD4 enhances T cell sensitivity to antigen by coordinating Lck accumulation at the immunological synapse.* Nature immunology, 2004. **5**(8): p. 791-799.

106. O'Rourke, A.M., J. Rogers, and M.F. Mescher, *Activated CD8 binding to class I protein mediated by the T-cell receptor results in signalling.* Nature, 1990. **346**(6280): p. 187-189.

107. Van Laethem, F., et al., *Deletion of CD4 and CD8 coreceptors permits generation of alphabetaT cells that recognize antigens independently of the MHC.* Immunity, 2007. **27**(5): p. 735-750.

108. Dockree, T., et al., *CD8(+) T-cell specificity is compromised at a defined MHCI/CD8 affinity threshold.* Immunology and cell biology, 2017. **95**(1): p. 68-76.

109. Casas, J., et al., *Ligand-engaged TCR is triggered by Lck not associated with CD8 coreceptor.* Nature communications, 2014. **5**: p. 5624.

110. Artyomov, M.N., et al., *CD4 and CD8 binding to MHC molecules primarily acts to enhance Lck delivery.* Proceedings of the National Academy of Sciences of the United States of America, 2010. **107**(39): p. 16916-16921.

111. Stepanek, O., et al., *Coreceptor scanning by the T cell receptor provides a mechanism for T cell tolerance.* Cell, 2014. **159**(2): p. 333-345.

112. Moogk, D., et al., *Constitutive Lck Activity Drives Sensitivity Differences between CD8+ Memory T Cell Subsets.* Journal of immunology (Baltimore, Md. : 1950), 2016.

113. Lévy, R. and M. Maaloum, *Measuring the spring constant of atomic force microscope cantilevers: thermal fluctuations and other methods.* Nanotechnology, 2002. **13**(1): p. 33.

114. Sung, C.L., et al., *Calibration for computer experiments with binary responses.* 2018.

115. Zhang, X., et al., *Atomic force microscopy measurement of leukocyte-endothelial interaction.* American journal of physiology. Heart and circulatory physiology, 2004. **286**(1): p. 67.

116. Chen, A. and V.T. Moy, *Cross-Linking of Cell Surface Receptors Enhances Cooperativity of Molecular Adhesion.* Biophysical Journal, 2000. **78**(6): p. 2814-2820.

117. Taubenberger, A., et al., *Revealing early steps of alpha2beta1 integrin-mediated adhesion to collagen type I by using single-cell force spectroscopy.* Molecular biology of the cell, 2007. **18**(5): p. 1634-1644.

118. Lehenkari, P.P. and M.A. Horton, *Single Integrin Molecule Adhesion Forces in Intact Cells Measured by Atomic Force Microscopy.* Biochemical and Biophysical Research Communications, 1999. **259**(3): p. 645-650.

119. Chaudhuri, O., et al., *Combined atomic force microscopy and side-view optical imaging for mechanical studies of cells.* Nature methods, 2009. **6**(5): p. 383-387.

120. Beicker, K., et al., *Vertical Light Sheet Enhanced Side-View Imaging for AFM Cell Mechanics Studies.* Scientific Reports, 2018. **8**(1): p. 1504.

121. Ounkomol, C., S. Yamada, and V. Heinrich, *Single-cell adhesion tests against functionalized microspheres arrayed on AFM cantilevers confirm heterophilic E- and N-cadherin binding.* Biophysical journal, 2010. **99**(12): p. 2.

122. Ounkomol, C., et al., *Versatile horizontal force probe for mechanical tests on pipette-held cells, particles, and membrane capsules.* Biophysical journal, 2009. **96**(3): p. 1218-1231.

123. Chesla, S.E., P. Selvaraj, and C. Zhu, *Measuring two-dimensional receptor-ligand binding kinetics by micropipette.* Biophysical journal, 1998. **75**(3): p. 1553-1572.

124. Fahmy, T.M., et al., *Increased TCR avidity after T cell activation: a mechanism for sensing low-density antigen.* Immunity, 2001. **14**(2): p. 135-143.

125. Pielak, R.M., et al., *Early T cell receptor signals globally modulate ligand:receptor affinities during antigen discrimination.* Proceedings of the National Academy of Sciences, 2017. **114**(46): p. 12190-12195.

126. Zarnitsyna, V.I., et al., *Memory in receptor-ligand-mediated cell adhesion.* Proceedings of the National Academy of Sciences of the United States of America, 2007. **104**(46): p. 18037-18042.

127. Cole, D.K., et al., *Hotspot autoimmune T cell receptor binding underlies pathogen and insulin peptide cross-reactivity.* The Journal of clinical investigation, 2016. **126**(6): p. 2191-2204.

128. Apgar, J.F., et al., *Stimulus design for model selection and validation in cell signaling.* PLoS computational biology, 2008. **4**(2).

129. Burchat, A.F., et al., *Pyrrolo[2,3-d]pyrimidines Containing an Extended 5-Substituent as Potent and Selective Inhibitors of lck II.* Bioorganic & Medicinal Chemistry Letters, 2000. **10**(19): p. 2171-2174.

130. Ikonen, E., *Cellular cholesterol trafficking and compartmentalization.* Nature Reviews Molecular Cell Biology, 2008. **9**(2): p. 125-138.

131. Gillespie, D.T., *Exact stochastic simulation of coupled chemical reactions.* The Journal of Physical Chemistry, 1977. **81**(25): p. 2340-2361.

132. Gillespie, D.T., *Stochastic simulation of chemical kinetics.* Annual review of physical chemistry, 2007. **58**: p. 35-55.

133. Katz, Z.B., et al., *A cycle of Zap70 kinase activation and release from the TCR amplifies and disperses antigenic stimuli.* Nature Immunology, 2016. **18**(1): p. 86-95.

134. Moogk, D., A. Natarajan, and M. Krogsgaard, *T cell receptor signal transduction: affinity, force and conformational change.* Current Opinion in Chemical Engineering, 2018. **19**: p. 43-50.

135. Gil, D., et al., *T cell receptor engagement by peptide-MHC ligands induces a conformational change in the CD3 complex of thymocytes.* The Journal of experimental medicine, 2005. **201**(4): p. 517-522.

136. Risueño, R.M., H.M. van Santen, and B. Alarcón, *A conformational change senses the strength of T cell receptor-ligand interaction during thymic selection.* Proceedings of the National Academy of Sciences of the United States of America, 2006. **103**(25): p. 9625-9630.

137. Beddoe, T., et al., *Antigen ligation triggers a conformational change within the constant domain of the alphabeta T cell receptor.* Immunity, 2009. **30**(6): p. 777-788.

138. Sykulev, Y., et al., *Peptide antagonism and T cell receptor interactions with peptide-MHC complexes.* Immunity, 1998. **9**(4): p. 475-483.

139. Krogsgaard, M., et al., *Agonist/endogenous peptide-MHC heterodimers drive T cell activation and sensitivity.* Nature, 2005. **434**(7030): p. 238-243.

140. Wylie, D.C., J. Das, and A.K. Chakraborty, *Sensitivity of T cells to antigen and antagonism emerges from differential regulation of the same molecular signaling module.* Proceedings of the National Academy of Sciences of the United States of America, 2007. **104**(13): p. 5533-5538.

141. François, P., et al., *Phenotypic model for early T-cell activation displaying sensitivity, specificity, and antagonism.* Proceedings of the National Academy of Sciences of the United States of America, 2013. **110**(10): p. 97.

142. Kumar, R., et al., *Increased sensitivity of antigen-experienced T cells through the enrichment of oligomeric T cell receptor complexes.* Immunity, 2011. **35**(3): p. 375-387.

143. Palmer, E. and D. Naeher, *Affinity threshold for thymic selection through a T-cell receptor-co-receptor zipper.* Nature reviews. Immunology, 2009. **9**(3): p. 207-213.

144. Thome, M., et al., *Syk and ZAP-70 mediate recruitment of p56lck/CD4 to the activated T cell receptor/CD3/zeta complex.* The Journal of Experimental Medicine, 1995. **181**(6): p. 1997-2006.

145. Thome, M., et al., *The p56lck SH2 domain mediates recruitment of CD8/p56lck to the activated T cell receptor/CD3/ζ complex.* European Journal of Immunology, 1996. **26**(9): p. 2093-2100.

146. Bell, G.I., *Models for the specific adhesion of cells to cells.* Science (New York, N.Y.), 1978. **200**(4342): p. 618-627.

147. Roh, K.-H.H., et al., *The coreceptor CD4 is expressed in distinct nanoclusters and does not colocalize with T-cell receptor and active protein tyrosine kinase p56lck.* Proceedings of the National Academy of Sciences of the United States of America, 2015. **112**(13): p. 13.

148. Borger, J.G., R. Zamoyska, and D.M. Gakamsky, *Proximity of TCR and its CD8 coreceptor controls sensitivity of T cells.* Immunology letters, 2014. **157**(1-2): p. 16-22.

149. Gupta, V.K., *Effects of cellular viscoelasticity in lifetime extraction of single receptor-ligand bonds.* Physical Review E, 2015. **91**(6): p. 62701.

150. Yachi, P.P., et al., *Altered peptide ligands induce delayed CD8-T cell receptor interaction--a role for CD8 in distinguishing antigen quality.* Immunity, 2006. **25**(2): p. 203-211.

151. Li, L., et al., *Ionic CD3-Lck interaction regulates the initiation of T-cell receptor signaling.* Proceedings of the National Academy of Sciences of the United States of America, 2017. **114**(29).

152. Viola, A., et al., *Quantitative Contribution of CD4 and CD8 to T Cell Antigen Receptor Serial Triggering.* The Journal of Experimental Medicine, 1997. **186**(10): p. 1775-1779.

153. Lorenz, U., *SHP-1 and SHP-2 in T cells: two phosphatases functioning at many levels.* Immunological reviews, 2009. **228**(1): p. 342-359.